Noise in IMPATT-diode oscillators

Citation for published version (APA):
Goedbloed, J. J. (1973). *Noise in IMPATT-diode oscillators*. [Phd Thesis 1 (Research TU/e / Graduation TU/e), Electrical Engineering]. Technische Hogeschool Eindhoven. https://doi.org/10.6100/IR106076

DOI:
10.6100/IR106076

Document status and date:
Published: 01/01/1973

Document Version:
Publisher’s PDF, also known as Version of Record (includes final page, issue and volume numbers)

Please check the document version of this publication:

• A submitted manuscript is the version of the article upon submission and before peer-review. There can be important differences between the submitted version and the official published version of record. People interested in the research are advised to contact the author for the final version of the publication, or visit the DOI to the publisher's website.
• The final author version and the galley proof are versions of the publication after peer review.
• The final published version features the final layout of the paper including the volume, issue and page numbers.

Link to publication

General rights
Copyright and moral rights for the publications made accessible in the public portal are retained by the authors and/or other copyright owners and it is a condition of accessing publications that users recognise and abide by the legal requirements associated with these rights.

- Users may download and print one copy of any publication from the public portal for the purpose of private study or research.
- You may not further distribute the material or use it for any profit-making activity or commercial gain
- You may freely distribute the URL identifying the publication in the public portal.

If the publication is distributed under the terms of Article 25fa of the Dutch Copyright Act, indicated by the “Taverne” license above, please follow below link for the End User Agreement:

www.tue.nl/taverne

Take down policy
If you believe that this document breaches copyright please contact us at:

openaccess@tue.nl

providing details and we will investigate your claim.

Download date: 05. Oct. 2023

NOISE
IN IMPATT-DIODE OSCILLATORS

J. J. GOEDBLOED

NOISE
IN IMPATT-DIODE OSCILLATORS

PROEFSCHRIFT

TER VERKRIJGING VAN DE GRAAD VAN DOCTOR
IN DE TECHNISCHE WETENSCHAPPEN AAN DE
TECHNISCHE HOGESCHOOL TE EINDHOVEN, OP
GEZAG VAN DE RECTOR MAGNIFICUS, PROF.
DR. IR. G. VOSSERS, VOOR EEN COMMISSIE AANGEWEZEN DOOR HET COLLEGE VAN DEKANEN IN
HET OPENBAAR TE VERDEDIGEN OP DINSDAG
6 NOVEMBER 1973 TE 16.00 UUR

DOOR

JASPER JAN GOEDBLOED

GEBOREN TE BIERVLIET

DIT PROEFSCHRIFT IS GOEDGEKEURD
DOOR DE PROMOTOR PROF. DR. H. GROENDIJK

Aan de nagedachtenis van mijn vader
Aan mijn moeder
Aan mijn vrouw

Acknowledgements

The research described in this work was carried out in the Philips Research Laboratories, Eindhoven, The Netherlands, to whose management I am greatly indebted for affording me the opportunity of publishing the results as a thesis.

I would like to express my gratitude to all those who have contributed to this work in any way. Many of the conclusions reached were made possible by the pool of know-how present in the Microwave Device Physics Group. For instance, I am much indebted to Dr. M. T. Vlaardingerbroek for the theoretical basis on which my own research was built up, and to Messrs. B. B. van Iperen and H. Tjassens for their microwave-impedance measuring system, without which my task would have been exceptionally more difficult. I am very grateful to Mr. J. H. Verduin for his skilful assistance with the experiments, and to Dr. D. de Nobel and Mr. H. G. Kock for making the diodes.

Special thanks are due to Dr. G. A. Acket and Mr. A. Smith-Hardy for their critical reading of the manuscript, and to Mrs. C. Oldenburg-Strating for the accurate typing work.

CONTENTS

1. INTRODUCTION

In March 1958 W. T. Read Jr., in his paper "A proposed high-frequency negative-resistance diode"[1]) put forward the suggestion that it should be possible to construct a microwave oscillator in which the active device is a semiconductor diode under breakdown conditions. In February 1965 the first experimental realisation of Read's proposal was reported by Johnston, DeLoach and Cohen[2])*). Since 1965 a large number of studies has been put forward concerning the excitation of microwaves using an avalanching diode, i.e. a diode under breakdown in which, due to impact-ionisation processes, an avalanche of charge carriers is created.

The operation of a microwave oscillator with avalanche diode is based on the fact that for certain conditions this diode shows an impedance with a negative real part. With the aid of this negative resistance the loss resistance of an oscillator loop can be cancelled out, thus making oscillations possible. The negative resistance is partly due to the nature of the avalanche process and partly due to transit-time effects. These two origins explain the designation IMPATT-diode oscillator, where the acronym IMPATT stands for $\overline{\text{IMP}}$act-ionisation, $\underline{\text{A}}$valanche and $\underline{\text{T}}$ransit-$\underline{\text{T}}$ime. The avalanche process turns out to be an inductive process, thus giving rise to a 90° phase shift between voltage and current. The additional phase shift needed to arrive at an impedance with a negative real part, is obtained by a phase delay due to the transit time of the carriers through the junction.

The practical application of an IMPATT-diode oscillator depends to a large extent on the noise characteristics of this oscillator. Hence soon after the oscillator became operational the first measurements of noise in these oscillators were already reported [4,5]). A large number of theoretical and experimental studies of noise in IMPATT diodes and IMPATT-diode oscillators followed. An excellent review of these studies, up to May 1971, has been presented by Gupta [6]). When reading the part of his review on noise in IMPATT-diode oscillators it strikes one that the number of papers is very limited in which the noise in these oscillators is discussed starting from the physical properties of the diode itself. Furthermore, a detailed experimental check of these theories is lacking.

The first theory of noise in IMPATT-diode oscillators has been presented by Hines [7]). His analysis, which he considers as a first approximation only, is based upon results of his small-signal analysis for IMPATT-diode amplifiers [8]). The first large-signal theory for noise in IMPATT-diode oscillators was pub-

---

*) From a paper by Val'd-Perlov, Tager and Krasilov [3]) dated November 1966 it can be concluded that they had already realised Read's proposal in 1959.

lished by Inkson [9]). He used the sharp-pulse approximation, already suggested by Read [1]), to describe the conduction current leaving the region of the junction where the impact ionisation takes place. This means that his theory is applicable to high-level operating oscillators only.

Vlaardingerbroek [10]) put forward an analytical theory which provides expressions for the output-power spectrum and the width of the output spectrum for IMPATT-diode oscillators operating at low signal levels. This theory, which is based on the fact that the output signal of an oscillating loop consists of narrow-band amplified noise, has been worked out in more detail by Vlaardingerbroek and the present author in ref. 9. In that paper the influence of low-frequency noise on the oscillator noise was also discussed. The paper in question formed the basis of the present study, in which we shall try to describe the noise in IMPATT-diode oscillators in terms of physical properties and dimensions of the diode itself. For this reason the circuits used were singly tuned and had a low-loaded quality factor of the cavity, so that the oscillator noise is affected as little as possible by the circuit.

The thesis is arranged as follows.

In chapter 2 the diode model used is introduced. This model is of great importance as we want to describe the oscillator noise analytically starting from the processes which take place inside the diode.

Chapter 3 deals with the small-signal and the large-signal behaviour of the noise-free IMPATT diode. The small-signal behaviour of the diode is of importance as it enables us to determine the value of several diode parameters. A study of the noise-free oscillator is of great interest because if the quasi-stationary quantities like output power and large-signal impedance cannot be described by the diode model used, we can have no illusions about the description of the oscillator noise using the same diode model.

In chapter 4 the noise of the non-oscillating diode is discussed. Special attention is paid to the intrinsic response time of the avalanche process which governs the internal noise properties of the diode.

Chapter 5 summarises briefly the general theory of oscillator noise which, in principal, is applicable to any oscillator, and it is applied to the special case of IMPATT-diode-oscillator noise. Furthermore, the oscillator-noise-measuring equipment is described.

In chapter 6 the basic idea that the output signal consists of narrow-band amplified noise is worked out and checked in detail experimentally. The theory presented is restricted to low signal levels so that the output power can be assumed mainly as linearly amplified noise, the only non-linearity taken into account being the determination of the output power level, as described in chapter 3.

Chapter 7 finally deals with up-converted and down-converted noise, i.e. with oscillator noise caused by low-frequency noise and the reverse. Furthermore, the deviations between the oscillator noise found experimentally and the noise predicted by the linear noise theory of chapter 6 are discussed. A comparison is made with recent theories [13-17]) in which the signal level is not restricted to low values.

2. IMPATT-DIODE MODEL

2.1. Introduction

Since the ultimate aim of the present study is to describe the noise of the IMPATT-diode oscillator, starting from the processes which take place inside the diode, the diode model to be used is of importance. Before this model is discussed in detail, some introductory observations will be made concerning the diode behaviour under reverse-bias and breakdown conditions [18]).

Let us consider a semiconductor diode, e.g. an abrupt p^+–n diode, where the superscript $+$ denotes material which is heavily doped compared to the adjacent material. There is an electric field across the metallurgical junction of the diode [19]). The magnitude of this field can be increased by applying a reverse bias voltage to the diode. For the present diode this means that a positive voltage is applied to the n-type material of the junction with respect to the p-type material. The layer in which the electric field is present is almost depleted of free carriers and is therefore called the depletion layer. The very small current (a few nano-amperes) which is still flowing through this layer is called the saturation current. This current is carried by electrons and holes generated thermally in the semiconductor material.

When an electron–hole pair is generated within the depletion layer it will be split immediately owing to the presence of the electric field. The electron moves towards the n-region, and the hole towards the p-region. Both carriers move with their corresponding drift velocity, which is defined as the average velocity component of the carrier parallel to the electric field. The velocity component is averaged over a time interval which is long compared to the average time between two collisions of the carrier with the crystal lattice.

At low values of the electric field the drift velocity increases with increasing field. For high values of the field the drift velocity more or less saturates. For electrons in silicon, for example, the drift velocity becomes saturated for field values larger than 20 kV/cm [20]).

Although the drift velocity saturates with increasing field, the kinetic energy acquired in the field by a carrier keeps increasing. If the electric field is high enough, a carrier can acquire so much energy that it will be able to ionise a lattice atom by impact, thus leading to the creation of an electron–hole pair [21]). The electron and hole of this pair, which are separated immediately, can in turn also ionise lattice atoms and create new electron–hole pairs, and so on. This process is called the avalanche process. It can give rise to large reverse currents and this phenomenon is known as junction breakdown. The capability for impact ionisation can be expressed by an ionisation coefficient, generally denoted by α for electrons and β for holes [22]). The ionisation coefficient gives the average number of electron–hole pairs created by one carrier per unit length n a direction parallel to the electric field. From experiments [23]) and from a theory by Shockley [24]) it is known that α and β can be expressed by

$$\alpha, \beta = a \exp{(-b/E)^m}, \tag{2.1}$$

where a, b and m are constants and E the magnitude of the electric field ($m = 1$ for silicon and germanium, and 2 for gallium arsenide [22])). The appearance of the exponential function in eq. (2.1) can be readily understood. If ε_i is the energy needed to ionise a lattice atom, then the carrier which ionises this atom by impact must have at least this energy in order to do so. A carrier has an energy ε_i when it has travelled a distance l_i given by $q\, l_i\, E = \varepsilon_i$, where q is the electronic charge. Let l be the average distance between two (non-ionising) collisions of the carrier with the lattice. Then the probability that the carrier travels the distance l_i without a collision is proportional to

$$\exp{(-\,l_i/l)} = \exp\left(-\frac{\varepsilon_i/q\,l}{E}\right). \tag{2.2}$$

It will be clear that the ionisation coefficient is proportional to this function.

Owing to the field dependence of α and β impact ionisation (or avalanche multiplication) generally occurs in a relatively narrow region of the depletion layer, namely the region with the highest values of the electric field. This region is generally called the avalanche region. The remaining part of the depletion layer is called the drift region, since the carriers only drift through it. In most practical situations it can be assumed that the carriers travel at saturated drift velocity throughout the depletion layer.

Since the carriers generated in the avalanche region reduce the electric field in that region once they have drifted out of the avalanche region, a steady-avalanche process is generally possible. In this steady avalanche the rate of ionisation is such that the mean number of electron–hole pairs created by an initial pair is unity if the number of thermally generated electron–hole pairs is negligible. When $\beta = \alpha$ the steady-avalanche condition is [1])

$$\int_0^{l_a} \alpha \, \mathrm{d}x = 1. \tag{2.3}$$

When $\beta \neq \alpha$, it is [25])

$$\int_0^{l_a} \alpha \exp{\left[\int_0^x (\beta - \alpha)\, \mathrm{d}\xi\right]} \mathrm{d}x = 1, \tag{2.4}$$

where l_a is the length of the avalanche region. Equation (2.4) can be reduced to

$$\alpha = \beta \exp\,[(\alpha - \beta)\, l_a], \tag{2.5}$$

when α and β do not depend on the position (x) in the avalanche region.

From the above it will be clear that the avalanche process is highly non-linear. This fact particularly affects the behaviour of the oscillating diode, not only the quasi-stationary quantities such as impedance and output power but also the fluctuating quantities. The fluctuations, i.e. the noise, are present due to the fact that both the thermal-generation process and the ionisation process are statistical processes.

All this will be discussed in detail later on in this study. From the introduction given, we derive the principal assumption on which the diode model used is based, namely:

In an avalanching junction carrier generation by impact ionisation and carrier drift occur in different regions of the depletion layer: the avalanche region and the drift region.

The avalanche region will be discussed in sec. 2.2, the drift region in sec. 2.3. In the course of our theoretical and experimental investigations it was found that the quantities which interest us can be described on the basis of a relatively simple diode model. The assumptions regarding this simple diode model are summarised in sec. 2.4.

2.2. The avalanche region

The avalanche multiplication which takes place in the avalanche region only, will be considered to be uniform over the diode area (one-dimensional problem). Moreover, we confine the analysis to the region of not too high frequencies, where the energy relaxation time and the momentum relaxation time can be neglected compared with the period of oscillation [26]). Under these conditions, and in the absence of noise and recombination effects, the kinetic equations for the electrons and holes are the continuity equations

$$\frac{\partial}{\partial t} n = \frac{1}{q}\frac{\partial}{\partial x} J_n + \alpha\, n\, v_n + \beta\, p\, v_p, \tag{2.6}$$

$$\frac{\partial}{\partial t} p = -\frac{1}{q}\frac{\partial}{\partial x} J_p + \alpha\, n\, v_n + \beta\, p\, v_p, \tag{2.7}$$

where n and p are the concentrations of electrons and holes, J_n and J_p the electron and hole current densities, α and β the ionisation coefficients of electrons and holes, v_n and v_p the saturated drift velocities of the electrons and holes, and q the electronic charge. All quantities in eqs (2.6) and (2.7) are positive and may depend (with, of course, the exception of q) on the position coordinate x

and the time coordinate t. The holes are assumed to drift in the positive x-direction.

The fluctuations of the avalanche process can be introduced into the mathematical description by adding a noise term to eqs (2.6) and (2.7), so that these equations take the form of a Langevin equation [27]). The noise will be left out of consideration in the present chapter and also in chapter 3. The introduction of the noise term into the description will be discussed in detail in sec. 4.1.

We continue the present section with the derivation of an expression for the total noise-free conduction current in the avalanche region. This expression, generally called the Read equation, has been the subject of several studies [28-30]). For this reason we will limit the derivation of the Read equation to the simplified case where $\alpha = \beta$, independently of x, and $v_n = v_p = v$, also independently of x. In this way the algebra is kept simple, while the principal assumptions to be made can still be stated. The Read equation will be subsequently refined to account for $\alpha \neq \beta$ and $v_n \neq v_p$.

Adding eqs (2.6) and (2.7) we find

$$\frac{1}{v}\frac{\partial}{\partial t} J_c = \frac{\partial}{\partial x}(J_n - J_p) + 2\,\alpha\, J_c, \tag{2.8}$$

while subtracting these equations yields

$$\frac{1}{v}\frac{\partial}{\partial t}(J_n - J_p) = \frac{\partial}{\partial x} J_c, \tag{2.9}$$

where $J_c = J_n + J_p$, and use has been made of the expressions $J_n = q\,n\,v$ and $J_p = q\,p\,v$. The expression for the total conduction current leaving the avalanche region is found after integration of eq. (2.8) over the length of the avalanche region:

$$\frac{1}{v}\int_0^{l_a} \frac{\partial}{\partial t} J_c \,\mathrm{d}x = (J_n - J_p)\Big|_0^{l_a} + 2\alpha \int_0^{l_a} J_c \,\mathrm{d}x. \tag{2.10}$$

The first term on the right-hand side of this equation can be written

$$(J_n - J_p)\Big|_0^{l_a} = -2\,J_c(0) + 2\,J_s, \tag{2.11}$$

where $J_c(0) = J_c(l_a)$ is the conduction current at the boundaries of the avalanche region, and $J_s = J_{ps} + J_{ns}$ is the saturation current entering the avalanche region. The second term on the right-hand side of eq. (2.10) can be worked out by means of partial integration. After some straightforward calculations, also using eq. (2.9), this yields

$$2\,\alpha \int_0^{l_a} J_c \,\mathrm{d}x = 2\,\alpha\, l_a\, J_c(0) - \frac{2\alpha}{v} \int_0^{l_a} x \frac{\partial}{\partial t} (J_n - J_p)\,\mathrm{d}x. \tag{2.12}$$

According to the mean-value theorem

$$J_c = J_c(0) + x \left(\frac{\partial}{\partial x} J_c \right)_{x=x_0} = J_c(0) + \frac{x}{v} \frac{\partial}{\partial t} (J_n - J_p)_{x=x_0},$$

where x_0 is a suitably chosen value of x in the interval $0 \leqslant x \leqslant l_a$. For the time derivative of J_c in the term on the left-hand side of eq. (2.10) we therefore find

$$\frac{\partial}{\partial t} J_c = \frac{\partial}{\partial t} J_c(0) + \frac{x}{v} \frac{\partial^2}{\partial t^2} (J_n - J_p). \tag{2.13}$$

We next assume the angular frequency (ω) considered in our studies to be so low that $(\omega\, l_a/v)^2 = (\omega\, \tau_a)^2 \ll 1$ (τ_a being the transit time of the carriers in the avalanche region). The term containing the second-order time derivative in eq. (2.13) can then be neglected. This means that J_c and also $J_n - J_p$ can be replaced by their quasi-stationary approximations

$$J_c = J_n + J_p = J_c(0)$$

and

$$J_n - J_p = J_c(0)\,(1 - 2\,\alpha\, x), \tag{2.14}$$

which can be obtained from eqs (2.6) and (2.7) with $\partial/\partial t = 0$. Substitution of eqs (2.11), (2.12) and (2.14) in eq. (2.10) yields

$$\tau_a\,(1 + \alpha\, l_a - \tfrac{4}{3}\,\alpha^2\, l_a^2) \frac{\partial}{\partial t} J_c(0) =$$

$$2\, J_c(0) \left[\alpha\, l_a \left(1 + \tfrac{2}{3}\, \tau_a \frac{\partial}{\partial t}\, \alpha\, l_a \right) - 1 \right] + 2\, J_s. \tag{2.15}$$

The ionisation coefficient α depends on the electric field E_a in the avalanche region. Representing α in the neighbourhood of the static field strength, E_{a0}, by its Taylor expansion, we obtain

$$\alpha\, l_a = \alpha(E_{a0})\, l_a + \left(\frac{\mathrm{d}\alpha}{\mathrm{d}E_a} \right)_{E_a = E_{a0}} v_a + \ldots = 1 + \alpha'\, v_a + \ldots, \tag{2.16}$$

where use has been made of the static breakdown condition, eq. (2.3), and $v_a = e_a l_a$, e_a being the time-dependent part of E_a, and v_a the time-dependent part of the voltage V_a across the avalanche region. In writing $v_a = e_a l_a$ we assume e_a to be independent of x.

We next assume that it is sufficient to expand α up to the first-order field derivative of α only. Then substitution of eq. (2.16) in the left-hand side of eq. (2.15) yields

$$\frac{\tau_a}{3}\left(1 - \tfrac{5}{2}\,\alpha'\,v_a\right)\frac{\mathrm{d}}{\mathrm{d}t}\,J_c(0) = J_c(0)\,(\alpha\,l_a - 1) + J_s, \tag{2.17}$$

where we have neglected terms containing v_a^2 and $\partial v_a/\partial t$. If $5\,\alpha'\,v_a/2 \ll 1$ eq. (2.17) reduces to the well-known Read equation

$$\frac{\tau_a}{3}\frac{\mathrm{d}}{\mathrm{d}t}\,J_c = J_c\,(\alpha\,l_a - 1) + J_s. \tag{2.18}$$

In the preceding derivation several rather crude assumptions were made:

(1) $(\omega\tau_a)^2 \ll 1$. For $\omega/2\pi = 10$ GHz and $v = 10^5$ m/s, $\omega\tau_a = 0{\cdot}63$ per micron length of the avalanche region, while $0{\cdot}6\ \mu\text{m} < l_a < 2{\cdot}2\ \mu\text{m}$ for the diodes we investigated (see chapter 3).

(2) Both the second- and higher-order field derivatives as well as the time derivatives of α' were neglected. In view of the strong field dependence of α (eq. (2.1)), this also is a questionable assumption. Some of the consequences of the second-order field derivative of α will be discussed in sec. 3.2.

(3) The assumption that $5\,\alpha'\,v_a/2 \ll 1$, and our neglect of terms containing v_a^2 and $\partial v_a/\partial t$ limit the validity of eq. (2.18) theoretically to rather low values of v_a. For example (see chapter 4) $\alpha' = 0{\cdot}3$ is found from the experimental data. This means that $5\,\alpha'/2 = 0{\cdot}75$.

However, nature is occasionally kind to the investigator. It is found that if *all* these three assumptions are made, eq. (2.18) is a good description of the conduction current over a considerable range of frequencies and voltages. This was shown by experiments (sec. 3.2) and is also suggested by results of detailed numerical calculations [31]). We will therefore continue to use eq. (2.18) in our calculations.

The time constant $\tau_a/3$ in eq. (2.18) can be considered as the intrinsic response time of the avalanche process [29]). This can be illustrated as follows. Suppose J_s to have a stationary value J_{s0} for $t < 0$. At $t = 0$, J_s rises to a value $J_{s0} + \Delta J_s$. This causes J_c to increase from its stationary value J_{c0}. For small values of t it follows from eq. (2.18) that the increase is given by

$$J_c - J_{c0} \approx \frac{t}{\tau_i}\,\Delta J_s,$$

where $\tau_i = \tau_a/3$ and where we assumed $\alpha' \, v_a \, t/\tau_i \ll 1$. In this simplified example, therefore, it takes τ_i seconds to increase the current J_{c0} caused by ΔJ_s by an amount ΔJ_s.

The intrinsic response time τ_i will prove to be of great importance in the description of the noise behaviour of the diode. We therefore give the following elucidation.

In a steady semiconductor avalanche the average number of electron–hole pairs involved is constant. For steady high-current avalanches where the number of thermally generated carriers is negligible, this means that every electron–hole pair leaving the avalanche region due to drift must be replaced by a new pair created by impact ionisation. During one transit time of the avalanche region, therefore, the average number of electron–hole pairs produced by an initial pair is unity. The intrinsic response time can be considered as the average time after which the initial pair creates the pair which succeeds it. The intrinsic response time is thus related to the transit time of the carriers in the avalanche region. It will be clear that the intrinsic response time in particular figures in the noise behaviour of the avalanche process, since all deviations from the ideal fluctuation-free situation in which any one pair produces exactly one new pair after a fixed time delay of τ_i seconds are noise contributions [8]). In the avalanche process these deviations abound, owing to the statistical character of this process and of the thermal-generation process from which the avalanche builds itself up. The intrinsic response time will be discussed further in chapter 4.

As shown by several authors [28,32-34]), the unequal ionisation coefficients and unequal drift velocities of electrons and holes will affect the final value of the intrinsic response time. Equation (2.18) can then be written in a generalised form [34,35]):

$$\tau_i \frac{\mathrm{d}}{\mathrm{d}t} I_c = I_c \left(\bar{\alpha} \, l_a - 1\right) + I_s, \tag{2.19}$$

where $I_c = A \, J_c$, $I_s = A \, J_s$, A is the junction area and τ_i is given by [32])

$$\tau_i = \tau_a \frac{2 \, (\alpha \, \beta)^{1/2}}{(\alpha - \beta)^2 \, l_a} \left[(\alpha + \beta) \, l_a - 2\right], \tag{2.20}$$

when α and β are independent of the position in the avalanche region. In eq. (2.20) τ_a is defined by

$$\tau_a = \frac{l_a}{2} \left(\frac{1}{v_n} + \frac{1}{v_p}\right), \tag{2.21}$$

and l_a can be found from the breakdown condition eq. (2.5). In eq. (2.19) $\bar{\alpha}$ is an average ionisation coefficient (averaged over α and β), the field derivative of which is well approximated by a relation given by Hulin et al. ^{36}):

$$\bar{\alpha}' = \frac{1}{2l_a}\left(\frac{\alpha'}{\alpha} + \frac{\beta'}{\beta}\right). \tag{2.22}$$

Thus far only the conduction current in the avalanche region has been considered. The total current I_t through that region is given by

$$I_t = I_c + C_a \frac{\mathrm{d}}{\mathrm{d}t} V_a, \tag{2.23}$$

where $C_a = \epsilon A/l_a$ is the "cold" capacitance of the avalanche region. In fig. 2.1 the currents and voltages of interest in the diode are presented in a vector diagram in the complex plane ^{37}). Suppose an alternating voltage v_t is applied to the avalanching junction. Part of this a.c. voltage (v_a) appears across the avalanche region. The voltage v_a causes an a.c. conduction current i_c in the avalanche region. It follows from eq. (2.19) that this current has a 90° phase lag with respect to v_a. The displacement current $C_a\,(\mathrm{d}V_a/\mathrm{d}t) = j\,\omega\,C_a\,v_a$ has a 90° phase lead with respect to v_a. We note that the conduction current and the displacement current are in anti-phase, so that for a given value of i_c, v_a and C_a the total a.c. current i_t is in phase with or in phase opposition to i_c, depending on the frequency ω. It is found that if i_t and i_c are in anti-phase the diode will have an impedance with a negative real part. The frequency at which $|i_c| = \omega\,C_a\,v_a$, and hence $i_t = 0$, is called the avalanche frequency. The condition for a negative resistance can then be formulated as follows: for a given i_c, v_a and C_a the frequency of the signal applied must be higher than the avalanche frequency.

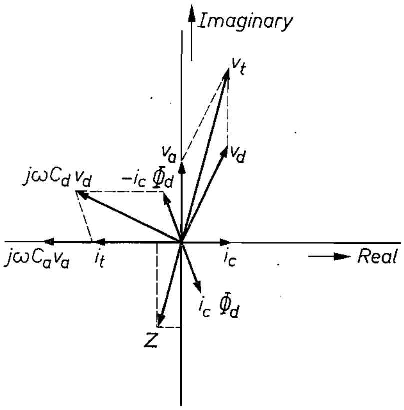

Fig. 2.1. Vector diagram in which the amplitudes and the phases of the various voltages and currents in the diode are represented in connection. The diode impedance $Z = v_t/i_t$.

2.3. The drift region

It is assumed that no impact ionisation takes place in the drift region, so that the carriers injected into this region from the avalanche region only drift through it. Furthermore, it is assumed that the carriers travel at saturated drift velocity.

If the current is injected into the drift region at $x = l_a$, it causes an induced current in the external circuit, the fundamental of which is given by

$$i_{\text{ind}} = \frac{1}{l_d} \int_{l_a}^{W} i_c \exp\left(-j \frac{\omega (x - l_a)}{v}\right) \mathrm{d}x \equiv \Phi_d \, i_c, \tag{2.24}$$

where W is the length of the depletion layer and $l_d = W - l_a$ is the length of the drift region. The current i_{ind} is also the average conduction current in the drift region (fig. 2.1). The transit-time function Φ_d, given by

$$\Phi_d = \frac{1 - \exp(-j\theta)}{j\theta}, \qquad \theta = \frac{\omega \, l_d}{v} \tag{2.25}$$

describes the phase delay with respect to i_c. (The velocity $v = v_n$ in the case of a p^+–n diode and v_p in the case of an n^+–p diode.)

The total a.c. current through the drift region is given by

$$i_t = i_c \, \Phi_d + j \, \omega \, C_d \, v_d \tag{2.26}$$

where $C_d = \epsilon A / l_d$ is the cold capacitance of the drift region and i_t is equal to the total a.c. current i_t through the avalanche region.

In the vector diagram the displacement current $j \, \omega \, C_d \, v_d$ can be found from $i_t - i_c \, \Phi_d$. The voltage v_d is delayed 90° in phase with respect to the displacement current.

The vector diagram can be finally completed by adding v_a and v_d, which gives the total a.c. voltage v_t across the depletion layer. In addition, the diode impedance Z is given by the ratio of v_t to i_t. As indicated in fig. 2.1, Z has indeed a negative real part. Furthermore, the imaginary part of Z is also negative, so that in an equivalent circuit Z can be represented by a negative resistance in series with a capacitance.

2.4. Summary of assumptions in the IMPATT-diode model

Except when explicitly stated otherwise, the following assumptions with regard to the IMPATT-diode model are made in the remaining part of our studies:

(1) the depletion layer can be divided into an avalanche region and a drift region;

(2) all the impact ionisation takes place in the avalanche region, for which it is also assumed that:

(a) transit time effects can be neglected;

(b) all relevant quantities are independent of the position in that region;

(c) the total conduction current is described by eq. (2.19), omitting the saturation-current term:

$$\tau_i \frac{\mathrm{d}}{\mathrm{d}t} I_c = I_c (\bar{\alpha}\, l_a - 1). \tag{2.27}$$

This assumption also includes the assumptions made in sec. 2.2 in order to arrive at eq. (2.19);

(d) it is sufficient to expand the ionisation coefficient to the first-order field derivative only:

$$\bar{\alpha} = \bar{\alpha}_0 + \bar{\alpha}'\, e_a;$$

(3) the electric-field configuration is such that only one drift region occurs;

(4) the drift velocities of electrons and holes are saturated throughout the depletion layer;

(5) the modulation of the width of the depletion layer in the presence of a.c. signals is neglected, as is the change of this width caused by a change of the direct current or of the junction temperature;

(6) the effects of carrier diffusion are neglected.

A further discussion of the assumptions made can be found in secs 3.1.5, 3.2.3, 3.2.5 and 4.4.

3. THEORY OF THE NOISE-FREE IMPATT DIODE

3.1. Small-signal theory

In chapter 2 several diode parameters were introduced, such as the length of the avalanche region (l_a), the transit-time function (Φ_d), the avalanche frequency (ω_a), etc. In the present section the determination of the values of these parameters will be discussed. For this purpose we first derive in sec. 3.1.1 an expression for the small-signal impedance of the diode on the basis of the assumptions for the diode model, summarised in sec. 2.4. The experimental determination of the small-signal impedance is also described in sec. 3.1.1. This impedance is determined at a fixed microwave frequency as a function of the bias current through the diode. In sec. 3.1.2 the calculation of the diode parameters from the measuring data is discussed. The results of this determination are given in sec. 3.1.3.

It is important to have some insight into the significance of the validity of the diode model used. To that end the diode model is extended in sec. 3.1.4 with respect to the model given in sec. 2.4. A method for the determination of the diode parameters from impedance data, using the extended model, is discussed. This method is applied to numerically calculated impedance data. In these numerical calculations the diode model was not subject to the assumptions made in sec. 2.4.

A discussion of the significance of the small-signal noise-free diode model as presented in sec. 2.4, and of the diode quantities derived in sec. 3.1.2 is given in sec. 3.1.5.

3.1.1. *Small-signal impedance*

Calculation of the small-signal impedance is based on the diode-model assumptions summarised in sec. 2.4. By taking the first-order perturbation of eq. (2.27), we obtain an a.c. equation at the angular frequency ω:

$$j\,\omega\,\tau_i\,i_{c1} = I_{c0}\,\overline{\alpha}'\,v_{a1}, \tag{3.1}$$

where the subscript 0 is used to denote a d.c. quantity, the lower-case character an a.c. quantity, and the subscript 1 a small-signal quantity. For example: i_{c1} is the small-signal a.c. component of the current I_c through the avalanche region, while I_{c0} is its d.c. component. The small-signal equation for the total current i_{t1} through the avalanche region is derived from eq. (2.23):

$$i_{t1} = i_{c1} + j\,\omega\,C_a\,v_{a1}. \tag{3.2}$$

After substitution of eq. (3.1) in eq. (3.2) we find

$$v_{a1} = \frac{i_{t1}}{j\,\omega\,C_a}\left(1 - \frac{1}{1-\omega^2/{\omega_{a1}}^2}\right), \tag{3.3}$$

where the small-signal angular avalanche frequency ω_{a1} is defined by

$$\omega_{a1}^2 = \frac{\overline{\alpha}'\, I_{c0}}{\tau_i\, C_a}. \tag{3.4}$$

The avalanche frequency can be considered as the resonance frequency of a parallel $L_a\, C_a$ circuit representing the avalanche region. The inductance L_a is given by

$$L_a = \frac{\tau_i}{\overline{\alpha}'\, I_{c0}}.$$

The equation for the total a.c. current in the drift region is now given by (eq. (2.26))

$$i_{t1} = i_{c1}\, \Phi_d + j\, \omega\, C_d\, v_{d1},$$

and substitution of eqs (3.1) and (3.3) yields

$$v_{d1} = \frac{i_{t1}}{j\, \omega\, C_d} \left(1 - \frac{\Phi_d}{1 - \omega^2/\omega_{a1}^2} \right). \tag{3.5}$$

Kirchhoff's law requires that (fig. 3.1)

$$i_{t1}\, Z_e + v_{a1} + v_{d1} + i_{t1}\, R_s = 0,$$

and after substitution of eqs (3.3) and (3.5) we find

$$i_{t1} \left(Z_e + R_s + \frac{1}{j\, \omega\, C_0} - \frac{\Phi}{j\, \omega\, C_d} \frac{1}{1 - \omega^2/\omega_{a1}^2} \right) = 0, \tag{3.6}$$

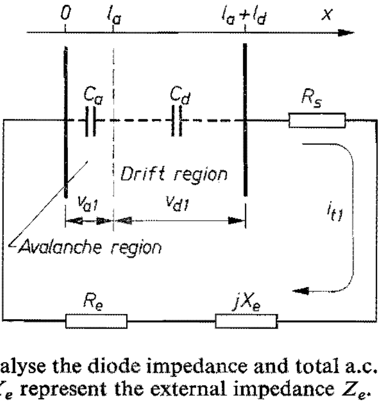

Fig. 3.1. Circuit used to analyse the diode impedance and total a.c. current. R_s is the parasitic diode resistance. R_e and jX_e represent the external impedance Z_e.

in which we use the abbreviations

$$C_0 = \frac{C_a\, C_d}{C_a + C_d} \qquad \text{and} \qquad \Phi = \frac{l_a}{l_d} + \Phi_d. \tag{3.7}$$

The small-signal impedance Z_1 of the diode follows from eq. (3.6) and can be written

$$Z_1 = R_s + \frac{1}{j\,\omega\, C_0} - \frac{\Phi}{j\,\omega\, C_d}\,\frac{1}{1 - \omega^2/\omega_{a1}{}^2}, \tag{3.8}$$

where we note that $R_s + 1/j\omega C_0$ is the impedance of the diode exactly at the point of breakdown ($I_{c0} \rightarrow 0$).

So much for the theoretical determination of the small-signal impedance. We measured the small-signal impedance of several diodes at a fixed frequency in the X-band as a function of the bias current through the diode. The measurements were carried out using the accurate microwave impedance bridge specially designed by Van Iperen and Tjassens [38]). On this bridge the small-signal impedance of the diode in its encapsulation is measured. The equivalent circuit of the diode in its encapsulation as used in the calculation of the diode impedance from the measuring data is given in fig. 3.2. The capacitance C_m of the encapsulation, typically 0·16 pF, was found by measuring empty encapsulations. The inductance L_m of the mounting wire, typically 0·5 nH, was found by comparing the capacitance of the diode measured at 10 GHz with its capacitance measured at a frequency of 1 MHz, where the influence of the mounting wire can be neglected. At 1 MHz the capacitance was measured with a Boonton Capacitance Bridge, Model 75D. A full discussion of the procedure described

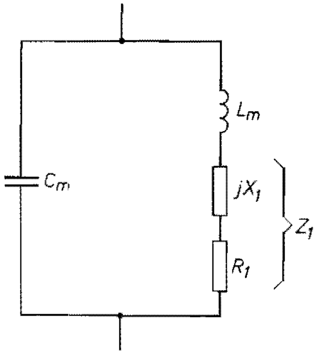

Fig. 3.2. Equivalent circuit of the diode in its encapsulation used in the calculation of the diode impedance from the measured impedance data. C_m is the capacitance of the encapsulation, and L_m is the inductance of the mounting wire.

above, including an extensive error treatment, is given in the above mentioned paper by Van Iperen and Tjassens [38]).

An example of the measured diode impedance is given in fig. 3.3. Before

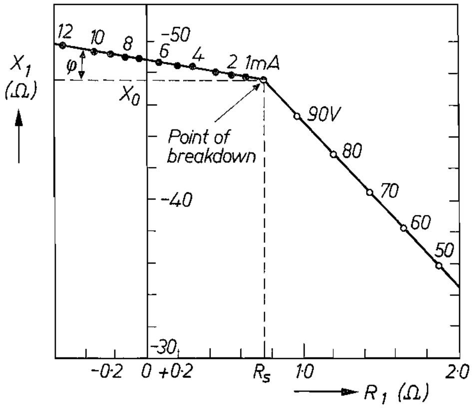

Fig. 3.3. Example of the measured small-signal impedance (diode no. 4 in table 3-II, sec. 3.1.3). The angle φ to be used in eq. (3.9) is indicated.

breakdown (circles) the bias voltage is the parameter; after breakdown (dots) the bias current is the parameter. The measuring frequency is 10 GHz. The figure shows that for the current range indicated a linear relation between the imaginary and real parts of the diode impedance is found. Indicated in fig. 3.3 is the angle φ to be used in the "tan φ" method for the determination of diode parameters. This method will now be discussed.

3.1.2. *Diode-quantity analysis;* tan φ *method*

In what follows we assume that we know the small-signal impedance data of the diode measured at a single microwave frequency as a function of the bias current through the diode. The values of the various diode parameters (diode quantities) used in the preceding section can be found from these measured data by assuming that they can be described by eq. (3.8), i.e. by our theoretical expression for the small-signal diode impedance.

If $Z_1 = R_1 + jX_1$ and $X_0 = 1/j\omega C_0$, it follows from eqs (2.25), (3.7) and (3.8) that tan φ, as indicated in fig. 3.3, is given by

$$\tan \varphi = \frac{X_1 - X_0}{R_1 - R_s} = -\frac{\mathrm{Re}\,\Phi}{\mathrm{Im}\,\Phi} = \frac{l_a/l_d + (\sin\theta)/\theta}{(1-\cos\theta)/\theta}. \qquad (3.9)$$

By way of example, tan φ is plotted in fig. 3.4 as a function of θ for several values of l_a/l_d.

From eq. (3.9) it is concluded that tan φ is a function of geometrical diode quantities and the frequency, but not of the bias current. The theory thus

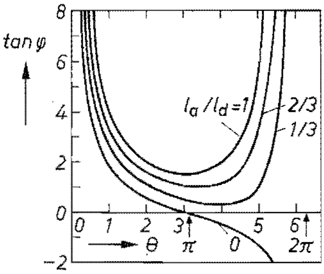

Fig. 3.4. The function tan φ, eq. (3.9), as a function of the transit angle θ for several values of the ratio l_a/l_d.

predicts the linear relationship between X_1 and R_1 as already mentioned at the end of sec. 3.1.1. For all diodes investigated experimentally this linear relationship was found for I_{c0} smaller than 10 to 15 mA. Deviations are found at higher values of the bias current. These deviations are due to the effect of the bias current on the width W of the depletion layer via Poisson's equation and via temperature effects (note that in our diode model W was assumed to be a constant; assumption (5) in sec. 2.4)

From the experimentally determined value of tan φ (eq. (3.9)) and the trivial relation

$$\theta = \theta_W \, (1 + l_a/l_d)^{-1}, \tag{3.10}$$

where $\theta_W = \omega \, W/v$, the ratio l_a/l_d and θ can be found [35]) if W and v are known. The width of the depletion layer was always calculated from the breakdown voltage and the manufacturing data of the diode, assuming a constant impurity distribution in the epitaxial layer. It was also assumed that the depletion layer was never restricted by the substrate on which the epitaxial layer was grown. In the case of the diodes investigated experimentally this assumption was verified by means of C–V measurements. In the calculations (see sec. 3.1.5) the saturated drift velocity v, also needed to calculated θ_W, was taken from table 3-I, i.e. from the literature. We shall come back to this particular choice of W and v at the end of this section.

TABLE 3-I

Table of constants used in the calculations

semi-conductor	m	α		β		v_n (m/s)	v_p (m/s)
		a (m^{-1})	b (V/m)	a (m^{-1})	b (V/m)		
Si	1	$2{\cdot}40 \, . \, 10^8$	$1{\cdot}60 \, . \, 10^8$	$1{\cdot}80 \, . \, 10^9$	$3{\cdot}20 \, . \, 10^8$	$1{\cdot}05 \, . \, 10^5$	$0{\cdot}96 \, . \, 10^5$
Ge	1	$1{\cdot}55 \, . \, 10^9$	$1{\cdot}56 \, . \, 10^8$	$1{\cdot}00 \, . \, 10^9$	$1{\cdot}28 \, . \, 10^8$	$0{\cdot}6 \, . \, 10^5$	$0{\cdot}6 \, . \, 10^5$
GaAs	2	$3{\cdot}50 \, . \, 10^7$	$6{\cdot}85 \, . \, 10^7$	$3{\cdot}50 \, . \, 10^7$	$6{\cdot}85 \, . \, 10^7$	$0{\cdot}9 \, . \, 10^5$	$0{\cdot}6 \, . \, 10^5$

Since we now know the values of W, l_a, l_d and θ, the transit-time function Φ is also known. Using the experimental value of X_0, the values of C_a and C_d can be calculated. The quantity $\bar{\alpha}'/\tau_i C_a$, which together with the bias current determines the avalanche frequency ω_{a1} (eq. (3.4)), can be found from the graph $R_1(I_{c0})$ or from the graph $X_1(I_{c0})$, using the following relations:

$$\left(\frac{\partial R_1}{\partial I_{c0}}\right)_{I_{c0}=0} = \left(\frac{\bar{\alpha}'}{\tau_i\, C_a}\right)\frac{\operatorname{Im}\Phi}{\omega^3\, C_d} \tag{3.11}$$

or

$$\left(\frac{\partial X_1}{\partial I_{c0}}\right)_{I_{c0}=0} = -\left(\frac{\bar{\alpha}'}{\tau_i\, C_a}\right)\frac{\operatorname{Re}\Phi}{\omega^3\, C_d}. \tag{3.12}$$

These relations are found after differentiation of the real and imaginary parts of eq. (3.8) with respect to the bias current.

Using the tan φ method, we thus determined all the diode quantities needed to calculate the diode impedance. It should be noted that this method does not provide for a value of $\bar{\alpha}'$ or τ_i. Only the ratio of these two quantities is known at this point of our investigation. In chapter 4 it will be shown that τ_i can be determined from microwave noise measurements on the non-oscillating diode; $\bar{\alpha}'$ can then be calculated from $\bar{\alpha}'/\tau_i$.

In the foregoing the value of W was calculated and that of v was taken from the literature. This might strike the reader as strange since the available impedance data can be arranged so that it is possible to determine θ and l_a/l_d (and hence Φ, C_a and C_d) from these data without making assumptions for W and v. It follows from eqs (3.4) and (3.8) that

$$(R_1 - R_s)^{-1} = \chi - \frac{\chi\, \omega^2\, \tau_i\, C_a}{\bar{\alpha}'}\,(I_{c0})^{-1}, \tag{3.13}$$

where $\chi = -\omega\, C_d/\operatorname{Im}\Phi$. From eqs (3.9) and (3.13) it then follows that

$$1 - \frac{\sin\theta}{\theta} + (\tan\varphi + \chi X_0)\left(\frac{1-\cos\theta}{\theta}\right) = 0, \tag{3.14}$$

and θ can be found from this relation if tan φ, X_0 and χ are known. The quantities tan φ and X_0 are determined as described before. The quantity χ follows from the graph $(R_1 - R_s)^{-1}$ as a function of ${I_{c0}}^{-1}$; χ can only be determined accurately when χ and the other terms in eq. (3.13) are of the same order of magnitude. This condition is satisfied for rather high values of I_{c0}. However, we then find that the diode model adopted is inadequate to describe the impedance data correctly. At these high bias currents the imaginary part of Z_1 is no longer proportional to the real part of Z_1. Moreover, eq. (3.14) cannot solve all our problems since to find the length of the drift region it is in any case necessary to make assumptions, either about v (l_d from θ) or about the actual junction area (l_d from C_d). Because of all these arguments we decided to calculate the value of W and to take the value of v from the literature.

3.1.3. *Experimental results*

With a view to studying the intrinsic response time in particular (chapter 4), we measured and analysed the small-signal impedance data of several diode structures: Si p^+–n, Si n^+–p, n-Si Schottky-barrier, Ge n^+–p and n-GaAs Schottky-barrier diodes. The results relevant to the measurements and analysis are summarised in table 3-II. All diodes are of the mesa type. In diodes 1–8 and diodes 10–12 the junction was formed by diffusion (diffusion depth about 1·5 μm) into an epitaxial layer on a good-conducting substrate. Diodes 1 and 2 were fabricated from the same slice of epitaxial material, as were diodes 7 and 8, and diodes 11 and 12. Diodes 9, 13 and 14 were of the Schottky-barrier type [39]). The metal used for diode 9 was palladium, while titanium was used for diodes 13 and 14.

TABLE 3-II

Diode quantities as determined from the measured impedance data; V_{BR} is the breakdown voltage of the diode

diode no.	material/ type	V_{BR} (V)	W (μm)	X_0 (Ω)	tan φ	θ (rad)	l_a/W	$\bar{\alpha}'/\tau_i\ C_a$ ($A^{-1}\ s^{-1}$)
1	Si p^+–n	65	3·0	46	2·8	1·14	0·38	46 . 10^{21}
2	Si p^+–n	66	3·1	36	2·7	1·16	0·37	31 . 10^{21}
3	Si p^+–n	68	3·2	48	3·3	1·05	0·43	48 . 10^{21}
4	Si p^+–n	100	5·3	47	1·9	1·83	0·42	22 . 10^{21}
5	Si n^+–p	70	3·3	22	1·1	1·82	0·18	23 . 10^{21}
6	Si n^+–p	110	5·8	34	0·8	2·68	0·28	16 . 10^{21}
7	Si n^+–p	111	5·8	43	1·0	2·55	0·33	18 . 10^{21}
8	Si n^+–p	111	5·8	41	1·0	2·55	0·33	19 . 10^{21}
9	n-Si S.B.	70	3·5	70	1·9	1·44	0·31	51 . 10^{21}
10	Ge n^+–p	32	2·6	30	1·6	1·82	0·34	36 . 10^{21}
11	Ge n^+–p	33	2·8	29	1·3	1·99	0·31	23 . 10^{21}
12	Ge n^+–p	33	2·8	25	1·4	1·93	0·33	21 . 10^{21}
13	n-GaAs S.B.	55	2·5	20	2·2	1·33	0·33	16 . 10^{21}
14	n-GaAs S.B.	50	2·2	31	2·0	1·22	0·23	25 . 10^{21}

The measuring frequency was 10 GHz for all diodes. The impedance data were obtained as described in sec. 3.1.1 and the data were analysed using the tan φ method. From the eighth column of table 3-II we find that the ratio l_a/W is $\approx 0{\cdot}4$, $0{\cdot}3$, $0{\cdot}3$ and $0{\cdot}3$ for the Si p^+–n, Si n^+–p, Ge n^+–p and n-GaAs Schottky-barrier diodes, respectively. Except for the Si n^+–p diodes these ratios agree fairly well with computer calculations of the diodes (see sec. 3.1.5). It can be shown that better agreement between theory and experiment can be obtained by taking the effect of diffusion of the free carriers in the depletion layer and the actual doping profile, and hence the actual field profile, into account [40]). Diffusion effects require a diode model whose large-signal and oscillator-noise behaviour in particular can hardly be traced analytically. However, for the diodes investigated on oscillator noise (chapter 6), it was found that neglecting the effects of carrier diffusion in the theory had no serious consequences. We therefore ignored these effects in our theoretical studies.

3.1.4. *Extension of the diode model*

To obtain some insight into the relevance of the data derived in the preceding section, we extend the diode model.

In sec. 3.1.2 we concluded that for the diode model used (sec. 2.4) the circuit representation of the avalanche region is a simple L_a C_a parallel circuit. From more-detailed studies it has been concluded that this circuit has to be extended when the model of the avalanche region is refined. We recall some of the major results of these studies without discussion:

(a) A resistance in series with the inductance L_a has to be added to account for the differential static resistance of the avalanche region and for transit-time effects on the conduction current in that region [41,42]). This differential resistance is, generally, negative and independent of the frequency ω. The effect of the transit time is generally also negative and is proportional to ω^2 [42]).

(b) A parallel resistance has to be added to the circuit to account for the carrier-induced displacement current [33,36]), which results from the fact that $\partial J_c/\partial x \neq 0$. The parallel resistance can be transformed into a resistance in series with L_a. This resistance is then proportional to ω^2. The effect of this displacement current may be positive or negative [33]).

(c) If the saturation current is taken into account, the d.c. current multiplication factor $M_0 = I_{c0}/I_s$ is no longer infinitely high. A finite M_0 can be represented by a series resistance of L_a. The value of this resistance is equal to $1/M_0\, \overline{\alpha}'\, I_{c0}$ [41]).

We now assume that all effects found from more-detailed studies of the avalanche-region properties may be represented by a resistance R_a in series with the inductance L_a [35]) (fig. 3.5):

$$R_a = R + S\,\omega^2,$$

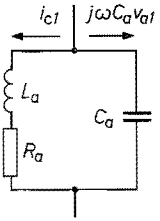

Fig. 3.5. Extended small-signal circuit representation of the avalanche region.

where R and S are independent of frequency. With this extended description of the avalanche region the expression for the diode impedance remains valid, provided we replace the avalanche frequency ω_{a1} by the complex avalanche frequency $\bar{\omega}_{a1}$ defined by

$$\bar{\omega}_{a1}^{\,2} = \omega_{a1}^{\,2}/(1 - j\sigma), \tag{3.15}$$

where $\sigma = r/\omega + s\,\omega$,
$r = R/L_a$,
$s = S/L_a$.

The equivalent expression for tan φ, eq. (2.9), is now given by

$$\tan \varphi = -\frac{\mathrm{Re}\,\Phi - h\,\mathrm{Im}\,\Phi}{\mathrm{Im}\,\Phi + h\,\mathrm{Re}\,\Phi}, \tag{3.16}$$

where

$$h = \sigma/(1 - \omega_{a1}^{\,2}/\omega^2). \tag{3.17}$$

From the foregoing discussion we expect σ to depend on the bias current. On the other hand it was found experimentally (fig. 3.3) that $(X_1 - X_0)/(R_1 - R_s)$ is a constant when the impedance is measured at a microwave frequency and at values of the bias current which are not excessively high. It can therefore be concluded that under these (experimental) conditions the terms containing h in eq. (3.16) can be neglected, since we know from the results given in table 3-II that tan φ is larger than zero. So h cannot be determined from the experimental data discussed. In principle it is possible to determine h from the small-signal impedance data of the diode measured as a function of frequency for a given value of the bias current. The value of the frequency should be varied from values well below ω_{a1} up to values well above ω_{a1}, while $\omega_{a1}/2\pi$ is of the order of magnitude of 3 GHz. These data, however, are difficult to obtain with sufficient accuracy. We therefore performed numerical calculations to obtain values of $Z_1(\omega)$, and used these values as "measuring data" in the analysis of the diode quantities in our extended analytical diode model.

In the computer calculations the drift velocity of the electrons and holes is assumed to be completely saturated throughout the depletion layer. The field dependence of the ionisation coefficient of the electrons, α, and that of the holes, β, is described by

$$\alpha, \beta = a \exp\left[-(b/E)^m\right].$$

The constants a, b and m, and the velocities v_n and v_p used in these calculations are listed in table 3-I. The static breakdown characteristics and the small-signal impedance were calculated numerically *). The latter calculations are analogous to those described by Gummel and Scharfetter [43]). Thus the continuity equations and current equations are solved directly without making the assumption that the depletion layer can be separated into an avalanche region and a drift region.

Calculations were made first for two silicon diodes: an n^+–p and a p^+–n diode, both having the same form of the impurity distribution $N(x)$:

$$N(x) = \mp 4{\cdot}7.10^{15} \pm 1{\cdot}2.10^{21} \operatorname{erfc}(1{\cdot}96.10^4\, x)\ \text{cm}^{-3}. \tag{3.18}$$

The current density J_{c0} was taken as 10^6 A/m² (= 10 mA/100² μm²) in accordance with a practical situation. Results relevant to the static behaviour of the diodes are summarised in table 3-III, where V_0 is the bias voltage and R_0 the static differential resistance (space-charge resistance) of the diode. The numerically calculated admittance as a function of frequency is represented by the dots in fig. 3.6. The continuous curves in this figure are calculated from the extended analytical diode model (in which a separation into an avalanche region and a drift region is assumed), after least-squares adjustment of the parameters r, s, $f_{a1} = \omega_{a1}/2\pi$, and l_d, using the dots in fig. 3.6 as "measuring points". The length W needed for this adjustment was taken from table 3-III. The results for the adjusted parameters are given in the left-hand section of table 3-IV. As shown in fig. 3.6, the analytical expression, viz. eq. (3.8) with the avalanche frequency ω_{a1} replaced by the complex avalanche frequency $\overline{\omega}_{a1}$ given by eq.

TABLE 3-III

Numerically calculated quantities relevant to the static behaviour of the two diodes of eq. (3.18). Current density 10^6 A/m²; junction area 10^{-8} m²

	n^+–p	p^+–n
V_0 (V)	109	103
W (μm)	5·66	5·50
R_0 (Ω)	102	48

---

*) The computer program was made by J. de Groot and H. Knoop of our laboratory.

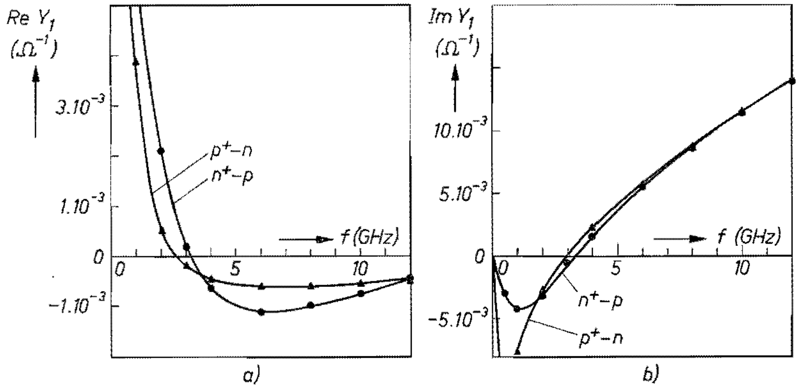

a) b)

Fig. 3.6. Small-signal admittance as a function of frequency for the two diodes of eq. (3.18). The marks (triangles: p^+–n, dots: n^+–p) refer to numerical calculations. The drawn curves were calculated from eq. (3.8), with $\omega_{a1} = \overline{\omega}_{a1}$ given by eq. (3.15), after least-squares adjustment to the numerically calculated points. Junction area 10^{-8} m^2; d.c. current 10^{-2} A; $R_s = 0$.
(*a*) Real part admittance; (*b*) imaginary part admittance.

TABLE 3-IV

Diode quantities relevant to the diode impedance as determined from the numerically calculated impedance data of the two diodes of eq. (3.18). Current density 10^6 A/m^2; junction area 10^{-8} m^2; (a) by the least-squares method; (b) by the tan φ approximation

	(a) least-squares		(b) tan φ approx.	
	n^+–p	p^+–n	n^+–p	p^+–n
r (s^{-1})	–0·4.10^9	–0·2.10^9	—	—
s (s)	–0·8.10^{-12}	–2·1.10^{-12}	—	—
f_a (GHz)	3·3	3·0	—	—
f_a (GHz) from eq. (3.11)	—	—	3·5	3·2
f_a (GHz) from eq. (3.12)	—	—	3·4	3·1
l_a (μm)	4·6	3·4	4·5	3·6
l_a/W	0·82	0·61	0·79	0·65
θ (rad), (f = 10 GHz)	3·03	2·01	2·95	2·15

(3.15), gives an excellent description of the numerically calculated points over a large range of frequencies. The assumption that all extensions of the model for the avalanche region can be combined into the series resistance $R_a = R + S\,\omega^2$ therefore also seems to be correct.

Secondly, calculations were made of the small-signal impedance for the same two diodes at a fixed frequency (10 GHz) as a function of the bias current. The results of these calculations are presented in fig. 3.7. From this figure it can be observed that a linear relationship exists between the real and imaginary parts of the impedance, as was found for the experimental data (sec. 3.1.1). Thus the influence of h on tan φ, eq. (3.16), is once again negligible. From eq. (3.17) it follows that $h \ll 1$ if $\sigma \ll 1$ and if, at the same moment, $\omega_{a1}{}^2/\omega^2 \ll 1$. Using the figures given in the left-hand section of table 3-IV it is found that $h = 0{\cdot}06$ and $0{\cdot}14$ for the n^+–p and p^+–n diode, respectively. It is therefore reasonable to state that for values of the bias current which are not too high, and for X-band frequencies, we may reduce eq. (3.16) to eq. (3.9) used in the tan φ method. When the latter method was used for the analysis of the computer data given in fig. 3.7, the figures in the right-hand section of table 3-IV were found. These figures show good agreement with the results obtained by the least-squares method using the extended analytical diode model. As mentioned before, the tan φ method gives us no information about r and s, and therefore none about h.

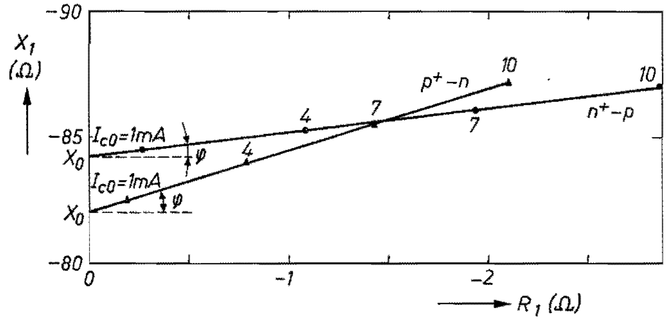

Fig. 3.7. Numerically calculated small-signal impedance as a function of the bias current for the two diodes of eq. (3.18). Junction area 10^{-8} m^2; frequency 10 GHz; $R_s = 0$. The angle φ, eq. (3.16), is indicated.

Thirdly, calculations *) were made for a silicon n^+–p diode as a function of frequency and the bias current, in order to obtain some insight in the current dependence of r, s, f_{a1}, W and l_a. The impurity distribution of this diode is given by

$$N(x) = 7{\cdot}5.10^{15} - 1{\cdot}2.10^{20}\ \mathrm{erfc}\,(2.10^4\,x)\ \mathrm{cm}^{-3}. \qquad (3.19)$$

---

*) In these calculations v_p(Si) was taken as $0{\cdot}75.10^5$ m/s, instead of $0{\cdot}96.10^5$ ms, which was used in all other calculations.

The results of the analysis of these data, using the least-squares adjustment to the extended, analytical expression of $Z_1(\omega)$, for several values of I_{c0}, are given in fig. 3.8. We conclude that $f_{a1}{}^2$ is indeed proportional to I_{c0} (see eq. (3.4)) and furthermore that the length of the depletion layer and that of the drift region increase slightly with increasing bias current, as is to be expected. The quantity s does not depend very markedly on I_{c0}, whereas the dependence of r on I_{c0} is more pronounced as will be shown in sec. 3.1.5. From fig. 3.8 it can be concluded that, at least for this diode, $\sigma = r/\omega + s\,\omega$ increases with increasing bias current.

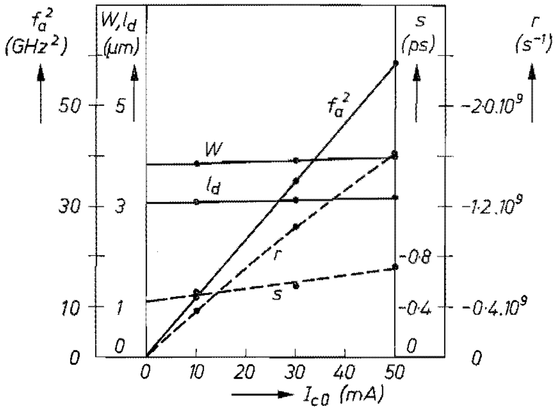

Fig. 3.8. Diode quantities for the diode of eq. (3.19) as a function of the bias current. The quantities were found after least-squares adjustment of eq. (3.8), with $\omega_{a1} = \overline{\omega}_{a1}$ given by eq. (3.15), to the numerically calculated small-signal impedance over a frequency range 0–12 GHz.

The ratio $\overline{\alpha}'/\tau_i$ can be determined from the data given in tables 3-III and 3-IV. For the known value of l_a the average electric field in the avalanche region can be found using the breakdown condition (eq. (2.5)). The value of $\overline{\alpha}'$ can then be calculated from eq. (2.22), so that τ_i is known. Using the figures given in the left-hand section of table 3-IV we thus find for the two diodes of eq. (3.18):

$$\text{Si } n^+\text{–}p,\ l_a = 1{\cdot}0\ \mu\text{m}: \quad \tau_i = 4{\cdot}3\ \text{ps},$$

$$\text{Si } p^+\text{–}n,\ l_a = 2{\cdot}1\ \mu\text{m}: \quad \tau_i = 6{\cdot}5\ \text{ps}.$$

The intrinsic response time τ_i will be discussed further in chapter 4. The above data are also presented in fig. 4.5.

3.1.5. *Discussion*

(1) The first assumption listed in the summary of assumptions in sec. 2.4 was that the depletion layer can be divided into an avalanche region and a drift region. From fig. 3.6 it can be concluded that the analytical model in which this division was made, accurately describes the numerical data, in the calculation

of which the division was not made. The first assumption in sec. 2.4 therefore seems to be appropriate, at least for the small-signal case.

(2) The second assumption made in sec. 2.4, resulting in the simple Read equation (2.27), placed fairly tight restrictions on the model of the avalanche region. However, comparing the data in the left-hand section of table 3-IV to those in its right-hand section, we draw the conclusion that if $\omega_{a1} < \omega$ and the value of the bias current is not too high, this second assumption is also appropriate. This conclusion is supported by the experimental data shown in fig. 3.3, which indicate that a current range exists in which X_1 depends linearly on R_1 as is demanded by the simple analytical model.

(3) The third assumption in sec. 2.4 states that we consider the diode to have only one drift region. Figure 3.9 gives the carrier-generation function for the two diodes of eq. (3.18), resulting from the numerical calculations of the static-behaviour characteristics. This generation function is defined as the absolute value of the space derivative of the normalised electron current density $|J_n/J_{c0}|$. The junction field strength is also shown and, drawn on this scale, is about the same for the two diodes. The relative length of the drift region as found by the least-squares method is also indicated. For the n^+–p diode it is then found by integration of the generation function that 96% of the carrier generation takes place outside the drift region, while the corresponding figure

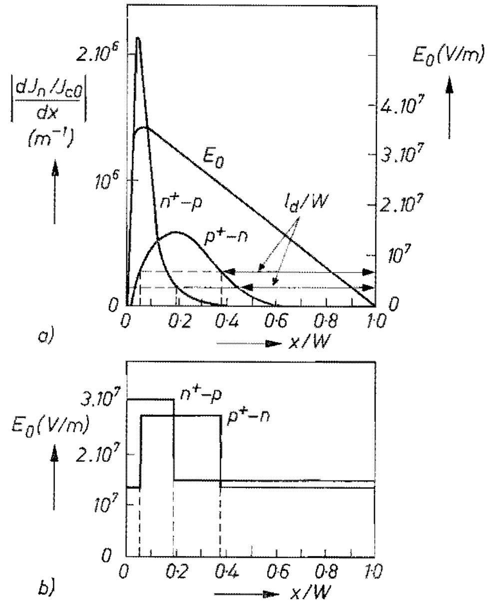

Fig. 3.9. (*a*) Electric-field distribution and carrier-generation function for the two diodes of eq. (3.18), as found from numerical calculations. The ratio l_d/W, as found from the least-squares adjustment (table 3-IV) is indicated for both diodes. (*b*) Equivalent field distribution.

for the p^+–n diode is found to be 90%. The generation function of the latter diode suggests, however, that a second drift region has to be taken into account on its left-hand side. Assuming somewhat arbitrarily that the generation function has the same value at the two boundaries of the avalanche region (as indicated by the dashed line in fig. 3.9), a relative thickness of 0·05 of the left-hand drift region is found. Then 89% of the generation takes place outside the two drift regions.

In the case of two drift regions eq. (3.9) has to be modified and becomes

$$\tan \varphi = \frac{(l_a + l_{d2})/l_{d1} + (\sin \theta_1)/\theta_1}{(1 - \cos \theta_1)/\theta_1}, \tag{3.20}$$

where the subscript 1 stands for the larger of the two drift regions and the subscript 2 for the other. When deriving eq. (3.20) it was assumed that

$$\frac{l_{d2}}{l_{d1}} \frac{1 - \cos \theta_2}{\theta_2} \ll \frac{1 - \cos \theta_1}{\theta_1}$$

and

$$(\sin \theta_2)/\theta_2 \approx 1.$$

Thus, if eq. (3.9) is used, it follows from eq. (3.20) that if $l_{d2} \ll l_{d1}$ the transit angle of the largest drift region is found, while the length of the avalanche region might be too large by an unknown amount l_{d2}.

With the assumptions made so far, together with the results obtained in sec. 3.1.4, the field profile given in fig. 3.9*a* can be reduced to those for the n^+–p and p^+–n diodes as shown in fig. 3.9*b*.

When the least-squares adjustment method, discussed in the preceding section, was extended to include a second drift region, again a relative thickness of $\approx$ 0·05 for this region was found in case of the p^+–n diode. The other diode quantities obviously change slightly in this process. However, none of the conclusions concerning h or σ is modified. In the remainder of our studies the possible effect of a second drift region is therefore neglected.

The saturation current I_s was neglected in all derivations and numerical examples. If I_s is taken into account $M_0 = I_{c0}/I_s < \infty$, while M_0 contributes to σ by an amount $1/\omega M_0 \tau_i$. At relevant values of the bias current M_0 is about 10^7. The intrinsic response time is about 5 ps, so that at microwave frequencies, say $\omega = 2\pi \,.\, 10^{10}\ \mathrm{s}^{-1}$, the contribution to σ is about $3 \,.\, 10^{-7}$ and hence negligible. At low frequencies and low bias currents a significant contribution of M_0 to σ is possible. That, however, is irrelevant to the present study.

Low-frequency measurements are found to be not very suitable for the determination of diode quantities. This can be illustrated as follows. From eqs (3.8) and (3.15) it can be calculated that

$$\lim_{\omega \to 0} Z_1 = R_s + \frac{l_a^2}{2\,\varepsilon\, v\, A} + \frac{r}{\omega_{a1}{}^2\, C_0} \equiv R_0. \tag{3.21}$$

The second term on the right-hand side of this equation is the well-known expression for the space-charge resistance of the drift region. The third term arises from the space-charge resistance of the avalanche region. It is found from experiments and from numerical calculations that, as a first-order approximation, R_0 is a constant at not too high values of the bias current. Hence r varies as a first-order approximation in the same way with I_{c0} as $\omega_{a1}{}^2$ does (see also fig. 3.7). The influence of $r/\omega_{a1}{}^2 C_0$ therefore cannot be eliminated by measuring R_0 at various values of I_{c0}. From the data given in tables 3-III and 3-IV it is found that for the two diodes of eq. (3.18) $r/\omega_{a1}{}^2 C_0$ is 5% and 6% of R_0 for the n^+–p and p^+–n diode, respectively. In an analysis[35]) similar to that performed in sec. 3.1.4 the present author has found values of 2% and 27% of R_0 to be possible for $r/\omega_{a1}{}^2 C_0$. Furthermore, the measured value of R_0 can be influenced by temperature effects (sec. 3.2.5). We therefore conclude that relatively large errors may be made when l_a is determined from R_0 without taking the space-charge resistance of the avalanche region into account.

3.2. Large-signal theory

When studying the noise properties of the oscillating diode it is important to know the behaviour of quasi-stationary quantities such as the large-signal impedance of the diode, and the signal level of the oscillations. Furthermore, it is very important to know the range of signal levels for which the large-signal theory used is valid.

The large-signal impedance is calculated in sec. 3.2.1. This is followed by a discussion of the oscillation condition in sec. 3.2.2. From this discussion we shall learn that, if the external circuit is fixed, both the oscillation frequency and the avalanche frequency in the model used are constants. In sec. 3.2.3 the range of validity of the noise-free large-signal model used is determined from simple output-power versus bias-current measurements.

Section 3.2.4 discusses the microwave impedance measurements. From the measuring data it is possible to determine the large-signal impedance of the diode, the circuit loss resistance, and the effective load resistance of the oscillator.

Finally, in sec. 3.2.5, the theory is extended to include the effect of the second-order field derivative of the ionisation coefficient, $\overline{\alpha}''$. By including $\overline{\alpha}''$ it should be possible to explain the rectification effects of the r.f. signal, the so-called "d.c. restorage". The experiments, however, are found not to confirm this; $\overline{\alpha}''$

is therefore left out of the theoretical description, except when in sec. 5.4.3 the "down-conversion" of oscillator noise is discussed.

3.2.1. *Large-signal impedance*

The large-signal impedance is calculated starting from the assumptions concerning the diode model summarised in sec. 2.4. We furthermore assume the diode to be placed in a singly tuned, low-Q circuit which at a fixed frequency may be described as shown in fig. 3.10. In this circuit we disregard the build-up of harmonic voltages and in our calculations we consider the fundamental harmonic of the a.c. current only. The bias current is assumed to be supplied from a constant current source.

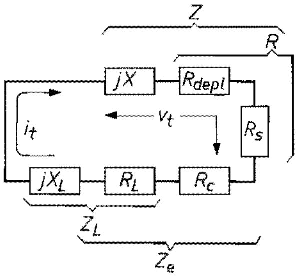

Fig. 3.10 Block diagram of the oscillating loop and definition of the impedances, see text.

The large-signal diode impedance is $Z = R + jX$. Its real part R is considered to consist of the resistance of the active part of the diode R_{depl}, and of a loss resistance R_s (see fig. 3.10). The circuit is represented by a loss resistance R_c and a load impedance $Z_L = R_L + jX_L$. Seen from the diode the external impedance is $Z_e = R_c + Z_L$. The r.f. current in the loop is i_t, the r.f. voltage across the diode v_t.

Let the voltage across the avalanche region be $V_a = V_{a0} + v_a \sin \omega t$, V_{a0} being the d.c. part and $v_a \sin \omega t$ the a.c. part, with v_a a real number. Integration of the Read equation (2.27) then yields

$$I_c = I_{00} \exp\left(\frac{\bar{\alpha}'}{\omega\,\tau_i}\, v_a\,(1 - \cos \omega t)\right), \tag{3.22}$$

where I_{00} is an integration constant. From this equation it follows that the fundamental harmonic i_c of I_c is given by [42,44])

$$i_c = -2\, I_{c0}\, \frac{I_1(\gamma v_a)}{I_0\,(\gamma v_a)} \cos \omega t, \qquad \gamma = \frac{\bar{\alpha}'}{\omega \tau_i}. \tag{3.23}$$

In the derivation of eq. (3.23) from eq. (3.22) use was made of the Fourier series [45])

$$\exp(-x\cos\omega t) = \sum_{\nu=-\infty}^{\infty} (-1)^{\nu} I_{\nu}(x) \exp(j\,\nu\,\omega\,t),$$

where $I_{\nu}(x)$ is the modified Bessel function of the first kind, with order ν and argument x. The time-independent factor in eq. (3.22) was removed by the requirement that the conduction current averaged over one period of ω be equal to the bias current I_{c0}, the latter being supplied from a constant current source. Equation (3.23) indicates that i_c lags 90° behind v_a. In fig. 3.12 in sec. 3.2.3 the ratio $I_1(\gamma v_a)/I_0(\gamma v_a)$ is represented by the drawn curve.

As in the small-signal case, v_a also excites a displacement current, given by $j\,\omega\,C_a\,v_a$. Addition of this current to the conduction current gives the total a.c. current i_t:

$$i_t = i_c + j\,\omega\,C_a\,v_a = j\,\omega\,C_a\,v_a\left(1-\frac{\omega_a^2}{\omega^2}\right) = i_c\left(1-\frac{\omega^2}{\omega_a^2}\right), \tag{3.24}$$

where the avalanche frequency ω_a is defined by

$$\frac{\omega_a^2}{\omega_{a1}^2} = \frac{2}{\gamma\,v_a}\,\frac{I_1(\gamma v_a)}{I_0(\gamma v_a)}, \tag{3.25}$$

ω_{a1}^2 being defined by eq. (3.4).

To find the total impedance of the diode we can proceed as in the small-signal case (sec. 3.1.1), since all further operations are linear operations. The same expression is found for this impedance as in the small-signal case, provided we replace the small-signal avalanche frequency in eq. (3.8) by the large-signal avalanche frequency defined by eq. (3.25). Hence Z is given by

$$Z = R_s + \frac{1}{j\,\omega\,C_0} - \frac{\Phi}{j\,\omega\,C_d}\,\frac{1}{1-\omega^2/\omega_a^2}. \tag{3.26}$$

It should be noted that in this expression ω_a is the only parameter that depends on the bias current and the signal level. We make use of this in a discussion of the oscillation condition below.

3.2.2. *Oscillation condition* [46])

For stable oscillation the oscillator loop must satisfy the condition that the total loop impedance vanishes at the oscillation frequency (ω_0). Using the impedance definitions given in fig. 3.10, this condition implies that

$$R_s + R_{\mathrm{depl}} + jX + Z_e = 0, \tag{3.27}$$

where $R_{\mathrm{depl}} + R_s = \mathrm{Re}\, Z$ and $X = \mathrm{Im}\, Z$. After substitution of eq. (3.26), this condition can be written

$$\frac{\omega_0^2}{\omega_a^2} = \frac{(1 - \Phi_d)/j\, \omega_0\, C_d + R_s + Z_e}{1/j\, \omega_0\, C_0 + R_s + Z_e} \equiv g(\omega_0). \tag{3.28}$$

For a given diode, i.e. for a given fixed set of geometrical diode quantities $\{l_a, l_d, A\}$, and a given fixed external circuit, the right-hand side of eq. (3.28) is a function of ω_0 only. This function is indicated by $g(\omega_0)$. Because the avalanche frequency ω_a defined in eq. (3.25) is a real quantity, the oscillation condition eq. (3.28) can now be expressed by the identities

$$\mathrm{Re}\, g(\omega_0) = \omega_0^2/\omega_a^2, \tag{3.29a}$$

$$\mathrm{Im}\, g(\omega_0) = 0. \tag{3.29b}$$

We observe that the oscillation frequency ω_0 is fully determined by eq. (3.29b) and is influenced neither by the a.c. voltage nor by the bias current, since $g(\omega_0)$ does not depend (in our model) on I_{c0} and v_a. Consequently, it follows from eq. (3.29a) that the avalanche frequency is a constant, too, and thus $\omega_a = \omega_{a,\mathrm{st}}$, where $\omega_{a,\mathrm{st}}$ is the small-signal avalanche frequency at the start of the oscillations (note that we assumed the external circuit to be fixed). Using eq. (3.4), eq. (3.25) can be written

$$\frac{\omega_a^2}{\omega_{a1}^2} = \frac{\omega_{a,\mathrm{st}}^2}{\omega_{a1}^2} = \frac{I_{\mathrm{st}}}{I_{c0}} = \frac{2}{\gamma\, v_a}\, \frac{I_1(\gamma v_a)}{I_0(\gamma v_a)}, \tag{3.30}$$

where I_{st} is the bias current at the start of the oscillations. We observe from this equation that if the bias current I_{c0} is varied the a.c. voltage v_a must vary in such a way that the avalanche frequency ω_a remains a constant equal to $\omega_{a,\mathrm{st}}$. The value of I_{st} follows, for example, from the real part of eq. (3.27):

$$R_L + R_s + R_c - \frac{\mathrm{Im}\, \Phi}{\omega_0\, C_d\, (1 - \omega_0^2/\omega_a^2)} = 0. \tag{3.31}$$

In the actual circuit I_{st} can be measured, and eq. (3.30) can be used to determine that value of $\gamma\, v_a$ for a given value of I_{c0} (fig. 3.11).

It should be emphasised that the above discussion is only valid if the shift of the oscillation frequency caused by varying I_{c0}, as is found in practice, has a negligible effect on the circuit impedance. For a discussion of the current dependence of ω_0 see the next section.

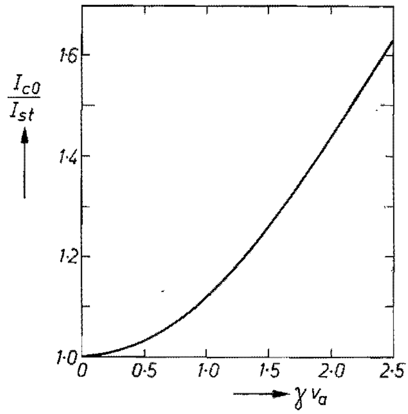

Fig. 3.11. The ratio of the bias current, I_{c0}, to the bias current at the start of the oscillations, I_{st}, as a function of γv_a, the normalised voltage across the avalanche region.

3.2.3. *Range of validity of the noise-free large-signal model (RVM)*

The range of validity of the noise-free large-signal diode model can easily be determined from output-power measurements using the results derived in secs 3.2.1 and 3.2.2. Throughout the remainder of our studies this range will be indicated by RVM, and it should be emphasised that the RVM only pronounces on the range of validity of the *noise-free* large-signal diode model.

The tuning procedure of the circuit will be described in sec. 3.2.4. After this tuning the circuit remains fixed and the only adjustable parameter left is the bias current. This current determines the value of the a.c. voltage v_a across the avalanche region in conformity with eq. (3.30), and consequently also the output power P_L dissipated in the load resistance R_L. After substitution of eq. (3.24) in the expression $P_L = \frac{1}{2}\,|i_t|^2\,R_L$ it follows that

$$P_L = [\tfrac{1}{2}\,\omega_0^2\,C_a^2\,(1 - \omega_{a,\mathrm{st}}^2/\omega_0^2)^2\,R_L]\,v_a^2 \equiv K\,v_a^2, \tag{3.32}$$

where K replaces the factor between square brackets. The factor K is a constant within the RVM because both ω_0 and $\omega_a = \omega_{a,\mathrm{st}}$ are constant. Hence the relative variation of P_L is

$$\frac{\delta P_L}{P_L} = 2\,\frac{\delta v_a}{v_a} + \left(\frac{\delta v_a}{v_a}\right)^2. \tag{3.33}$$

Differentiation of eq. (3.30) yields the relation

$$\frac{\delta I_{c0}}{I_{c0}} = [1 - D(\gamma v_a)]\,\frac{\delta v_a}{v_a}, \tag{3.34}$$

where

$$D(\gamma v_a) = \frac{\mathrm{d}}{\mathrm{d}\gamma v_a}\left(\frac{I_1(\gamma v_a)}{I_0(\gamma v_a)}\right)\frac{\gamma v_a}{I_1(\gamma v_a)/I_0(\gamma v_a)} =$$

$$= \gamma v_a\left(\frac{I_0(\gamma v_a)}{I_1(\gamma v_a)} - \frac{I_1(\gamma v_a)}{I_0(\gamma v_a)}\right) - 1. \tag{3.35}$$

We note that eq. (3.35) represents the ratio of the slopes of the tangent to the chord of the function $I_1(\gamma v_a)/I_0(\gamma v_a)$ which is represented by the drawn curve in fig. 3.12. The dashed curve in this figure represents the function $[1-D(\gamma v_a)]^{-1}$.

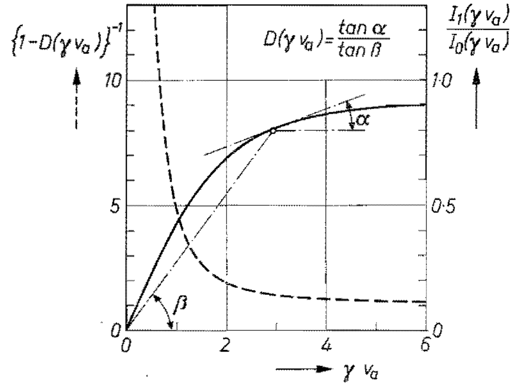

Fig. 3.12. The function $I_1(\gamma v_a)/I_0(\gamma v_a)$ (drawn curve) from which $D(\gamma v_a)$ can be determined, and the function $[1-D(\gamma v_a)]^{-1}$ (dashed curve), which relates the output-power variations to the bias-current variations.

If we apply an artificial variation in I_{c0}, small enough for the second term on the right-hand side of eq. (3.33) to be negligible, we find

$$\frac{2}{1-D(\gamma v_a)} = \frac{\delta P_L/\delta I_{c0}}{P_L/I_{c0}}, \tag{3.36}$$

and hence the function $D(\gamma v_a)$ can be determined from the $P_L(I_{c0})$ characteristics as γv_a follows from eq. (3.30), i.e. from the ratio I_{st}/I_{c0}. Figure 3.13*a* gives an example of the measured $D(\gamma v_a)$ compared with the theoretical $D(\gamma v_a)$ for an Si n^+–p diode and an *n*-GaAs Schottky-barrier diode (see also chapter 5, table 5-I). In these two examples the diodes have an RVM up to $\gamma v_a \approx 1{\cdot}8$ and $\gamma v_a \approx 2{\cdot}2$, respectively. It should be noted that to determine the RVM it is sufficient to know the $P_L(I_{c0})$ characteristic only. Neither the diode impedance nor the circuit impedance need therefore be known.

In sec. 3.2.4 it will be shown that it is possible to establish the value of the effective load resistance R_L and the value of the total a.c. voltage v_t across the diode. If we define the modulation depth m by

$$m = v_t/V_{\mathrm{BR}} \tag{3.37}$$

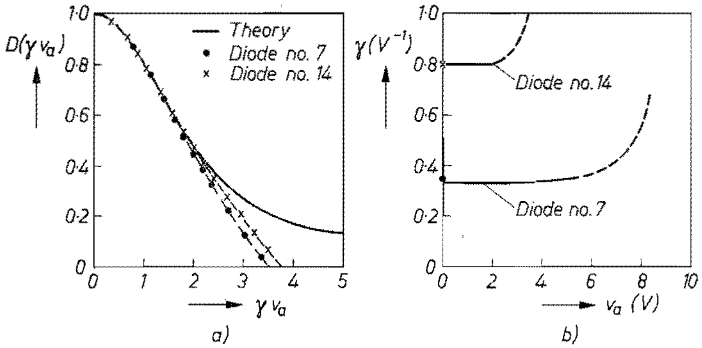

Fig. 3.13. (*a*) Experimental values of $D(\gamma v_a)$ derived from the $P_L(I_{c0})$ characteristics for a Si n^+–p diode (dots) and an n-GaAs Schottky-barrier diode (crosses). Oscillation frequency 9 GHz. The drawn curve represents the theoretical values of $D(\gamma v_a)$. (*b*) γ as a function of v_a for the same diodes, and under the same experimental conditions as under (*a*). The values $\gamma(0)$ derived from the quantities given in table 3-II are indicated. The range in which γ is a constant determines the RVM.

where V_{BR} is the breakdown voltage of the diode, we find an RVM up to $m_{max} \approx$ 0·12 and $m_{max} \approx 0{\cdot}22$ for the silicon and the gallium-arsenide diode of fig. 3.13, respectively, while the optimum modulation depth for these diodes is m_{opt}(Si) $\approx$ 0·37 and m_{opt}(GaAs) $\approx$ 0·50. The optimum modulation depth, as defined by Van Iperen and Tjassens [38,47]), is the modulation depth corresponding to the maximum output power for a given value of the bias current when the load resistance is varied. The optimum modulation depth is found to be nearly independent of the bias current. As shown by Van Iperen and Tjassens [38,47]), and as also follows from our large-signal impedance measurements, the maximum attainable modulation depth is slightly higher. Thus we find that our large-signal diode model describes about 40% of the possible range of modulation depths.

It might be felt that the model is useful in only a small range. However, neither an analytical nor a numerical diode model has yet been reported in the literature that describes the diode impedance over a substantially larger range of modulation depths. Moreover, as will be clear later on in our studies, the RVM covered by our model is still of interest in the study of noise in IMPATT-diode oscillators.

Since, as mentioned, R_L can be found from large-signal impedance measurements, the constant K in eq. (3.32) can be determined, as all diode quantities are known from the analysis of the small-signal impedance measurements. v_a can therefore be calculated since P_L can be read from a power meter. Thus γ can be determined as a function of v_a. The results for $\gamma(v_a)$ for the diodes of fig. 3.13*a* are given in fig. 3.13*b*. In fig. 3.13*b* the RVM is given by the range in which γ is a constant (indicated by the drawn curves), since our diode model demands for a constant γ (the RVM which can be read from fig. 3.12*a* is of course the same as the RVM which can be read from fig. 3.13*b*). Also indicated in fig. 3.13*b* is $\gamma(0)$, calculated from the small-signal data given in table 3-II. Taking into account the rather large number of independent measurements needed to arrive at fig. 3.13*b*, it is concluded that the internal consistency of the data is good (for the diodes summarised in table 5-I it was found that the two values of γ at $v_a = 0$ matched within 16%).

We next consider the shift of the oscillation frequency which is found in practice when the bias current is varied (as mentioned before, the oscillator circuit is fixed). When the bias current is varied, we observe a variation of the bias voltage. The latter means that the width of the depletion layer also varies and hence the cold capacitance C_0 of the diode. If we assume (a) that for the diodes studied $1/C_0^2 \propto V_0$, (b) that $X_L = \omega L$ where L is a constant, and (c) that the variation of the oscillation frequency is predominantly caused by the variation of C_0, it can be easily demonstrated that the fourth power of the oscillation frequency is proportional to the diode bias voltage. As shown in fig. 3.14, this relationship is satisfied very well within the RVM of the diodes.

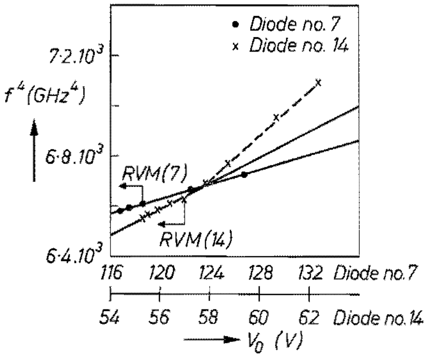

Fig. 3.14. Fourth power of the oscillation frequency as a function of the bias voltage across the oscillating diode for an Si n^+-p diode (dots) and an n-GaAs S.B. diode (crosses). The RVM is indicated for both diodes.

Furthermore, we conclude that within the RVM the total frequency shift is smaller than 1%. This was found to be so for all diodes investigated. We therefore neglected this frequency shift as far as it concerns the diode impedance and the output power for which the RVM is applicable. This frequency shift was also neglected when the intrinsic oscillator noise, chapter 6, was studied.

The diode loss resistance R_s was always taken from the small-signal impedance data at the point of breakdown, as indicated in fig. 3.3. It should, however, be emphasised that at very high r.f. signal levels and at high input levels R_s can depend to an appreciable extent on the signal level [48]) and on the temperature. Within the RVM of the diode the r.f. signal and the input level are relatively low. We therefore assumed R_s to be constant.

3.2.4. *Microwave impedance measurements*

The large-signal diode impedance, Z, and the circuit quantities such as the circuit loss resistance R_c and the load resistance R_L were measured by a method outlined by Van Iperen and Tjassens [38,47]). We shall briefly recapitulate the steps in the measuring procedure.

(a) The small-signal impedance of the diode at a fixed frequency, say 9 GHz, is measured as a function of the bias current up to a value of R_1 which is somewhat higher (to account for R_c) than the highest value of R_L to be used. In this way the small-signal impedance will be known at all values of the start oscillation current that are of interest to us.

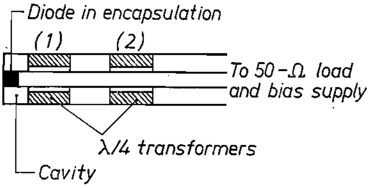

Fig. 3.15. Schematic diagram of the coaxial oscillator circuit.

(b) The diode is mounted in a coaxial oscillator circuit as sketched in fig. 3.15. The circuit is tuned in such a way that the oscillations start at the frequency at which the small-signal impedance was measured (9 GHz in our example). If one slug is used, the tuning procedure is trivial. If two slugs are used, the tuning procedure is as follows. Slug 1, which is closest to the diode, is tuned so that the oscillations start at 9 GHz. At a bias current slightly higher than the start oscillation current slug 2 is tuned for maximum output power. The latter tuning causes a small shift of the oscillation frequency. In an iterative procedure slugs 1 and 2 are then readjusted so that the desired start oscillation frequency and maximum output power "coincide". We never used more than two slugs. It is felt that in this way the oscillator is always singly tuned correctly.

(c) After tuning the circuit remains fixed. Then the output power dissipated in the load resistance is measured. Since the diode impedance is known at the start of the oscillations, $\{R_1, X_1\}$, we also know the total circuit impedance, which is the complementary impedance $\{-R_1, -X_1\}$. Various values of the circuit impedance were obtained by inserting slugs of various inside diameters. We thus obtained (fig. 3.16) a plot of the output power as a function of $R_1 = R_L + R_c$, with the bias current as a parameter. The point $P_L = 0$ to which all the curves converge gives us the value of R_c. Hence we also know R_L.

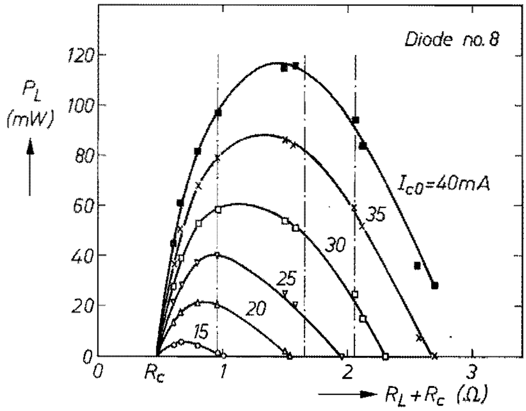

Fig. 3.16. Output power dissipated in the load resistance, P_L, as a function of $R_c + R_L = |R_1|$, as measured on an Si n^+–p diode. The vertical lines indicate the values of $R_c + R_L$ for which the oscillator noise of this diode will be studied (diode no. 8 in table 5-I, sec. 5.4.1).

From the results given in fig. 3.16 it is possible to calculate the amplitude of the r.f. current i_t from the relationship $P_L = \frac{1}{2}\,|i_t|^2\,R_L$, and the amplitude of the r.f. voltage v_t across the diode from

$$v_t = (R_1{}^2 + X_1{}^2)^{1/2}\,|i_t|\,. \tag{3.38}$$

Figure 3.17 shows R_{depl} and X as a function of i_t with I_{c0} as parameter for an n-GaAs S.B. diode (diode no. 14 in table 5-I). From these curves the diode impedance as a function of the bias current with the r.f. current as parameter can easily be derived. The results presented in fig. 3.17 will be used in chapter 5.

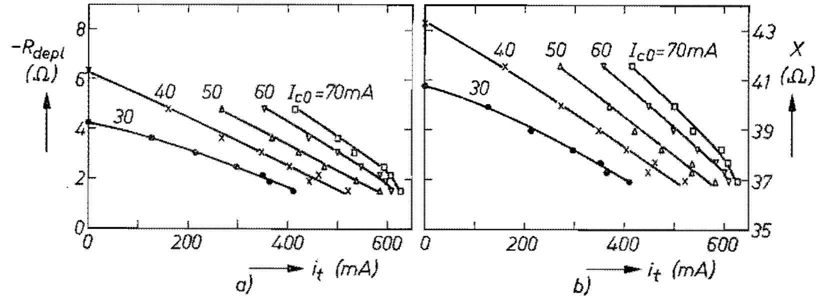

Fig. 3.17. Large-signal impedance of the active layer of an n-GaAs S.B. diode as a function of the total r.f. current i_t. The bias current I_{c0} is parameter (diode no. 14 in table 5-I, sec. 5.4.1). (*a*) Real part of the impedance ($R_{\mathrm{depl}} = R - R_s$); (*b*) imaginary part of the impedance.

3.2.5. *D.c. restorage*

When measuring at equal values of the bias current the d.c. voltage across the oscillating diode is found to differ from that across the non-oscillating diode, the temperature of the heat sink of the diode being kept constant. This difference is partly caused by temperature effects (δV_{th}), due to differences in power dissipation. The other part is thought to be caused by rectification effects of the r.f. signal (δV_{0r}), the so-called d.c. restorage. If δV_0 is the difference in bias voltage between the oscillating and the non-oscillating state, than

$$\delta V_0 = \delta V_{\mathrm{th}} + \delta V_{0r}, \tag{3.39}$$

where

$$\delta V_{\mathrm{th}} = (\delta V_0\, I_{c0} - P_{\mathrm{out}})\, R_{\mathrm{th}} \frac{\mathrm{d}V_0}{\mathrm{d}T}. \tag{3.40}$$

In the latter expression R_{th} is the thermal resistance of the diode, $\mathrm{d}V_0/\mathrm{d}T$ describes the change of the bias voltage with temperature, and P_{out} is the microwave power which leaves the oscillating diode and thus does not contribute to the heating of the diode. δV_{0r} can therefore be found from eq. (3.39) once δV_0 and δV_{th} are known.

The thermal resistance needed in eq. (3.40) can be measured as follows [42,49]. At a constant bias current the absolute value of the small-signal impedance of the diode $|Z_1|$ is measured as a function of frequency (fig. 3.18). The simplest circuit with which the impedance data can be approximated is shown in the insert in fig. 3.18. In ref. 42 it has been shown that R_{th} can be calculated from

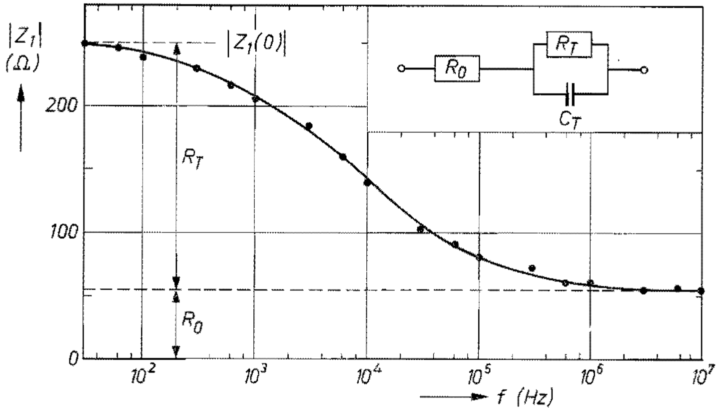

Fig. 3.18. Example of the low-frequency impedance as a function of frequency (diode no. 6 in table 3-II). The insert shows the simplest circuit with which the impedance data can approximated. R_T and C_T are the temperature resistance and capacitance of the diode, respectively.

$$R_{\mathrm{th}} = R_T \left[V_0 \left(\frac{\mathrm{d}V_0}{\mathrm{d}T} \right)_{I_{c0}} \right]^{-1} \ {}^{\circ}\mathrm{C/W}, \tag{3.41}$$

where $R_T = |Z_1(0)| - R_0$ (see fig. 3.18). The quantity $(\mathrm{d}V_0/\mathrm{d}T)_{I_{c0}}$ can be measured with the diode placed in an oven. Results for R_{th} for several diodes, measured at $I_{c0} = 10$ mA, are given in chapter 5, table 5-I. It should be noted that R_{th} is temperature-dependent, so that it depends on the bias current [50]).

The precise form of the curve in fig. 3.18 contains information concerning the quality of the thermal contacts [42,47]). We also note that eq. (3.21), which describes the low-frequency diode resistance, is valid in this case for $f > 1$ MHz, i.e. for $f \gg 1/2\pi R_T C_T$.

A theoretical estimate of δV_{0r} can be found only when the second- and higher-order field derivatives of the ionisation coefficient are taken into account. Limiting the Taylor expansion of $\bar{\alpha}$ to the second-order term, we find after integration of the Read equation:

$$I_c = I_{00} \exp \left\{ \frac{1}{\tau_i} \left[\left(\bar{\alpha}\, l_a - 1 + \frac{\bar{\alpha}''}{4 l_a} v_a^2 \right) t + \frac{\bar{\alpha}'}{\omega} (1 - \cos \omega t)\, v_a + \right.\right.$$

$$\left.\left. - \frac{\bar{\alpha}''}{8\, \omega\, l_a} v_a^2 \sin 2\omega t \right] \right\}; \qquad (3.42)$$

see also eq. (3.22).

For periodic oscillations the coefficient of t in eq. (3.42) must vanish, so that

$$\bar{\alpha}\, l_a - 1 + \frac{\bar{\alpha}''}{4 l_a} v_a^2 = 0. \qquad (3.43)$$

If δV_{a0} is the change of the d.c. voltage V_{a0} across the avalanche region caused by the d.c. restorage, it is easily found from eq. (3.43) that δV_{a0} is well approximated by [42])

$$\delta V_{a0} = - \frac{1}{4 l_a} \frac{\bar{\alpha}''}{\bar{\alpha}'} v_a^2, \qquad (3.44)$$

where $\delta V_{a0} = l_a\, \delta E_{a0}$.

A change δV_{a0} also influences the d.c. voltage V_{d0} across the drift region. An estimate for this voltage change is

$$\delta V_{d0} = \frac{1}{2} \frac{l_d}{l_a} \delta V_{a0}$$

and hence an estimate for δV_{0r} is given by

$$\delta V_{0r} = - \frac{2 l_a + l_d}{8 l_a^2} \frac{\bar{\alpha}''}{\bar{\alpha}'} v_a^2. \qquad (3.45)$$

Combining eqs (3.32) and (3.45), we see that δV_{0r} is proportional to the output power of the oscillator. Furthermore, since $\bar{\alpha}''$ and $\bar{\alpha}'$ are positive numbers δV_{0r} is negative. Figure 3.19 gives the measured d.c. restorage for diodes 14 and 7 of table 5-I in sec. 5.4.1 as a function of P_L. The dots represent the δV_0 and the circles δV_{0r} according to eqs (3.39) and (3.40), where P_{out} was taken to be the output power dissipated in $(R_c + R_L)$. The latter choice is somewhat arbitrary since a part of the output power dissipated in a part of R_s might also be taken into account. In the case of the GaAs diode (diode no. 14), where the ionisation coefficients of electrons and holes are equal, δV_{0r} can be calculated according to eq. (3.45). The calculated δV_{0r} for this diode is also given in fig. 3.19*a*. From this figure we conclude that there is no agreement between theory and experiment for this diode. The measured δV_{0r} in fact becomes positive within the RVM of the diode. For the silicon diode, where the ionisation coefficients are unequal, we have no expression available to calculate $\bar{\alpha}''$. Hence, for this diode we have plotted δV_0, and the measured δV_{0r} only. It is seen from this figure that δV_{0r} is negative for all values of P_L investigated. However, the experimental curve for δV_{0r} contains a part where the slope of the tangent is positive, which is contrary to the theory.

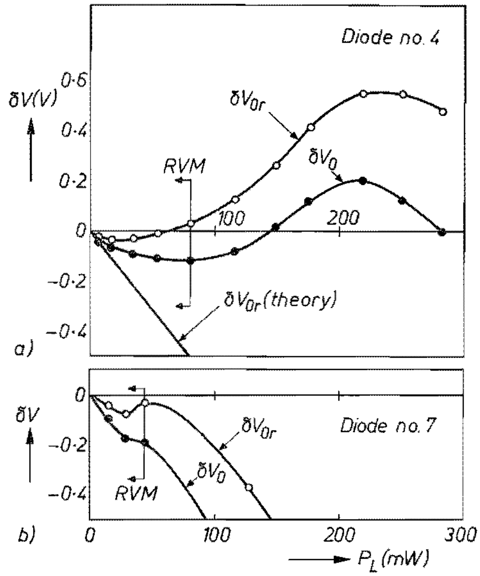

Fig. 3.19. Change of the bias voltage of the oscillating diode with respect to that of the non-oscillating diode as a function of the output power dissipated in the load resistance. The total change δV_0 was measured for equal values of the bias current, and at a fixed temperature. δV_{0r} is δV_0 corrected for temperature effects ($\delta V_{0r} = \delta V_0 - \delta V_{th}$). The RVM is indicated. (*a*) *n*-GaAs Schottky-barrier diode (diode no. 14). The calculated d.c. restorage is indicated; (*b*) Si n^+–p diode (diode no. 7).

The deviations mentioned were found to be the rule rather than the exception. We therefore conclude that our diode model is inadequate to describe this second-order effect. The quantitative description of the d.c. restorage, in particular the positive d.c. restorage which has also been observed by others [31]), is still unexplained. D.c. restorage, has, however, been mentioned in this section because it plays a part in the down-conversion of r.f. noise in bias-current noise.

4. NOISE OF THE NON-OSCILLATING DIODE

The output power of an oscillating loop can be considered to consist of narrow-band amplified noise, as will be discussed in chapter 6. This noise is generated predominantly within the avalanche region of the diode. In the present chapter the noise of the non-oscillating diode is discussed, because at the start of the oscillations the oscillator signal builds up itself from this noise. Furthermore, the intrinsic response time τ_i which governs the internal noise properties of the diode, can be determined from noise measurements on the non-oscillating diode.

Many studies have been devoted to the subject of noise in non-oscillating diodes [6]). We first give a brief historical review. The first theory to describe the current fluctuations in the avalanche process was presented by Tager [51]). He assumed that the fluctuations of the conduction current flowing out of the avalanche region are due to the shot noise of the thermally generated current and to the fluctuations in the number of electron–hole pairs created by each primary electron–hole pair. The diode model used by Tager was Read's diode model where, among other assumptions, $v_n = v_p$ and $\alpha = \beta$. Tager's theory was further developed by McIntyre [52]), who derived a more general expression for the noise generated in the avalanche region. His theory allows for $v_n \neq v_p$, $\alpha \neq \beta$ and an arbitrary electric-field profile. Both authors considered the fluctuation of the conduction current in the avalanche region only, i.e. they considered the primary noise current to be discussed in sec. 4.2. However, the total noise current flowing through the diode is also influenced by displacement currents and the transit-time effect of the carriers in the drift region. These effects were first studied theoretically by Hines [8]), who used an analysis based on the small-signal-impedance theory given by Gilden and Hines [53]). The total noise current caused by the noise source to be introduced in sec. 4.1, will be calculated in sec. 4.2.

The studies on noise in avalanche photodiodes have also contributed to the understanding of the noise behaviour of the avalanche process. Of these studies we mention the theoretical work of Emmons and Lukovsky [28]) and the experimental work of Melchior and Lynch [54]). These four workers were especially interested in the frequency dependence of the noise current at low values of the bias current, such that the carrier multiplication factor has to be considered as finite.

Of more recent date is the theoretical work of Claassen [32]), Kuvås and Lee[33]) and Convert[34]). From these studies we can obtain explicit expressions for the intrinsic response time which governs the internal noise properties of the diode, i.e. the primary noise current. All investigations mentioned above deal with the noise problem analytically. A numerical investigation has been made by Gummel and Blue [55]).

In the literature there is very little quantitative information, based on experiments, available on the intrinsic response time. We therefore carried out noise and impedance measurements at microwave frequencies in order to determine τ_i experimentally. The measurements will be described in sec. 4.4. Low-frequency noise measurements will be discussed in sec. 4.5.

In sec. 4.3 the influence of the extension of the diode model, as described in sec. 3.1.4, on the noise properties of the non-oscillating diode will be discussed. In that section, too, the possibility of noise sources other than the one introduced in sec. 4.1 will be explored.

4.1. Introduction of the noise source

The total noise current flowing through the diode is predominantly caused by the noise of the random impact-ionisation process. Therefore in the present section only the conduction current in the avalanche region is considered.

For the description of the noise behaviour of a device one seeks for the place in the description of the device where it is justifiable to introduce a white noise source. After introducing this source the total noise current through the device caused by this source is determined. In our opinion it is correct to introduce the white noise source in the continuity equations for the electrons and holes, eqs (2.8) and (2.9). For the sum of the continuity equations we then obtain

$$\frac{1}{v}\frac{\partial}{\partial t} I_c = \frac{\partial}{\partial x}(I_n - I_p) + 2\,\alpha\, I_c + 2\, g_n, \tag{4.1}$$

while the difference of the two equations remains unaltered:

$$\frac{1}{v}\frac{\partial}{\partial t}(I_n - I_p) = \frac{\partial}{\partial x} I_c. \tag{4.2}$$

The noise generation is represented by g_n in eq. (4.1). The latter equation has the form of a Langevin equation [27]). For simplicity of presentation we once again, as in the derivation of the Read equation, eq. (2.18), limit the calculations to the case $\beta = \alpha$, $v_n = v_p = v$, where α and v are assumed to be independent of the position. The final equations will be refined afterwards.

The white noise source represented by g_n is assumed to be a shot-noise source of the following. From the condition of a steady, high-current avalanche where the number of thermally generated electron–hole pairs can be neglected, we know that the average number of electron–hole pairs created by an initial pair during its transit through the avalanche region is unity. The length l_a of the avalanche region is of the order of 1 μm. The energy of a carrier needed to make an ionising collision possible is about 3/2 times the band-gap energy of the semiconductor [24]). Hence, for silicon the carrier must have an energy ε_i of about 1·5 eV. A carrier has gained this energy from the electric field E when it has travelled a distance $l_i = \varepsilon_i/qE$. A typical value of E in silicon is $3{\cdot}5 . 10^7$ V/m. Thus for silicon $l_i \approx 0{\cdot}04$ μm, and hence $l_i \ll l_a$ (the same arguments apply to germanium and gallium arsenide). We therefore think it justifiable to state that the ionisation probability of a carrier depends on its instantaneous energy only and not on the previous carrier history. As a result, if we consider an infinitesimal volume at a fixed position within the avalanche region, we know that a large number of ionisations take place in this volume but that the probability that a carrier will ionise precisely in this volume is completely random. Hence the mean-square value of the fluctuations of the conduction current $\mathrm{d}I_c$ generated within this volume is given by the shot-noise relation

$$\langle(\mathrm{d}I_c - \langle \mathrm{d}I_c \rangle)^2\rangle = 2\,q\,\langle \mathrm{d}I_c\rangle\,\mathrm{d}f,$$

where $\mathrm{d}f$ is the bandwidth considered.

The next step to be made is to calculate the influence of the shot noise generated in the fixed infinitesimal volume, on the total conduction current leaving the avalanche region. In addition we must integrate over the shot-noise contributions of all infinitesimal volumes which together form the avalanche region. From the foregoing it will be clear that we can assume that all volumes give the same initial shot-noise contribution.

4.2. The total noise current

For the calculation of the total noise current through the diode we assume the diode to be placed in a circuit similar to that of fig. 3.1. Proceeding upon the lines along which the Read equation, eq. (2.18), has been derived, it is easily found from eqs (4.1) and (4.2) that

$$\frac{\tau_a}{3}\frac{\mathrm{d}}{\mathrm{d}t} I_c = I_c\,(\alpha\, l_a - 1) + g_n(x), \tag{4.3}$$

where we neglected the saturation current, and where $g_n(x)$ is the initial shot-noise source at the position x in the avalanche region, as described in sec. 4.1. The conduction current I_c consists of a d.c. component I_{c0} and a noise component i_{nc}. After linearisation of eq. (4.3) we obtain the relation

$$j\,\omega\frac{\tau_a}{3}\,i_{nc} = I_{c0}\,\alpha'\,v_{na} + g_n(x). \tag{4.4}$$

In like manner as in the calculation of the small-signal impedance, see eqs (3.1) to (3.8), we find for the total noise current $\mathrm{d}i_{nt}$ flowing through the diode caused by $g_n(x)$:

$$\mathrm{d}i_{nt}\,(Z_1 + Z_e) = \frac{g_n(x)}{j\,\omega\,\tau_a/3}\,\frac{\Phi}{j\,\omega\,C_d}\,\frac{1}{1-\omega_{a1}{}^2/\omega^2}\,. \tag{4.5}$$

Since we are dealing with noise, the mean-square value of $\mathrm{d}i_{nt}$ is of interest, hence

$$\langle(\mathrm{d}i_{nt})^2\rangle = \frac{2\,q\,\langle \mathrm{d}I_c\rangle\,\mathrm{d}f}{\omega^2\,(\tau_a/3)^2}\left|\frac{\Phi}{\omega\,C_d}\,\frac{1}{1-\omega_{a1}{}^2/\omega^2}\,\frac{1}{Z_1+Z_e}\right|^2. \tag{4.6}$$

In this equation $g_n{}^2(x)$ is replaced by the shot-noise relation, where $\langle \mathrm{d}I_c\rangle$ is the average current generated in the infinitesimal volume at x in the avalanche region. The total noise current caused by all initial shot-noise sources in the avalanche region is found after integration to be

$$\langle i_{nt}{}^2\rangle = \int_0^{l_a} \langle(\mathrm{d}i_{nt})^2\rangle\,. \tag{4.7}$$

So we have to calculate the integral

$$\int_0^{l_a} \langle \mathrm{d}I_c\rangle = \int_0^{l_a} \langle\alpha\,(I_n+I_p)\rangle\,\mathrm{d}x = \alpha_0\,I_{c0}\,l_a = I_{c0}.$$

After generalisation to $\alpha \neq \beta$, $v_n \neq v_p$, as in eqs (2.19) to (2.22), we find:

$$\langle i_{nt}{}^2\rangle = \frac{2\,q\,I_{c0}\,\mathrm{d}f}{\omega^2\,\tau_i{}^2}\left|\frac{\Phi}{\omega\,C_d}\,\frac{1}{1-\omega_{a1}{}^2/\omega^2}\,\frac{1}{Z_t}\right|^2, \tag{4.8}$$

where $Z_t = Z_1 + Z_e$. Equation (4.8) is equivalent to eq. (19) of Hines's original noise theory [8]). Although Hines introduced his noise source in a completely different way we both find the same expression for the total noise current. It might be the subject of a separate study to investigate whether the two derivations of the total noise current should indeed give the same answer or that the equivalence of eq. (4.8) and eq. (19) of ref. 8 is quite fortuitous.

Equation (4.8) can formally be written

$$\langle i_{nt}{}^2\rangle = \langle i_{n0}{}^2\rangle\,|F|^2,$$

where F is a transfer function. The noise current i_{n0} is generally called the primary noise current. This current is the noise current which would flow in the avalanche if it were possible to maintain the electric field constant (in time) at the exact critical value needed to maintain a steady avalanche [8]). Since

$$\langle i_{n0}{}^2\rangle = \frac{2\,q\,I_{c0}\,\mathrm{d}f}{\omega^2\,\tau_i{}^2}, \tag{4.9}$$

it should be noted that τ_i is the only diode parameter that determines the primary noise current.

We finally mention that eq. (4.8) is based on the assumptions on the diode model summarised in sec. 2.4, and that this equation can also be found starting from eq. (4.4) where $g_n(x)$ has been replaced by $(2\,q\,I_{c0}\,\mathrm{d}f)^{1/2}$, i.e. from [11])

$$j\,\omega\,\tau_i\,i_{nc} = I_{c0}\,\overline{\alpha}'\,v_{na} + (2\,q\,I_{c0}\,\mathrm{d}f)^{1/2}. \qquad (4.10)$$

Then, of course, the integration eq. (4.7) must be skipped. Furthermore, the values of i_{nc} and v_{na} are r.m.s. values in this case.

4.3. Extension of the diode model; discussion

In secs 4.1 and 4.2 it was assumed that the dominant noise source is the noise generated in the avalanche process. Further possible noise sources are:

(1) The thermal noise from the passive diode resistance and circuit resistance. The noise contributions of these resistors follow from the well-known Nyquist theorem: $\overline{v_n^2} = 4\,kT\,R\,\mathrm{d}f$. It was found that in all experimental situations this noise contribution could be neglected.

(2) The thermal noise generated in the drift region of the diode. This noise contribution can be estimated from the "impedance-field method" developed by Shockley et al. [56]), which gives the noise voltage induced at the terminals of a device by the thermal velocity fluctuations of carriers at an arbitrary place within that device. For the mean-square open-circuit noise voltage per unit bandwidth the impedance-field method yields the following expression in the case of a one-dimensional structure of length $(W - l_a)$ and area A [56]):

$$\frac{\langle v_{n0}{}^2\rangle_d}{\mathrm{d}f} = 4\,q^2\,A \int_{l_a}^{W} n(x)\,D(x) \left|\frac{\partial Z_n(x)}{\partial x}\right|^2 \mathrm{d}x. \qquad (4.11)$$

In this expression n is the time-average density of the free carriers, D the diffusion constant of the carriers, and $\partial Z_n/\partial x$ the impedance-field vector with respect to the terminal. For the drift region, in which the carriers travel at saturated drift velocity v, it is then found [57]) that

$$\frac{\langle v_{n0}{}^2\rangle_d}{\mathrm{d}f} = \frac{8\,q\,D\,I_{c0}}{v\,l_a\,\omega^2\,C_d^2}\left(1 - \frac{\sin\theta}{\theta}\right), \qquad (4.12)$$

where use has been made of $I_{c0} = n\,q\,v\,A$, since n is indepeneent of x. The diffusion constant D was assumed to be independent of x, since we are interested here in an estimate of the noise source only. In fig. 4.1 eq. (4.12) is presented graphically for diode no. 6 of table 4-I (sec. 4.4), assuming $I_{c0} = 10$ mA and $D = 80$ cm^2/s. This value of D is the average high-field dif-

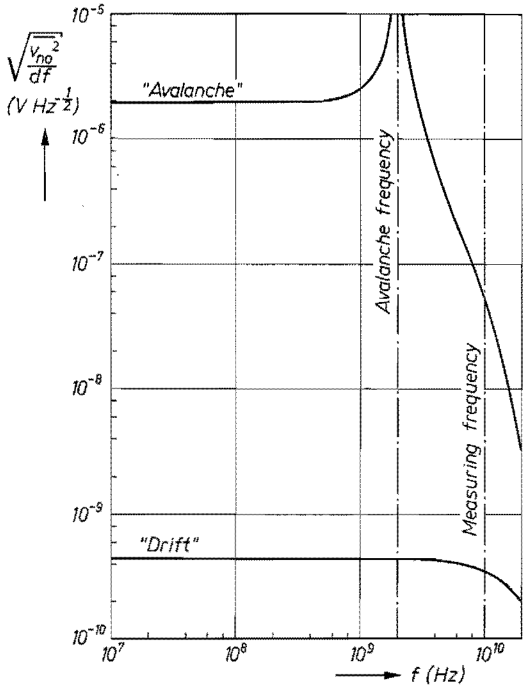

Fig. 4.1. Calculated open-circuit noise voltage per unit bandwidth (for diode no. 6 of table 4-I) as a function of frequency, at a bias current of 10 mA, caused by the noise generated in the avalanche region and in the drift region.

fusion constant ($E = 400$ kV/cm) for electrons and holes in an avalanche in silicon [58-60]). It is felt that this value leads to a reasonable upper limit of the noise contribution of the drift region. Also presented in fig. 4.1 is the open-circuit noise voltage per unit bandwidth which follows from eq. (4.8):

$$\frac{\langle v_{n0}{}^2\rangle_a}{\mathrm{d}f} = \frac{2\,q\,I_{c0}}{\omega^2\,\tau_i{}^2}\,\frac{|\Phi|^2}{\omega^2\,C_d{}^2}\,\frac{1}{(1-\omega_{a1}{}^2/\omega^2)^2}\,. \tag{4.13}$$

The value of the intrinsic response time needed in the calculation was obtained from eqs (2.5) and (2.20), using the constants given in table 3-I. We conclude that for this diode the noise generated in the avalanche is indeed the dominant noise contribution. Within the range of frequencies of interest this was found to be the case for all diodes investigated, as will be discussed further at the end of sec. 4.4. Below, therefore, we shall consider the noise generated in the avalanche only.

In sec. 3.1.4 the diode model was extended with respect to that summarised in sec. 2.4. In the extended model we accounted for the differential static resistance of the avalanche region, for transit-time effects in that region, etc.

It was found in sec. 3.1.4 that all effects which were found from a more detailed study of the avalanche region could be summed up in the parameter σ, which gives rise to a complex avalanche frequency $\overline{\omega}_{a1}$ defined by eq. (3.15):

$$\overline{\omega}_{a1}{}^2 = \omega_{a1}{}^2/(1-j\sigma).$$

When this extension of the diode model is applied to the description of the noise behaviour of the diode we find for the total noise current:

$$\langle i_{nt}{}^2\rangle_{\text{ext}} = \frac{2\,q\,I_{co}\,\mathrm{d}f}{\omega^2\,\tau_i{}^2\,(1+\sigma^2)} \left| \frac{\Phi}{\omega\,C_a}\;\frac{1}{1-\omega_{a_1}{}^2/\omega^2}\;\frac{1}{Z_t} \right|^2. \tag{4.14}$$

The difference between eqs (4.8) and (4.14) is that τ_i has been replaced by $\tau_i\,(1-j\sigma)$. This leads to the complex avalanche frequency $\overline{\omega}_{a1}$ of eq. (3.15) and to $\tau_i{}^2\,(1+\sigma^2)$ in the denominator of the primary noise current (see eq. (4.9)). Equation (4.14) can be rewritten as

$$\langle i_{nt}{}^2\rangle_{\text{ext}} = \langle i_{nt}{}^2\rangle/(1+h^2), \tag{4.15}$$

where $h = \sigma/(1-\omega_{a1}{}^2/\omega^2)$, as in eq. (3.17). In sec. 3.1.4 it was concluded that at not too high values of the bias current and at microwave frequencies, so that $\omega_{a1}{}^2/\omega^2 \ll 1$, the value of σ was small compared to unity, and hence $h \ll 1$. We then can conclude from eq. (4.15) that under the same conditions i_{nt} is correctly described by the simple-model equation (4.8). At low frequencies a significant contribution of σ is possible, but the condition $h \ll 1$ can be satisfied at values of the bias current such that $\omega_{a1}{}^2 \gg |\sigma|\,\omega^2$. In practice this means that I_{co} should be larger than, say, 10 μA. In the remainder of our studies we are interested in the noise behaviour of the diode at a frequency of 200 kHz and at X-band frequencies, say 9–10 GHz, while the bias current is always large enough. Therefore, we shall use eq. (4.8), which is based on the assumptions summarised in sec. 2.4.

Finally, in this section we mention that at values of the bias current and at values of the frequency such that $\omega_{a1}{}^2 \ll \omega^2$, eq. (4.8) predicts that the noise power is proportional to the bias current, and inversely proportional to ω^4 if the frequency dependence of Φ is neglected. These predictions have been verified by experimental studies carried out by Constant et al. [61]) and by Haitz and Voltmer [62]). An example of the bias-current dependence of the noise power at 10 GHz for two of our diodes investigated is given in fig. 4.4 in sec. 4.4.

4.4. R.f. noise measurements

The r.f. noise current was measured to obtain, in combination with the impedance measurements discussed in sec. 3.1, an experimental value of the intrinsic response time [35,63]). For the noise measurements the diode (in its encapsulation) was placed in a mount connected to an X-band radiometer. The

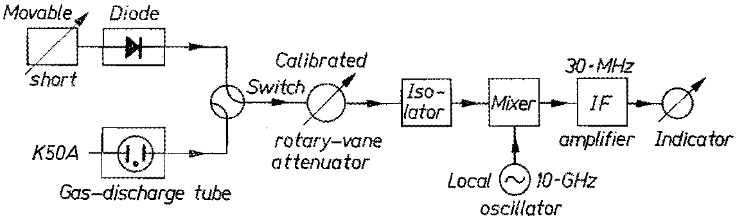

Fig. 4.2. Block diagram of the noise-measuring circuit.

block diagram of this radiometer is shown in fig. 4.2. At a bias current of 10 mA the movable short connected to the mount was adjusted for maximum output power. The position of this short was then fixed during the remainder of the measurements. (The bias current of 10 mA was the maximum value of this current used because the condition $h \ll 1$ has to be fulfilled, and temperature effects and the change of the width of the depletion layer caused by I_{c0} must be negligible.) The local oscillator of the radiometer was tuned at 10 GHz, the centre frequency of the IF amplifier was 30 MHz, and the bandwidth of this amplifier about 3 MHz. The exact value of the bandwidth is not important because in this radiometer the noise power delivered by the diode to the characteristic impedance of the transmission line (Z_0) is measured relative to the known noise power delivered by a K50A gas-discharge tube.

It was next assumed that for the whole frequency band used, the equivalent circuit of the diode in its encapsulation and mount may be represented by that of fig. 4.3. Thus no corrections were made to impedance and noise-current data to account for the fact that the noise was measured at 10 GHz ± 30 MHz, while the impedance data were all obtained at 10 GHz.

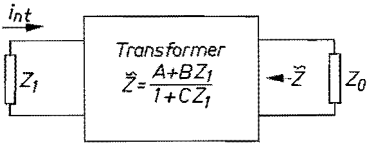

Fig. 4.3. Equivalent circuit of the noise-measuring circuit. Z_0 is the characteristic impedance of the transmission line. The transformer between the diode and Z_0 is described by the parameters A, B and C.

The parameters A, B and C of the transformer, fig. 4.3, were found by measuring the impedance $\tilde{Z}$ of he diode in the mount (without changing the position of the short), and then using the impedance of the diode itself, which is already known from sec. 3.1.1, as a calibration. Since A, B and C now have known values, the circuit of fig. 4.3 can be reduced to that of fig. 3.1, so that the total noise current $i_{nt}(I_{c0})$, as well as the total loop impedance $Z_t(I_{c0}) = Z_1(I_{c0}) + Z_e$ can be found. The value of X_e/R_t calculated from the measuring data was $\leqslant 8$.

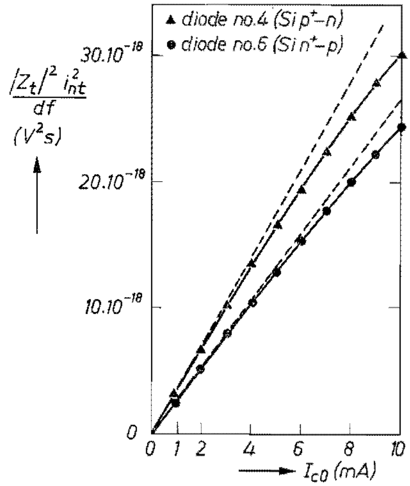

Fig. 4.4. Example of the quantity $i_{nt}^2\,|Z_t|^2/\mathrm{d}f$ as a function of the bias current as found from the experiments. The diode nos. 4 and 6 refer to the diodes in table 4-I.

This justifies the assumption that we may use the circuit of fig. 4.3 with frequency-independent values of the parameters over the frequency range 10 GHz ± 30 MHz.

Figure 4.4 gives an example of the parameter $i_{nt}^2\,|Z_t|^2/\mathrm{d}f$ as a function of the bias current. The intrinsic response time was determined from the slope of the tangent through the origion of the graph:

$$\tau_i^2 = \frac{2q\,|\Phi|^2}{\omega^4\,C_d^2}\left(\frac{\partial}{\partial I_{c0}}\,\frac{\langle i_{nt}^2\rangle\,|Z_t|^2}{\mathrm{d}f}\right)^{-1}_{I_{c0}=0}, \qquad (4.16)$$

using the data obtained from the impedance measurements summarised in table 3-II.

The data relevant to the measurements and analysis described are summarised in table 4-I. The results for τ_i as a function of the length of the avalanche region (see also table 3-II) are presented graphically in fig. 4.5, together with the theoretical curves of τ_i obtained from eq. (2.20). Also plotted in this figure are the values of τ_i for the two diodes of eq. (3.18), sec. 3.1.4, and the point $\{\tau_i = 3$ ps, $l_a = 0{\cdot}3$ μm$\}$ reported by Melchior and Lynch for a germanium avalanche photodiode [54]). From fig. 4.5 we conclude that eq. (2.20) correctly predicts the dependence of τ_i on l_a in the range investigated. However, we also conclude that there is a systematic discrepancy between the numerical experimental and theoretical values. This discrepancy, which has also been observed by Naqvi [64]) and by Kuvås and Lee [65]), can be removed by taking the effect of carrier diffusion into account [60,65,66]). The effect of carrier diffusion is to

TABLE 4-I

Diode quantities as determined from the measured noise current and impedance data for the same diodes as given in table 3-II, and the ratio $\langle v_{n0}^2\rangle_d/\langle v_{n0}^2\rangle_a$, see text

diode no.	material/ type	V_{BR} (V)	l_a (μm)	τ_i (ps)	$\overline{\alpha}'$ (V^{-1})	$\langle v_{n0}^2\rangle_d/\langle v_{n0}^2\rangle_a$ (%)
1	Si p^+–n	65	1·2	3·6	0·15	0·1
2	Si p^+–n	66	1·2	3·6	0·14	0·1
3	Si p^+–n	68	1·4	3·8	0·14	0·1
4	Si p^+–n	100	2·2	6·1	0·11	0·3
5	Si n^+–p	70	0·6	2·7	0·25	0·2
6	Si n^+–p	110	1·6	4·0	0·10	0·5
7	Si n^+–p	111	1·9	5·0	0·10	0·6
8	Si n^+–p	111	1·9	4·6	0·10	0·6
9	n-Si S.B.	70	1·1	3·6	0·13	0·1
10	Ge n^+–p	32	0·9	6·8	0·35	2·0
11	Ge n^+–p	33	0·9	7·7	0·30	3·2
12	Ge n^+–p	33	0·9	7·5	0·31	2·9
13	n-GaAs S.B.	55	0·8	7·7	0·28	4·6
14	n-GaAs S.B.	50	0·6	6·4	0·29	3·7

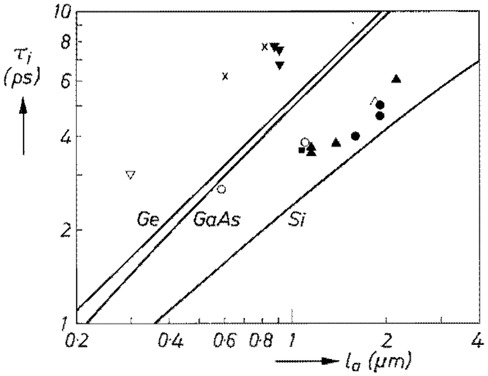

Fig. 4.5. The intrinsic response time as a function of the length of the avalanche region, as found from the experiments. Black triangles: Si p^+–n, dots: Si n^+–p, black square: n-Si Schottky barrier, black triangles upside down: Ge n^+–p, crosses: n-GaAs Schottky barrier, and as estimated for the two diodes of eq. (3.18), open triangles: Si p^+–n, circles: Si n^+–p; open triangles upside down: Melchior and Lynch [54]). The drawn curves where calculated from eq. (2.20) using the constants of table 3-I.

increase the intrinsic response time since, owing to back-stream diffusion of carriers, the after-effect of a deviation from the steady state lasts longer. If the effect of carrier diffusion is taken into account, then the influence of this diffusion on the passage of the carriers through the drift region must also be taken into account. This, of course, influences the value of τ_i determined from the experiments, as has been shown by Hulin et al. [60]). However, diffusion effects are not considered in the theoretical part of our studies, in order, particularly, to keep the large-signal theory analytically traceable. On the other hand, when in the remainder of our studies we compare theory and experiment, the value of τ_i found experimentally, as given in table 4-I, will be used.

Finally, we shall look at the noise contribution of the drift region, as discussed in sec. 4.3. From eqs (4.12) and (4.13) we obtain the relation

$$\frac{\langle {v_{n0}}^2 \rangle_d}{\langle {v_{n0}}^2 \rangle_a} = \frac{4\,D\,\omega^2\,{\tau_i}^2}{v\,l_d\,|\Phi|^2} \left(1 - \frac{\sin\theta}{\theta}\right) \left(1 - \frac{{\omega_{a1}}^2}{\omega_2}\right)^2 . \tag{4.17}$$

At microwave frequencies and for not too high values of the bias current, such that ${\omega_{a1}}^2/\omega^2 \ll 1$, the last term between brackets is almost unity, thus making the ratio given by eq. (4.17) independent of I_{c0}. The ratio (in %) is given in the last column of table 4-I for the diodes investigated, using the data given in tables 3-I, 3-II and 4-I, and the average high-field diffusion constants $D(\mathrm{Si}) = 80\,\mathrm{cm^2/s}$ for $E = 400\,\mathrm{kV/cm}$ [58-60]), $D(\mathrm{Ge}) = 100\,\mathrm{cm^2/s}$ for $E = 200\,\mathrm{kV/cm}$ [60]), and $D(\mathrm{GaAs}) = 250\,\mathrm{cm^2/s}$ for $E = 400\,\mathrm{kV/cm}$ [60]). Since we took D constant in the drift region and the values of D used are maximum values, we may conclude from the last column that only a small error in τ_i is made when the noise contribution of the drift region is neglected.

4.5. L.f. noise measurements

In chapters 5 and 7 it will be discussed that low-frequency noise, so fluctuations of the bias current, under certain conditions in the bias circuit of the oscillator can give a contribution to the oscillator noise. Therefore, it is of relevance to consider the low-frequency noise of the non-oscillating diode first.

The expression for the total noise current through the diode, eq. (4.8), contains the total loop impedance $Z_1 + Z_e$. We assume the frequency to be so low that only the real part of Z_e has to be considered, and that $\mathrm{Re}\,Z_e = R_B$, where R_B is the bias resistance. In sec. 3.1.5 (eq. (3.21)) and in sec. 3.2.5 (fig. 3.18) we have seen that the simple diode model used can give rise to relatively large errors in the calculation of R_0, the low-frequency limit of Z_1, and also that temperature effects can influence the actual value of R_0. Therefore, we consider the total noise current to be generated by a noise voltage source $\langle {v_{n0}}^2 \rangle^{1/2}$ in series with the diode. From eq. (4.8) it follows for $\omega \to 0$ that

$$\underset{(\omega \to 0)}{\langle v_{n0}{}^2 \rangle} = \frac{2\,q\,W^2}{(\bar{\alpha}'\,l_a)^2}\,\frac{1}{I_{c0}}\,\mathrm{d}f, \tag{4.18}$$

where use has been made of

$$\lim_{\omega \to 0} |\Phi|^2 = \frac{W^2}{l_d{}^2}\,.$$

Equation (4.18) predicts that $\langle v_{n0}{}^2 \rangle$ is inversely proportional to the bias current I_{c0}. This prediction has been verified in a comprehensive study of the homogeneity of the avalanche breakdown of a junction by Haitz [67]). A plot of the noise voltage per unit bandwidth for diode no. 7 of table 4-I is presented in fig. 4.6. This experimental curve was traced from the continuously recorded curve on an x–y recorder. For a comparison with theory we must know the value of $\bar{\alpha}'$. This value can be obtained from the factor $\bar{\alpha}'/\tau_i C_a$ given in table 3-II, since C_a and τ_i are now known quantities, while the factor $\bar{\alpha}'/\tau_i C_a$ was not used in the calculation of τ_i from the experimental data, as can be concluded from eq. (4.16). The results of the calculation of $\bar{\alpha}'$ are given in the sixth column of table 4-I, and presented graphically as a function of l_a in fig. 4.7. Also given in this figure are the theoretical curves calculated from eq. (2.22), and it is concluded that the experimental data are in close agreement with the theory.

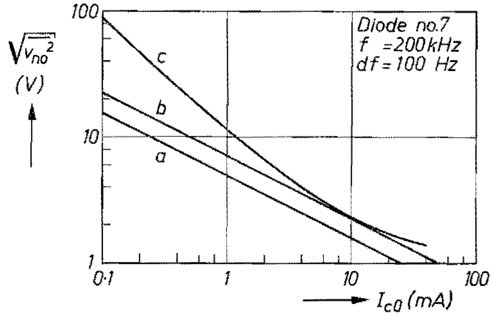

Fig. 4.6. Open-circuit noise voltage as a function of the bias current for diode no. 7 of table 4-I. Curve a was calculated from eq. (4.18) using $\bar{\alpha}'\,l_a = 1{\cdot}90 \,.\, 10^{-7}$ m/V (see table 4-I); for curve b $\bar{\alpha}'\,l_a = 1{\cdot}48 \,.\, 10^{-7}$ m/V is used, which follows if carrier diffusion is taken into account [40]). Curve c is the experimental curve.

In fig. 4.6, two theoretical curves are drawn relating $\langle v_{n0}{}^2 \rangle$ to I_{c0}. The lower curve was calculated from eq. (4.18) and from the relevant quantities given in tables 3-II and 4-I obtained from the microwave measurements. For diode no. 7 the quantity $\bar{\alpha}'\,l_a$ is equal to $1{\cdot}9 \,.\, 10^{-7}$ m/V. If the microwave measurements are analysed, as is done in ref. 60, i.e. carrier diffusion is taken into account, and

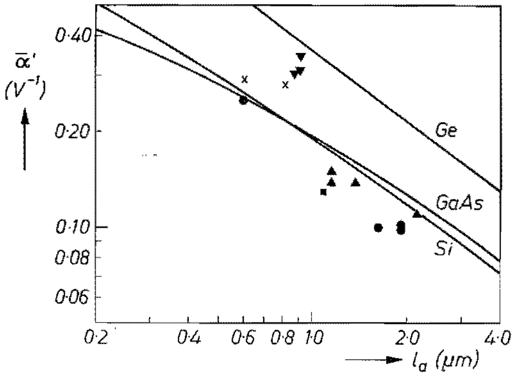

Fig. 4.7. The field derivative of the average ionisation coefficient as a function of the length of the avalanche region, as found from the experiments (black triangles: Si p^+–n, dots: Si n^+–p, black square: n-Si Schottky barrier, black triangles upside down: Ge n^+–p, crosses: n-GaAs Schottky barrier). The drawn curves were calculated from eq. (2.22) using the constants of table 3-I.

the actual doping profile is also taken into account, it is found for diode no. 7 that $\int_0^W \bar{\alpha}' \, \mathrm{d}x = 1{\cdot}48 . 10^{-7}$ m/V [40]. Using $\bar{\alpha}' \, l_a = 1{\cdot}48 . 10^{-7}$ V/m in eq. (4.18), the upper theoretical curve in fig. 4.7 is found. We conclude that in the intermediate bias-current range there is good agreement between theory and experiment, particularly if we reckon with (1) the large number of independent measurements needed to arrive at the diode quantities, and (2) with the fact that all diode quantities were determined from measuring data at microwave frequencies. At low values of the bias current we measure some excess noise due to the fact that the avalanche in this diode is not completely uniform over the junction area [66]. At higher currents, too, excess noise is found, due to thermal effects: the current in the centre of the diode becomes lower than in the periphery of the diode [67]. Furthermore the temperature affects the value of $\bar{\alpha}$ and as a result the value of $\bar{\alpha}'$. Both $\bar{\alpha}$ and $\bar{\alpha}'$ decrease with increasing temperature [68]. In addition, l_a and W are influenced by the temperature of the junction.

Finally, we mention that the pole at $I_{c0} = 0$ in eq. (4.18) is only an apparent one, the main reason being that eq. (4.18) is not valid at very low values of I_{c0}. At very low values of the bias current eq. (4.15) should be used.

5. OSCILLATOR NOISE

5.1. Introduction

The practical application of an IMPATT-diode oscillator depends to a large extent on its noise characteristics, i.e. on the amplitude and frequency fluctuations of the output signal of the oscillator. In this chapter we first shall briefly discuss some of the ways one can describe the fluctuations, and give measures commonly used to quantify the fluctuations (sec. 5.1). This is followed in sec. 5.2 by a description of the noise-measuring equipment. In sec. 5.3 a very brief survey will be given of the general, phenomenological theory of oscillator noise which, in principle, is applicable to any oscillator. This chapter ends with an application of the general oscillator-noise theory to the special case of our IMPATT-diode oscillators.

The simplest way to look at the "quality" of the output signal is to use a spectrum analyser. This apparatus displays the output power P_L dissipated in the load resistance as a function of frequency. The output power is measured in a narrow frequency band df, averaged over a time interval which is long compared to $1/df$. The resulting "picture" is called the spectrum, an example of which is given in fig. 5.1. The centre frequency f_0 of the spectrum is called the oscillation frequency or carrier frequency. A measure for the quality of the spectrum of the output signal is its width $2\,\Delta f_0$ which is the frequency interval around f_0 determined by $P_L(f_0 \pm \Delta f_0) = \frac{1}{2}P_L(f_0)$. The spectrum width is indicated in fig. 5.1. For a spectrum of the form as given in this figure it applies

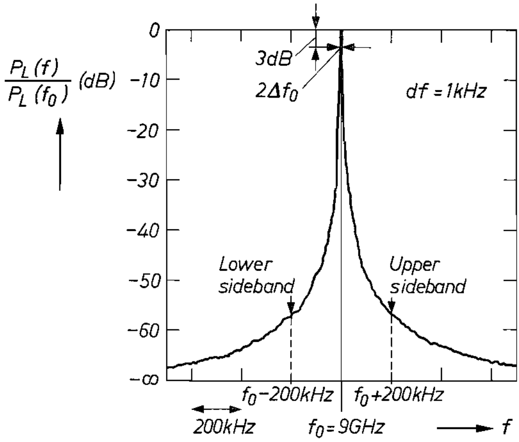

Fig. 5.1. Spectrum of the output signal of diode no. 7 in table 5-I, oscillation level such that $\gamma v_a = 0{\cdot}6$. Horizontal scale 200 kHz/division, vertical scale 10 dB/division. The spectrum width $2\,\Delta f_0$ around the oscillation or carrier frequency f_0 is indicated, as are the upper and lower sidebands, of width 1 kHz, at a distance of 200 kHz from the carrier. The spectrum was displayed with an HP852A spectrum analyser, dynamic range 60 dB.

that the smaller the spectrum width the better the quality of the output signal, i.e. the lower the oscillator noise. The bandwidth df used when measuring the output power should be small compared to the spectrum width, $2\,\Delta f_0$.

When using a spectrum analyser we face two problems. The first problem is that it is impossible to conclude from the spectrum displayed whether it is brought on by amplitude fluctuations (AM noise), by frequency fluctuations (FM noise) or by a mixture of both. The second problem is the rather small dynamic range of the analyser (for example 60 dB), which limits the measurable ratio $P_L(f)/P_L(f_0)$. Therefore another measuring technique has to be applied. This technique, for which a more detailed description of the spectrum is needed, will be discussed in sec. 5.2. This description is based on the fact that most of the output power is contained in a rather narrow band around f_0 (fig. 5.1). Therefore, the output spectrum can be thought to consist of a carrier of frequency f_0 containingall the output power, and an upper ($f > f_0$), and a lower ($f < f_0$) noise continuum. It is useful to subdivide the noise continuum into a large number of strips of bandwidth df[69]). The noise power within each strip (sideband) may then be replaced by a sinusoidal voltage source of frequency f and voltage v_n. The frequency f is the mean frequency of the noise sideband considered. The frequency f_m, defined by $f_m = f - f_0$, gives the distance (in frequency) of the sideband from the carrier at f_0. In our studies we shall only consider the noise sidebands for which $2\,\Delta f_0 \ll f_m \ll f_0$. Furthermore, we restrict the discussion to those cases where the carrier power is very much larger than the noise power in the sideband considered.

We next consider the carrier and the noise sidebands at $\Omega = 2\,\pi f_m$ from the carrier. In fig. 5.2a the three corresponding voltage vectors are drawn in the complex plane. The carrier vector rotates at frequency ω_0 anti-clockwise in this plane. The amplitude of the carrier voltage is a constant. The noise vector of the upper sideband rotates anti-clockwise at frequency Ω with respect to the carrier, while that of the lower sideband rotates clockwise at Ω with respect to the carrier. The circle in fig. 5.2a indicates schematically the r.m.s. value of v_n, which is assumed to be the same for the upper and lowerside bands (symmetrical spectrum). Addition of the two noise vectors to the carrier vector gives the instantaneous signal voltage v_s.

The signal can also be considered as a carrier which is simultaneously amplitude-modulated and phase-modulated by the noise. If v_{nr} is the resultant of the two noise vectors, the amplitude modulation is determined by its component parallel to the carrier vector, and the phase modulation by its component perpendicular to the carrier vector. We illustrate this as follows. In fig. 5.2b the upper-sideband noise vector is decomposed by replacing it by two parallel vectors $v_n{}^*$ of length $v_n/2$, both rotating anti-clockwise at frequency Ω. A noise vector $v_{\mathrm{am}}{}^*$ of length $v_n/2$ rotating clockwise at frequency Ω is added symmetrically with respect to the carrier. The vector $v_{\mathrm{am}}{}^*$ is compensated at any

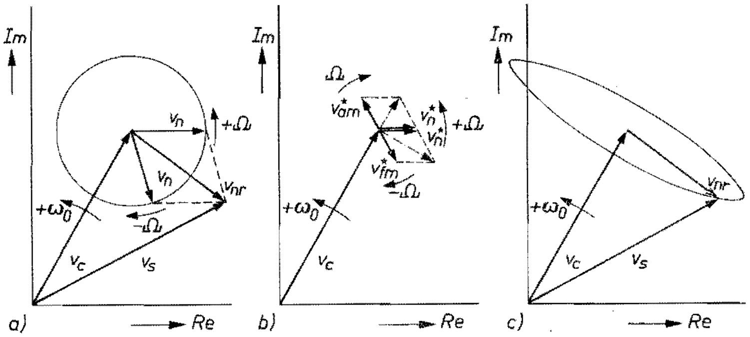

Fig. 5.2. Vector diagram of the carrier voltage v_c, and the upper- and lower-sideband voltage v_n at angular frequencies ω_0, $\omega_0 + \Omega$, and $\omega_0 - \Omega$, respectively.
(*a*) Considering the carrier and the noise sidebands at Ω from the carrier only, the signal voltage $v_s = v_c(\omega_0) + v_n(\omega_0 + \Omega) + v_n(\omega_0 - \Omega)$. The upper- and lower-sideband vectors rotate at angular frequencies Ω and $-\Omega$, respectively, with regard to the carrier.
(*b*) Decomposition of the upper-sideband noise vector into AM (v_{am}^*, v_n^*) and FM (v_{fm}^*, v_n^*) noise vectors. $|v_n^*| = |v_n|/2$; $|v_n^*| = |v_{am}^*| = |v_{fm}^*|$. The resultant of v_{am}^* and v_n^* is always parallel to v_c, the resultant of v_{fm}^* and v_n^* is always perpendicular to v_c. A similar decomposition can be made for the lower-sideband noise vector.
(*c*) On the average, the end point of the resultant v_{nr} of the upper- and lower-sideband noise vectors will be on an oval as indicated.

time by the vector v_{fm}^*. The resultant of the vectors v_n^* and v_{fm}^* is always perpendicular to the carrier vector, and determines the phase fluctuations. A similar decomposition can be made for the lower-sideband noise vector. The decomposition is based on the relation for an amplitude-modulated signal,

$$v_{s,a} = [v_c + v_n \cos(\Omega t + \psi)] \cos \omega_0 t =$$

$$= v_c \cos \omega_0 t + \frac{v_n}{2} \cos [(\omega_0 + \Omega)\, t + \psi] + \frac{v_n}{2} \cos [(\omega_0 - \Omega)\, t + \psi], \quad (5.1)$$

and that for a phase-modulated signal ($v_n \ll v_c$),

$$v_{s,f} = v_c \cos\left(\omega_0 t + \frac{v_n}{v_c} \sin(\Omega t + \psi)\right) =$$

$$= v_c \cos \omega_0 t + \frac{v_n}{2} \cos [(\omega_0 + \Omega)\, t + \psi] - \frac{v_n}{2} \cos [(\omega_0 - \Omega)\, t + \psi]. \quad (5.2)$$

From fig. 5.2*a*, *b* and eqs (5.1) and (5.2) we conclude that for each sideband the AM noise power is equal to the FM noise power (white noise). However, it is found experimentally that, in general, the AM noise power is about 40 dB below the FM noise power, as will be discussed in detail in sec. 5.4.2. This can be understood by recalling that the non-linearity of the oscillating diode limits the magnitude of the output signal. Thus the diode has a kind of built-in automatic gain control [70]) which limits the amplitude fluctuations of the signal voltage. A comparable mechanism is not present for the phase fluctuations, so that these are larger than the amplitude fluctuations. We conclude that there must be a strong correlation between the upper- and the lower-sideband noise vector, in such a way that the resultant of these vectors predominantly gives rise to phase fluctuations. This is illustrated in fig. 5.2*c*, where it is indicated that, on the average, the end point of the resultant of the noise vectors and that of the signal voltage are on an oval. The length of the short axis of the oval is determined by the amplitude fluctuations, while that of the long axis is determined by the phase fluctuations.

The instantaneous signal voltage can be written as

$$v_s(t) = [v_c + v_{\mathrm{am}} \cos(\Omega t + \psi)] \cos\left(\omega_0 t + \frac{v_{\mathrm{fm}}}{v_c} \sin(\Omega t + \varphi)\right), \tag{5.3}$$

where v_{am} and v_{fm}/v_c are the instantaneous magnitude of the amplitude and phase fluctuations, respectively, and where v_{am}, v_{fm}, ψ and φ are assumed to be slowly varying functions of time compared to Ω^{-1}. Since the instantaneous signal frequency ω is equal to the time derivative of the second cosine term in eq. (5.3), i.e. equal to

$$\omega = \omega_0 + \frac{v_{\mathrm{fm}}}{v_c} \Omega \cos(\Omega t + \varphi), \tag{5.4}$$

we can also speak of frequency modulation instead of phase modulation.

A measure for both the AM and FM oscillator noise is the ratio, expressed in dB, of the noise power in one sideband (of width $\mathrm{d}f$, at f_m from the carrier) to the carrier power.

A frequently used measure for the FM noise is the root-mean-square frequency deviation Δf_{rms}. This quantity tells us how much, in frequency, the signal frequency periodically shifts at a frequency f_m, as shown by eq. (5.4). The relation between Δf_{rms} and the noise-power to carrier-power ratio mentioned above is given by [69])

$$\frac{P_{\mathrm{FM}}}{P_c} = \frac{(\Delta f_{\mathrm{rms}})^2}{2 f_m^2}. \tag{5.5}$$

In the case of a symmetrical spectrum of the form $1/(1 + x^2)$, i.e. the spectrum can be described by a Lorentz curve, the spectrum width $2\,\Delta f_0$ is related to Δf_{rms} by the expression [11])

$$(\Delta f_{\mathrm{rms}})^2 = \frac{1}{2\pi} 2\,\Delta f_0\,\mathrm{d}f, \tag{5.6}$$

where it was assumed that $f_m \gg 2\,\Delta f_0$ and that the spectrum width was caused by FM noise only.

5.2. Experimental arrangement

In this section we describe the equipment used to measure AM and FM oscillator noise, and bias-current noise. A diagram of the system, subdivided into 7 parts, is given in fig. 5.3. The oscillator-noise receiver, given in part 7, is based on ideas set forth by Ondria [69]), and Schiek and Köhler [71]). The

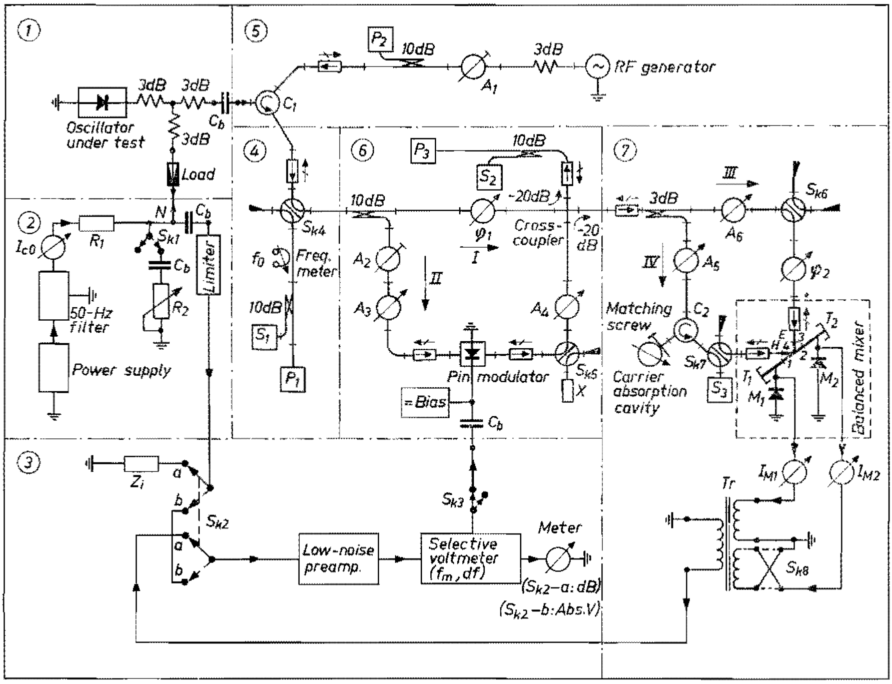

Fig. 5.3. Diagram of the noise-measuring system (see text).

⊢◀	microwave load,
⊢∿∿⊣	fixed attenuator,
A⌀	adjustable attenuator,
A⌀	calibrated rotary-vane attenuator,
φ⌀	phase shifter,
⋈	directional coupler,
⇥	isolator,
⟳	3-port circulator,
⊘	microwave switch,
P	thermistor power meter,
S	spectrum analyser.

calibration bridge, given in part 6, has been described by Schreiber and Hecker [72]). We shall now first discuss the seven parts of the diagram individually, after which the AM-noise-measuring procedure and the FM-noise-measuring procedure will be described.

Part 1. Oscillator under test

The coaxial oscillator used has already been described in sec. 3.2.4. The oscillator signal is fed into a 3-dB power divider which is terminated on one port by a microwave load and on the other port by the circulator C_1 in part 5. The oscillator is biased via the inner conductor of the load and the power divider by means of the circuit of part 2. Used in this way, the power divider and load prevent the occurrence of spurious oscillations at high output levels of the oscillator in most cases.

Part 2. Bias circuit

The bias current is furnished by the power supply via a 50-Hz (mains frequency) suppression filter and the resistor R_1 (about 2 kΩ) which prevents short-circuiting of the noise voltage present at the nodal point N, by the power supply. The variable resistor R_2 in series with the blocking condensor C_b can be switched to the circuit by switch S_{k1}. We can thus vary the total a.c. bias resistance "seen" by the diode. The limiter prevents large voltage swings from damaging the low-noise pre-amplifier (part 3) when the bias voltage is applied to the diode.

Part 3. Selective-voltmeter circuit

With the switch S_{k2} in position b, the noise voltage of the bias circuit (point N, part 2) is measured by a selective voltmeter (HP 3591 A) via a low-noise pre-amplifier. The selective voltmeter is tuned to the frequency $f_m = \Omega/2\pi$, see sec. 5.1, which in all our reported experiments is 200 kHz. The frequency band $\mathrm{d}f$ around f_m is adjustable (10, 100, 1000 and 3100 Hz), but all results reported will be reduced to $\mathrm{d}f = 100$ Hz. With S_{k2} in position b, the selective voltmeter is read in absolute volts.

With S_{k2} in position a, the noise coming from the noise receiver (part 7) is measured and the selective voltmeter is read in dB. With S_{k2} in position a, the limiter of part 2 is connected to an impedance Z_i which represents the input impedance of the pre-amplifier (at 200 kHz). In this way the a.c. conditions in the bias circuit (part 2) remain unchanged when S_{k2} is switched. The selective voltmeter furnishes a sinusoidal signal of adjustable amplitude at a frequency of f_m (= 200 kHz) which, via the switch S_{k3}, can be applied to the bias circuit of the *p–i–n* modulator of part 6.

Part 4. Monitor arm

This arm contains a frequency meter, a thermistor power meter P_1 and a YIG-tuned spectrum analyser S_1 (EIP, Model 101 B). This analyser facilitates the tuning procedure as described in sec. 3.2.4, while, in addition, the oscillator signal can easily be inspected for spurious oscillations over a broad frequency band (18 GHz). The oscillator signal is applied from the circulator C_1 (part 5), via an isolator and the switch S_{k4}.

Part 5. Injection-phase-locking arm

Via the circulator C_1 a small r.f. signal can be supplied to the oscillator under test for locking-range experiments. From these experiments the cavity-loaded quality factor Q_L was determined from the relation [11])

$$Q_L = 2 \frac{f_0}{\delta f_L} \sqrt{\frac{P_i}{P_L}}, \tag{5.7}$$

where δf_L is the total locking range and f_0 the oscillation frequency. For P_i and P_L we took the power of the injected signal and the output power of the unlocked oscillator respectively, measured between coaxial oscillator and power divider (part 1). P_i can be adjusted by the attenuator A_1 and is proportional to the reading of the thermistor power meter P_2. The locking range δf_L was read from the spectrum analyser S_2 (HP 852 A) in part 6. Q_L was determined from eq. (5.7) for the power range of P_i where in fact $(\delta f_L)^{-1} P_i^{1/2}$ is constant. Since the aim of our study is the understanding of the noise behaviour of the IMPATT diode, we always used a singly tuned, low-Q_L circuit (for example $Q_L < 22$ in the investigation of diode 14 of table 5-I, see sec. 5.4.1). In consequence of this, the noise behaviour of the diode comes to the fore very well.

Part 6. Calibration bridge [72])

With the aid of this circuit it is possible to add sidebands (at $f_0 \pm f_m$) of a known sideband-power to carrier-power ratio, to the signal entering the noise receiver of part 7. Moreover, by proper adjustment of the phase shifter φ_1 the sidebands can be added to the signal entering the receiver as pure AM sidebands or as pure FM sidebands. We thus have a calibrated modulation signal which in the receiver undergoes the same operations as the noise sidebands (at $f_0 \pm f_m$) we are interested in.

The signal entering this bridge from S_{k4} (part 4) is split into two paths by means of a 10-dB directional coupler. Part of the signal goes along path I, the other part (—10 dB) goes along path II. The thermistor power meter P_3, via the cross-coupler, receives —20 dB*) of the signal going along path I, and also receives the signal going along path II and the cross-coupler. The calibrated modulation signal is now obtained as follows. First the bridge is balanced for zero signal on P_3 by means of the phase shifter φ_1 and the adjustable attenuator A_2. When balancing the bridge the following conditions are fulfilled:

---

*) In this description we used rounded-off values for the sake of simplicity.

(a) The calibrated rotary vane attenuators A_3 and A_4 are placed in the "zero" position. We took 2 dB as the "zero" position of the attenuator, to avoid a possible phase shift which can occur [38]) if the attenuator is used from 0 dB on.
(b) The *p–i–n* modulator is d.c. biased only (approximately 1 mA).
(c) The position of the switch S_{k5} is as indicated in fig. 5.3.

Once the bridge is balanced, the carrier power in path II entering the cross-coupler is 20 dB*) below the carrier power in path I. Hence the signal entering the noise receiver (part 7) coupled out via the cross-coupler from path II, is 2 times 20 dB, i.e. 40 dB, below the signal entering the noise receiver from path I.

After the bridge is first balanced, it is unbalanced by a known amount by introducing a 1-dB additional attenuation with A_3. This results in a particular reading on P_3. A_3 is reset to its "zero" position and the sinusoidal modulation signal (frequency f_m, in our case 200 kHz) from the selective-voltmeter circuit (part 3) is applied to the *p–i–n* modulator to such an amount that P_3 shows the same reading. In this way —20 dB*) AM sidebands below the carrier are introduced in path II. Since the cross-coupler couples out the signal in path II —20 dB to the noise receiver, the modulation sidebands entering the receiver are 3 times 20 dB, i.e. 60 dB*), below the carrier. With A_3 and A_4 (50-dB attenuation maximum each) the modulation-power to carrier-power ratio of the signal entering the receiver can be adjusted between —60 and —156 dB.

It can be shown that by unbalancing the bridge by an amount of 0·915 dB instead of 1 dB, a —20-dB modulation-power to carrier-power ratio is obtained. However, since 1 dB is easier to adjust, we used this value which resulted in a —19·3-dB ratio. This was verified experimentally by using the crystal X (via switch S_{k5}) and the AM measuring procedure as described by Ondria [69]). Since the ratio is but —19·3 dB, this verification could be performed accurately. We measured the actual coupling factor of the cross-coupler separately as a function of frequency. The upper limit (—60 dB) of the modulation-power to carrier-power ratio of the signal entering the receiver can be extended, for example to —50 dB, by inserting a 10-dB attenuator in path I after the modulation procedure has been performed.

Part 7. Oscillator-noise receiver

The basics of this receiver have been described by Ondria [69]). At the input of the receiver the signal is split into two paths (III and IV) by a 3-dB directional coupler. Afterwards the two paths meet via the E and H ports of a hybrid-T balanced mixer, where the signal is detected for fluctuations by the mixer diodes M_1 and M_2 with tuning shorts T_1 and T_2 in arms 1 and 2 of the balanced mixer respectively. The signal coming through the E port enters arms 1 and 2 in phase, the signal coming through the H port enters arms 1 and 2 in anti-phase. The

---

*) In this description we use rounded-off values for the sake of simplicity.

signals of M_1 and M_2 (at a frequency around f_m) are fed into the balanced l.f. transformer Tr. With the commutator switch S_{k8} the signals from M_1 and M_2 can be added (mixer diodes in series) or subtracted (mixer diodes in anti-series). The output signal of the transformer is fed into the pre-amplifier (part 3, switch S_{k2} in position a, selective voltmeter reading in dB). Furthermore, the transformer produces a short circuit for the d.c. component of the detected signal. The resulting d.c. current can be read from the current meters I_{M1} and I_{M2}. The d.c. short reduces the intrinsic noise of the mixer diodes. The signal level on the mixer diodes, a measure for which is the current read from I_{M1} and I_{M2}, can be adjusted by the rotary-vane attenuators A_5 and A_6.

After this description of the noise-measuring equipment we end this section with a description of the AM- and FM-noise-measuring procedures.

(1) AM-noise-measuring procedure

When measuring AM noise, only path III of the noise receiver (part 7 of fig. 5.3) and the balanced mixer are used. The attenuator A_5 is set to maximum attenuation and path IV is connected to the load by switch S_{k7}. AM noise can be measured relatively simply since amplitude fluctuations of the signal entering the mixer are readily detected by M_1 and M_2, whereas phase or frequency fluctuations have to be "transformed" to amplitude fluctuations before they can be detected (see below). The AM noise is measured as follows:

(a) The calibrated modulation is brought on as described under part 6. The attenuators A_3 and A_4 are in the "zero" position.

(b) With the mixer diodes in series (S_{k8}), the phase shifter φ_1 (part 6) is adjusted for maximum output on the selective voltmeter. The calibrated modulation signal is now added to the original signal as pure AM modulation. In terms of the vector diagram of fig. 5.2*b* this means that the upper- and the lower-sideband vectors of the calibrated modulation signal are at any time parallel to the vectors v_n^* and v_{am}^* respectively.

(c) With the mixer diodes in anti-series (S_{k8}), the tuning shorts T_1 and T_2 are adjusted for minimum output on the selective voltmeter (while it can be concluded from I_{M1} and I_{M2} that we are not measuring a nodal point of the standing wave pattern in the mixer arm). Now the mixer is balanced, and the mixer diodes are connected in series (S_{k8}) again. We generally find a change of signal level of 30–40 dB at the selective voltmeter when switching from anti-series to series after balancing the mixer. Note that we used the strong modulation signal to adjust the mixer correctly. Steps (b) and (c) are repeated.

(d) Attenuators A_3 and A_4 are set to maximum attenuation. Now only the AM noise on the signal is detected. After this the attenuation of the modulation signal is reduced (by A_3 and A_4) until the reading at the selective voltmeter has increased by 3 dB. Then we have equal noise and modulation powers. Using the rounded-off numbers as given in part 6, the ratio of the single-sideband noise power to the carrier power is then given by

$$P_{\text{noise}}/P_c = -[(A_3-2)+(A_4-2)+60+3-1{\cdot}06]\ \text{dB}, \qquad (5.8)$$

where A_3 and A_4 are the readings of the attenuators A_3 and A_4, —2 dB accounts for the "zero" position of A_3 and A_4, 60 dB for the calibrated modulation, 3 dB to arrive at a single-sideband value and —1·06 dB $(= 10\,.\,{}^{10}\log(4/\pi))$ because the selective voltmeter is calibrated for sinusoidal signals and we assume the measured noise to have a Gaussian distribution[70,73]).

(2) FM-noise-measuring procedure

As already mentioned, a detector diode can detect amplitude fluctuations only, frequency modulations have to be "transformed" to amplitude fluctuations first before they can be detected. In fig. 5.2*b* we have seen that the resultant of the AM-noise vectors (that is of v_{am}^* and v_n^*) is always parallel to the carrier vector, while the resultant of the FM-noise vectors (that is of v_{fm}^* and v_n^*) is always perpendicular to the carrier vector. The trick in transforming FM into AM noise is obviously to "remove" the carrier from the signal affected by FM noise and to "add" the carrier shifted over 90° so that the carrier is now parallel to the resultant of the original FM-noise vectors, so that they are transformed into AM-noise vectors. The removal of the carrier is done with a carrier-suppression filter in path IV. This filter consists of a high-Q reflection-type resonator giving an attenuation of the carrier of at least 20 dB, as can easily be checked on the spectrum analyser S_3 connected to switch S_{k7}. After the signal in path IV has passed the filter, only the noise sidebands are left and are added in the balanced mixer to the carrier coming along path III (the signal coming along path III acts as a local-oscillator signal). The 90° phase shift needed is obtained by appropriate adjustment of the phase shifter φ_2.

The FM-noise-measuring procedure is as follows:

(a) Perform steps (a), (b) and (c) of the AM-noise-measuring procedure. Now the mixer is balanced and we have a calibrated modulation signal.

(b) The signal in path III is removed from the balanced mixer (switch S_{k6}); attenuator A_5 is set to a suitable value; the signal in path IV is switched to the balanced mixer (switch S_{k7}); the mixer diodes are connected in anti-series. Then the carrier-suppression filter is adjusted for minimum output on the selective voltmeter, which means maximum suppression of the carrier, as can easily be checked by switching path IV to the spectrum analyser S_3 using switch S_{k7}. The spectrum analyser S_2 of part 6 was used for S_3.

(c) Path IV is switched off (S_{k7}); path III is switched on (S_{k6}); mixer diodes are connected in series. Then the phase shifter φ_1 (part 6) is adjusted for minimum output on the selective voltmeter: now the calibrated modulation signal is added as pure FM modulation to the carrier entering the oscillator-noise receiver. In terms of the vector diagram of fig. 5.2*b* this means that the upper- and the lower-sideband vectors of the calibrated modulation signal are parallel at any time to the vectors $v_n{}^*$ and $v_{\mathrm{fm}}{}^*$ respectively.

(d) The signal of path IV is added ($\mathrm{S_{k7}}$) to the balanced mixer; mixer diodes are connected in anti-series. The phase shifter φ_2 in path III is then adjusted for maximum output on the selective voltmeter. Now the 90° phase shift needed between the FM sidebands and the original carrier is obtained and the single-sideband FM noise-power to carrier-power ratio can be found according to step (d) of the AM-noise-measuring procedure, again using eq. (5.8).

It should be noted that in the first instance the exact frequency behaviour of the carrier suppression filter is unimportant since the calibration signal is treated in the same way as the noise sidebands we are interested in.

5.3. General oscillator-noise theory

In this section we briefly recall results of the general, phenomenological theory of oscillator noise. In sec. 5.4 this general theory will be applied to the special case of an IMPATT-diode oscillator. The present section is based on the oscillator-noise theory put forward by Vlaardingerbroek [12]).

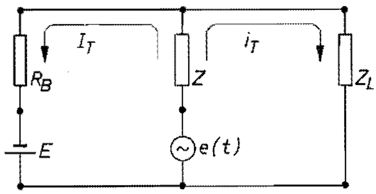

Fig. 5.4. Schematic drawing of the oscillator circuit. The diode, represented by Z, is part of the r.f. loop with load impedance Z_L and r.f. current i_T, and also part of the l.f. loop with bias resistance R_B, bias voltage source E and l.f. current I_T. The noise generated primarily within the IMPATT diode is transformed to a driving noise source $e(t)$ outside the diode.

In his theory, Vlaardingerbroek combines different aspects of oscillator-noise theories reported by several authors [74-79]). The oscillator circuit to be considered is shown in fig. 5.4. The circuit consists of an r.f. loop in which the current is

$$i_T(t) = [i_t + \delta i_t(t)] \cos [\omega_0 t + \varphi(t)] \tag{5.9}$$

by analogy with eq. (5.3). The AM noise is described by $\delta i_t(t)$, the FM noise by $\delta\omega(t) = \mathrm{d}\varphi(t)/\mathrm{d}t$. The current in the l.f. loop of the circuit, the bias current, is

$$I_T(t) = I_{c0}(t) + \delta I_{c0}(t), \tag{5.10}$$

where $\delta I_{c0}(t)$ is the noise component of the bias current. The "noisy diode" is represented by its impedance Z in series with a *driving noise source* $e(t)$. This noise source represents the noise generated within the diode, transferred to a source outside the diode. In this section we only state that there is such a driving noise source. In chapters 6 and 7 this noise source will be interpreted in terms of the specific behaviour of an IMPATT diode.

Two frequency ranges are of interest to $e(\omega)$, the Fourier transform of $e(t)$:

(1) The r.f. range with frequencies ω around the oscillation frequency. This r.f. part is the so-called *intrinsic oscillator noise*. The phenomenological description of the intrinsic noise (AM and FM) has been formulated in detail by Kurokawa[74,75]).

(2) The l.f. range with frequencies Ω from zero frequency up to the highest frequency difference between carrier and noise sideband of interest. This l.f. part, which causes fluctuations of the bias current, can influence the amplitude and frequency of the output signal, and thus give rise to the so-called *up-converted oscillator noise*. The phenomenological description of AM and FM up-converted noise has been presented by Thaler et al. [76]).

As has been discussed in sec. 3.2.5, the bias loop receives information about the manner of oscillating of the diode via d.c. restorage (rectification effects). Hence, oscillator noise can be converted into l.f. noise. Thus we also distinguish *down-converted oscillator noise*. The latter noise, in turn, can influence the oscillator noise via up-conversion. Effects of down-converted oscillator noise have been studied by Weidmann [77,78]) and Mouthaan and Rijpert [79]).

Vlaardingerbroek worked out the following matrix equation which gives the relation between the three measurable noise quantities $\{\delta i_t, \delta\omega, \delta I_{c0}\}$ and the driving noise source e:

$$\begin{pmatrix} R_{i_t} + j\dfrac{\Omega}{i_t}X_{t\omega_0} & R_{t\omega_0} & R_{I_{c0}} \\ X_{i_t} - j\dfrac{\Omega}{i_t}R_{t\omega_0} & X_{t\omega_0} & X_{I_{c0}} \\ \delta V_{i_t} & \delta V_{\omega_0} & R_{Bt} \end{pmatrix} \begin{pmatrix} \delta i_t(\Omega) \\ \delta\omega(\Omega) \\ \delta I_{c0}(\Omega) \end{pmatrix} = \begin{pmatrix} -\dfrac{e_c}{i_t}(\Omega) \\ +\dfrac{e_s}{i_t}(\Omega) \\ -e_l(\Omega) \end{pmatrix}, \qquad (5.11)$$

where e_c, e_s and e_l will be discussed below, $Z = R + jX$ is the (large-signal) diode impedance, $Z_t = Z + Z_e = R_t + jX_t$ is the total oscillator-loop impedance, and R_{Bt} the total bias-loop resistance at frequency Ω, which is equal to the bias resistance $R_B(\Omega)$ plus the equivalent resistance of the oscillating diode at frequency Ω. In eq. (5.11)

$$R_{i_t} = \left(\frac{\partial}{\partial i_T}R\right)_{i_T=i_t}, \quad R_{t\omega_0} = \left(\frac{\partial}{\partial\omega}R_t\right)_{\omega=\omega_0}, \quad R_{I_{c0}} = \left(\frac{\partial}{\partial I_T}R\right)_{I_T=I_{c0}},$$

etc., and

$$\delta V_{i_t} = \left(\frac{\partial}{\partial i_T}\,\delta V_{0r}\right)_{i_T = i_t}, \quad \delta V_{\omega_0} = \left(\frac{\partial}{\partial \omega}\,\delta V_{0r}\right)_{\omega = \omega_0},$$

where δV_{0r} is the d.c. voltage change across the diode as defined in sec. 3.2.5. Since the lines along which eq. (5.11) was derived are clearly described in refs 12 and 75, this equation has simply been stated here. We consider it to be sufficient to make the following remarks about the derivation of eq. (5.11). The first two rows of eq. (5.11) arise from a discussion of the r.f. loop of the oscillator: one row for the cosine terms and one for the sine terms arising in the loop equation after slight deviations from a stable oscillation condition are considered. The slight deviations are caused by the driving noise source $e(t)$. The noise voltages $e_c(\Omega)$ and $e_s(\Omega)$ are the Fourier transform of $e_c(t)$ and $e_s(t)$, respectively, where $e_c(t)$ and $e_s(t)$ are related to $e(t)$ by

$$\left.\begin{matrix} e_s(t) \\ e_s(t) \end{matrix}\right\} = \frac{2}{T_0} \int\limits_{t}^{t+T_0} e(t) \begin{Bmatrix} \cos\left[\omega_0 t + \varphi(t)\right] \\ \sin\left[\omega_0 t + \varphi(t)\right] \end{Bmatrix} \mathrm{d}t, \tag{5.12}$$

where $e(t)\cos\left[\omega_0 t + \varphi(t)\right]$ and $e(t)\sin\left[\omega_0 t + \varphi(t)\right]$ are the in-phase and out-phase components of $e(t)$ with respect to i_t, respectively, and $T_0 = 2\,\pi/\omega_0$. Due to this averaging process, carried out during the deduction of eq. (5.11) to remove the cosine and sine factors, the spectral densities of e_c and e_s contain only low frequencies Ω. The noise voltages e_c and e_s account for the r.f. noise generated at a distance $|\Omega|$ from the carrier. The last row of eq. (5.11) arises from the bias loop. Only the equation for the real parts of this loop is considered, since Ω is assumed to be low in our studies ($\Omega = 2\pi . 200$ kHz in all our experiments). The low-frequency part of the driving noise source is represented by e_l.

If $R_{I_{c0}}$, $X_{I_{c0}}$, δV_{i_t}, δV_{ω_0}, δI_{c0} and e_l are all equal to zero eq. (5.11) describes the intrinsic oscillator noise. If only δV_{i_t} and δV_{ω_0} are zero eq. (5.11) describes the intrinsic as well as the up-converted oscillator noise, while eq. (5.11) without zeros describes intrinsic, up-converted and down-converted noise.

It should be emphasized that this general oscillator-noise theory does not provide an expression for the driving noise voltages e_c, e_s and e_l for the special case of the IMPATT-diode oscillator, so that these noise voltages are unknown. However, in secs 5.4.2 and 5.4.3 it will be shown that still useful expressions can be derived from eq. (5.11). These expressions will not contain one of the noise voltages e_c, e_s or e_l.

5.4. Application of the general oscillator-noise theory to IMPATT-diode oscillators

Equation (5.11) will next be applied to the special case of our IMPATT-diode oscillator. First some general conclusions will be drawn. In sec. 5.4.2 a relation for the ratio of the intrinsic AM and FM noise is derived and checked experimentally. The diode and circuit quantities of the oscillators under test used are summarised in sec. 5.4.1. Section 5.4.3 deals with some aspects of modulation noise, i.e. with up-converted and down-converted oscillator noise.

Inversion of eq. (5.11) yields the explicit relation for the measurable noise quantities $\{\delta i_t,\ \delta\omega,\ \delta I_{c0}\}$ expressed in the driving noise sources $\{e_c,\ e_s,\ e_l\}$. In general, this inversion results in a complicated expression which, however, in the case of an IMPATT-diode oscillator can be simplified considerably by taking into account the following remarks:

(1) The d.c. restorage, δV_{0r}, is independent of the r.f. signal frequency, as shown in sec. 3.2.5, eq. (3.45). In spite of the fact that our model could not explain the experimentally found values of δV_{0r}, we still assume in what follows that δV_{0r} is independent of ω_0. This makes $\delta V_{\omega_0} = 0$.

(2) In sec. 3.2.1 it has already been mentioned that in the expression for the large-signal impedance, eq. (3.26), the avalanche frequency ω_a is the only parameter which depends on the bias current and the signal level (in our diode model *all* other parameters are independent of these two quantities). So $Z\ (\omega_0, i_t, I_{c0}) = Z\ (\omega_0, \omega_a\ (i_t, I_{c0}))$. Furthermore, in sec. 3.2.2 it has been explained that for the oscillating diode both the oscillation frequency and the avalanche frequency are constants. From these observations it follows that

$$\frac{R_{i_t}}{R_{I_{c0}}} = \frac{X_{i_t}}{X_{I_{c0}}} = \frac{\partial\omega_a{}^2/\partial i_t}{\partial\omega_a{}^2/\partial I_{c0}} \tag{5.13}$$

and

$$R_{i_t} = -\,R_{I_{c0}}\frac{\mathrm{d}I_{c0}}{\mathrm{d}i_t}\,,\quad X_{i_t} = -\,X_{I_{c0}}\frac{\mathrm{d}I_{c0}}{\mathrm{d}i_t}\,. \tag{5.14}$$

Substitution of all these results into the inverse of eq. (5.11) yields the matrix equation

$$\begin{pmatrix} \delta i_t \\ \delta\omega \\ \delta I_{c0} \end{pmatrix} = \frac{1}{N}\begin{pmatrix} -X_t & -R_{t\omega_0} & -\dfrac{\Gamma}{R_{Bt}} \\ -X_{I_{c0}}\,\varrho(1+\Lambda) & -R_{I_{c0}}\,\varrho(1+\Lambda) & 0 \\ X_{t\omega_0}\,\varrho\Lambda & -R_{t\omega_0}\,\varrho\Lambda & -\dfrac{\varrho\Gamma}{R_{Bt}} \end{pmatrix}\begin{pmatrix} e_c \\ e_s \\ i_t e_l \end{pmatrix}, \tag{5.15}$$

where we used the abbreviations

$$\varrho = \frac{\mathrm{d}I_{c0}}{\mathrm{d}i_t}, \quad \Gamma = R_{t\omega_0} X_{I_{c0}} - R_{I_{c0}} X_{t\omega_0}, \quad \Lambda = \frac{\delta V_{i_t}}{\varrho\, R_{Bt}},$$

and where the denominator N is given by

$$N = i_t\, \varrho\, (1 + \Lambda)\, \Gamma.$$

In the derivation of eq. (5.15) from eq. (5.11) the distance from the carrier Ω was assumed to be so small that the terms proportional to Ω in eq. (5.11) could be neglected.

The following are some of the conclusions arising out of eq. (5.15) [12]:

(a) The zero in the 3×3 matrix shows that there is no up-conversion of l.f. noise into FM oscillator noise. This is in accordance with the conclusion derived from eq. (3.29b) in sec. 3.2.2, which states that the oscillation frequency is influenced neither by the bias current nor by the signal level. Equation (3.29) was already verified experimentally in an indirect way when it was found in sec. 3.2.3 that a range of validity for our diode model (RVM) in fact exists. We shall discuss this point further in sec. 7.2.

(b) If $\Gamma = 0$, the denominator $N = 0$, and the oscillator is unstable. We found experimentally that if the oscillator circuit used was adjusted as described in sec. 3.2.4, the oscillator did not become unstable (within the range of validity of the diode model), nor did the oscillation frequency, as a function of the bias current, show any discontinuities. Such discontinuities have been observed where the oscillator circuit was not adjusted as stipulated in sec. 3.2.4. Further conclusions from eq. (5.15) will be mentioned at appropriate places in the following pages.

5.4.1. *Summary of diode and circuit parameters*

The values obtained for the diodes and circuits used in the remainder of this study in the investigation of oscillator noise are summarised in table 5-I. The diode numbers are the same as in preceding tables. It is seen in table 5-I that some of the diodes were investigated for more than one value of the load resistance. The values of all parameters were obtained as described in the preceding chapters, which means that the data given in

(a) column 3 were read from a voltmeter;

(b) column 4 were calculated from the manufacturing data, see sec. 3.1.2;

(c) columns 5 to 9 inclusive and column 13 were obtained from small-signal-impedance measurements, see secs 3.1.2 and 3.2.3;

(d) column 10 were obtained from noise measurements on the non-oscillating diode, see sec. 4.4;

TABLE 5-I

Diode and circuit parameters

1	2	3	4	5	6	7	8	9	10	11	12	13	14	15	16	17	18	19
no.	mat./ type	V_{BR} (V)	W (μm)	W/l_d	θ (rad)	$\lvert\Phi\rvert^2$	$1-\frac{\sin\theta}{\theta}$	$\bar{\alpha}'/\tau_i C_a$ ((A s)$^{-1}$)	τ_i (ps)	γ (V^{-1})	$(\gamma v_a)_{max}$	R_s (Ω)	R_c (Ω)	R_L (Ω)	f_0 (GHz)	I_{st} (mA)	$\frac{\omega_{a,st}^2}{\omega_0^2}$	R_{th} (°C W^{-1})
2	Si p^+–n	66	3·1	1·59	1·2	2·17	0·21	31.10^{21}	3·6	0·68	1·8	0·70	0·40	3·1	10	31·0	0·24	24
											1·8			3·8	10	34·4	0·27	
4	Si p^+–n	100	5·3	1·69	1·9	1·92	0·49	22.10^{21}	6·1	0·34	1·4	0·78	0·85	1·6	10	29·4	0·16	18
7	Si n^+–p	111	5·8	1·49	2·3	1·29	0·67	18.10^{21}	5·0	0·37	1·8	0·75	0·50	0·5	9	14·9	0·08	20
8	Si n^+–p	111	5·8	1·49	2·3	1·19	0·67	19.10^{21}	4·6	0·35	1·8	0·94	0·46	0·5	9	14·8	0·09	18
										0·34	1·9			1·2	9	20·7	0·13	
										0·34	1·7			1·6	9	25·9	0·16	
10	Ge n^+–p	32	2·6	1·53	1·6	1·66	0·47	36.10^{21}	6·8	0·79	1·9	0·56	0·30	6·8	9	34·6	0·39	25
											1·9			5·1	9	27·6	0·31	
14	n-GaAs S.B.	50	2·2	1·29	1·1	1·46	0·19	25.10^{21}	6·4	0·80	2·2	0·60	0·75	2·2	9	26·5	0·21	15

(e) columns 11 and 12 were found from output-power measurements, see sec. 3.2.3;

(f) columns 14 and 15 were determined from large-signal-impedance measurements, see sec. 3.2.4;

(g) columns 16 and 17 were read from meters;

(h) column 18 were calculated from the data given in columns 9, 16 and 17;

(i) column 19 were obtained from measurements as described in sec. 3.2.5, where the bias current was taken equal to 10 mA.

5.4.2. *The ratio of the intrinsic AM to FM noise power*

In chapter 6 it will be shown that it is possible to derive an analytical expression for the intrinsic FM oscillator noise starting from the processes which take place inside the diode. That expression contains diode and circuit data which can all be measured as described in chapters 3 and 4, and others which can be obtained simply from reading the meters (bias current, output power). However, the theory of chapter 6 does not provide an expression for the intrinsic AM oscillator noise. In the present section we shall see that the general oscillator-noise theory described can provide an expression for the ratio of the intrinsic AM to FM noise and that this ratio can be expressed in terms of diode and circuit data only. So this ratio does not contain the unknown values of e_c and e_s. Combining the expression for this ratio with the expression for the FM noise, to be derived in sec. 6.4, yields an expression for the intrinsic AM noise only.

From eq. (5.15) it follows that

$$\delta i_t = -\frac{X_{t\omega_0}\, e_c + R_{t\omega_0}\, e_s}{i_t\, \varrho\, (1 + \Lambda)\, \Gamma} - \frac{e_l}{R_{Bt}\, \varrho\, (1 + \Lambda)}, \tag{5.16}$$

$$\delta\omega = -\frac{X_{I_{c0}}\, e_c + R_{I_{c0}}\, e_s}{i_t \Gamma}. \tag{5.17}$$

The first term on the right-hand side of eq. (5.16) represents the intrinsic AM noise which, via Λ, can be influenced by effects of down-conversion. The second term describes the up-converted noise, which also is a function of Λ. We now assume that the total bias resistance R_{Bt} is so high that $\Lambda \ll 1$ and that the second term on the right-hand side of eq. (5.16) is very much smaller than the first term (note that $\delta\omega$ in eq. (5.17) is independent of Λ). On the assumption that e_c and e_s are uncorrelated, we obtain from eqs (5.14) to (5.17):

$$\langle \delta i_t^{\,2} \rangle = \frac{|Z_{t\omega_0}|^2}{|Z_{I_{c0}}|^2}\, \frac{1}{\varrho^2} \langle \delta\omega^2 \rangle = \frac{|X_{t\omega_0}|^2}{|Z_{i_t}|^2} \langle \delta\omega^2 \rangle, \tag{5.18}$$

where $\langle\ \rangle$ indicates averaging over a long period. Using the definitions of the AM and FM-noise-power to carrier-power ratio, as given at the beginning of this chapter, eq. (5.18) can be rewritten as

$$\frac{P_{\mathrm{AM},i}}{P_{\mathrm{FM},i}} = 2\,\frac{\Omega^2}{i_t^2}\,\frac{|Z_{t\omega_0}|^2}{|Z_{i_t}|^2}, \tag{5.19}$$

the subscript i denoting intrinsic noise.

The next step is to express $Z_{t\omega_0}$ and Z_{i_t} in measurable diode and circuit quantities. For the determination of $Z_{t\omega_0}$ we assume that for the singly tuned oscillator circuit, with its low-loaded quality factor Q_L, the oscillator loop may be considered as a simple LCR series resonance circuit with a very high internal quality factor. In chapter 6 we shall see that such an assumption is reasonable for our IMPATT-diode oscillator, and also that the real part R_t of Z_t is the nearly zero resistance left in the oscillating loop due to the presence of the driving noise source (in the absence of the noise source $R_t = 0$). We assume here that R_t is almost independent of ω, such that $R_{t\omega_0} \ll X_{t\omega_0}$, and hence $|Z_{t\omega_0}| = |X_{t\omega_0}|$. For the simple LCR circuit it is easily found that $|X_{t\omega_0}| = 2/\omega_0^2 C$, where $\omega_0^2 = 1/LC$ determines the oscillation frequency ω_0. Hence

$$|Z_{t\omega_0}|^2 = 4/\omega_0^4 C^2. \tag{5.20}$$

In this expression C is the capacitance of the oscillating diode given by

$$C = C_d\,(1-\omega_a^2/\omega^2)\left[\frac{W}{l_d} - \left(1-\frac{\sin\theta}{\theta}\right)\frac{\omega_a^2}{\omega^2}\right]^{-1}, \tag{5.21}$$

as is easily found from the imaginary part of eq. (3.26).

The quantity Z_{i_t} can be found from straightforward calculations, using eqs (2.24)–(2.26). Since $|Z_{i_t}|^2 = R_{i_t}^2 + X_{i_t}^2$, it suffices to trace the steps along which R_{i_t} is derived. From eq. (3.26) it follows that

$$R = R_s - \frac{\mathrm{Im}\,\Phi}{\omega\,C_d}\,\frac{1}{1-\omega^2/\omega_a^2},$$

and hence

$$\frac{\partial R}{\partial i_t} = \frac{\mathrm{Im}\,\Phi}{\omega^3\,C_d}\,\frac{1}{(1-\omega_a^2/\omega_0^2)^2}\,\frac{\partial \omega_a^2}{\partial i_t}. \tag{5.22}$$

From eq. (3.25) we find after differentiation that

$$\frac{\partial \omega_a^2}{\partial i_t} = \frac{\omega_a^2}{\gamma v_a}\,[1 - D(\gamma v_a)]\,\frac{\partial}{\partial i_t}(\gamma v_a), \tag{5.23}$$

where $D(\gamma v_a)$ is defined by eq. (3.35). The a.c. voltage v_a across the avalanche region is $v_a = i_t\, Z_a$, where

$$Z_a = \frac{1}{j\,\omega\, C_a}\,\frac{1}{1-\omega_a{}^2/\omega^2},$$

as is easily found by inspection of eq. (3.24). Since $\gamma v_a = \gamma\, i_t\, Z_a$ we have

$$\frac{\partial}{\partial i_t}(\gamma v_a) = \gamma\, Z_a + \frac{\gamma v_a}{\omega^2}\,\frac{1}{1-\omega_a{}^2/\omega^2}\,\frac{\partial \omega_a{}^2}{\partial i_t}\,. \tag{5.24}$$

Eliminating $\partial(\gamma v_a)/\partial i_t$ from eq. (5.23) using eq. (5.24) and substituting the result into eq. (5.20) yields

$$R_{i_t} = \frac{\operatorname{Im} \Phi}{\omega_0\, C_a}\,\frac{1}{1-\omega_a{}^2/\omega_0{}^2}\,\frac{1}{i_t}\,\frac{1}{B(\gamma v_a)}\,. \tag{5.25}$$

Similarly we obtain

$$X_{i_t} = \frac{\operatorname{Re} \Phi}{\omega_0\, C_a}\,\frac{1}{1-\omega_a{}^2/\omega_0{}^2}\,\frac{1}{i_t}\,\frac{1}{B(\gamma v_a)}\,. \tag{5.26}$$

In eqs (5.25) and (5.26) $B(\gamma v_a)$ is defined by

$$B(\gamma v_a) = \frac{D(\gamma v_a) - \omega_0{}^2/\omega_a{}^2}{1-D(\gamma v_a)} =$$

$$= -1 + \frac{1-\omega_0{}^2/\omega_a{}^2}{2+\gamma v_a\,[I_1(\gamma v_a)/I_0(\gamma v_a) - I_0(\gamma v_a)/I_1(\gamma v_a)]}\,. \tag{5.27}$$

For $\gamma v_a \rightarrow 0$, $|B(\gamma v_a)| \rightarrow \infty$, and for $\gamma v_a \rightarrow \infty$, $|B(\gamma v_a)| \rightarrow \omega_0{}^2/\omega_a{}^2$. Finally, substitution of eqs (5.21), (5.25) and (5.26) into eq. (5.20) yields for the ratio of the intrinsic AM to FM noise power (both measured in the same bandwidth at a distance of Ω from ω_0):

$$\frac{P_{\mathrm{AM},i}}{P_{\mathrm{FM},i}} = \frac{8}{|\Phi|^2}\,\frac{\Omega^2}{\omega_0{}^2}\left[\frac{W}{l_d} - \left(1-\frac{\sin\theta}{\theta}\right)\frac{\omega_{a,\mathrm{st}}{}^2}{\omega_0{}^2}\right]^2 B^2(\gamma v_a), \tag{5.28}$$

where ω_a has been replaced by $\omega_{a,\mathrm{st}}$ as discussed in sec. 3.2.2 (also in the expression for $B(\gamma v_a)$, ω_a has to be replaced by $\omega_{a,\mathrm{st}}$). From the data given in table 5-I it can be concluded that in all cases investigated eq. (5.28) can be approximated by

$$\frac{P_{\mathrm{AM},i}}{P_{\mathrm{FM},i}} = \frac{8\,\Omega^2\,W^2}{\omega_0{}^2\,|\Phi|^2\,l_d{}^2}\,B^2(\gamma v_a). \tag{5.29}$$

Figure 5.5 shows an example of the ratio $P_{\mathrm{AM},i}/P_{\mathrm{FM},i}$ as a function of γv_a for diode no. 2 in table 5-I. The ratio was calculated from eq. (5.28) for three values of the ratio $\omega_{a,\mathrm{st}}^2/\omega_0^2$. Note that in sec. 3.2.3 in the case of $\omega_{a,\mathrm{st}}^2/\omega_0^2$ the RVM found experimentally is given by $(\gamma v_a)_{\max} = 1{\cdot}8$. For $\gamma v_a \to 0$ the ratio $P_{\mathrm{AM},i}/P_{\mathrm{FM},i} \to \infty$ is as expected, since at "zero" output power the only "signal" left are the amplitude fluctuations of the bias current.

Experimental and theoretical results of $P_{\mathrm{AM},i}/P_{\mathrm{FM},i}$ as a function of the modulation depth are presented in fig. 5.6 for diodes no. 7 and no. 14 of table 5-I (as will be shown in sec. 7.2 the up-converted and down-converted noise can be made negligibly small compared to the intrinsic noise). The modulation depth m, defined by eq. (3.37), was chosen as abscissa because this parameter can be determined experimentally for all signal levels, whereas γv_a can only be determined within the RVM of the diode. The maximum modulation depth $m_{\max}$ within the RVM of the diode is indicated in the figure. The theoretical curves were calculated from eq. (5.28) for $m \leqslant m_{\max}$ and from eqs (5.19) and (5.20) for $m \geqslant_{\max}$. The procedure by which the results given in fig. 5.6 were obtained for $m \leqslant m_{\max}$ will be described in sec. 6.3. In the case $m \geqslant m_{\max}$ the values of $|Z_{t_t}|$ and $|Z_{t\omega_0}|$ were obtained from results of large-signal-impedance

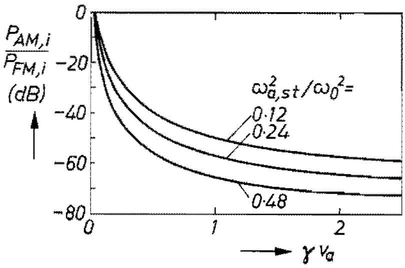

Fig. 5.5. The ratio $P_{\mathrm{AM},i}/P_{\mathrm{FM},i}$ as a function of γv_a for diode no. 2 in table 5-I. The ratio is calculated for $\omega_{a,\mathrm{st}}^2/\omega_0^2$ equal to 0·12, 0·24 and 0·48, respectively. In the case $\omega_{a,\mathrm{st}}^2/\omega_0^2 = 0{\cdot}24$, the RVM found experimentally is given by $(\gamma v_a)_{\max} = 1{\cdot}8$.

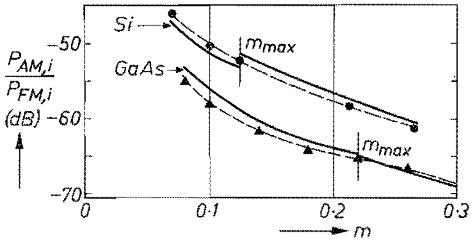

Fig. 5.6. Experimental and theoretical results for the ratio of the intrinsic AM to FM noise power as a function of the modulation depth for the Si n^+–p diode no. 7 and the n-GaAs S.B. diode no. 14 in table 5-I. For $m \leqslant m_{\max}$ the theoretical curves were calculated from eq. (5.28), for $m \geqslant m_{\max}$ from eqs (5.19) and (5.20).

measurements as described in sec. 3.2.4. An example of these impedance data has been given in figs 3.16 and 3.17.

We conclude from fig. 5.6 that for all values of m there is good agreement between theory and experiment. For $m \geqslant m_{\max}$ this also implies an experimental verification of parts of the theory given in refs 12 and 65. Furthermore, the assumption that our circuit may be considered as a simple LCR circuit seems to be correct.

5.4.3. *Up-converted and down-converted oscillator noise*

The influence of bias-current noise on the oscillator noise (up-conversion), and the reverse effect, the influence of oscillator noise on the bias-current noise (down-conversion), will briefly be discussed next, starting from eq. (5.15). In sec. 7.2 these types of noise will be discussed on the basis of our diode model, and a comparison with the experiments will be made in that section too.

It has already been concluded from eq. (5.15) that in our model there is no up-conversion of bias-current noise into FM oscillator noise. Since the output power very much depends on the bias current we may expect that up-converted AM oscillator noise can be present. We shall derive an expression for the latter type of noise first. For this purpose we need the equation for the bias-current noise. From eq. (5.15) we find that

$$\delta I_{c0} = \frac{(X_{t\omega_0}\, e_c + R_{t\omega_0}\, e_s)\, \Lambda}{i_t\, \Gamma\, (1 + \Lambda)} - \frac{e_l}{R_{Bt}\, (1 + \Lambda)} . \tag{5.30}$$

In the calculation of the amount of up-converted noise we assume that in eqs (5.16) and (5.30) the first term on the right-hand side is much smaller than the second term, so that

$$\langle \delta i_t^{\,2} \rangle = \frac{\langle \delta I_{c0}^{\,2} \rangle}{\varrho^2} = \left(\frac{\mathrm{d}i_t}{\mathrm{d}I_{c0}} \right)^2 \langle \delta I_{c0}^{\,2} \rangle . \tag{5.31}$$

Note that this equation does not contain the unknown voltages e_c, e_s and e_l. The next step is to calculate $\mathrm{d}i_t/\mathrm{d}I_{c0}$. From eqs (5.13) and (5.14) it follows that

$$\frac{\mathrm{d}i_t}{\mathrm{d}I_{c0}} = - \frac{\partial \omega_a^{\,2}/\partial I_{c0}}{\partial \omega_a^{\,2}/\partial i_t} . \tag{5.32}$$

The calculation of $\partial \omega_a^{\,2}/\partial i_t$ follows after elimination of $\partial(\gamma v_a)/\partial i_t$ from eqs (5.23) and (5.24) to be given by

$$\frac{\partial \omega_a^{\,2}}{\partial i_t} = \frac{\omega^2}{i_t} \left(1 - \frac{\omega_a^{\,2}}{\omega^2} \right) \frac{1}{B(\gamma v_a)} , \tag{5.33}$$

where use has been made of eq. (5.27); $\partial\omega_a{}^2/\partial I_{c0}$ can be found in a similar way. Thus first $\partial\omega_a{}^2/\partial I_{c0}$ is expressed in terms of $\partial(\gamma v_a)/\partial I_{c0}$, then $\partial(\gamma v_a)/\partial I_{c0}$ is calculated and from both relations obtained $\partial\omega_a{}^2/\partial I_{c0}$ can be calculated. This procedure yields the expression

$$\frac{\partial\omega_a{}^2}{\partial I_{c0}} = -\frac{\omega^2}{I_{c0}}\frac{1-\omega_a{}^2/\omega^2}{D(\gamma v_a)-\omega^2/\omega_a{}^2} + \frac{\omega^2}{i_t}\left(1-\frac{\omega_a{}^2}{\omega^2}\right)\frac{1}{B(\gamma v_a)}\frac{\mathrm{d}i_t}{\mathrm{d}I_{c0}}, \tag{5.34}$$

while substitution of eqs (5.33) and (5.34) into eq. (5.32) yields

$$\frac{\mathrm{d}i_t}{\mathrm{d}I_{c0}} = \frac{1}{2}\frac{i_t}{I_{c0}}\frac{1}{1-D(\gamma v_a)}. \tag{5.35}$$

The function $[1-D(\gamma v_a)]^{-1}$ was already shown in fig. 3.11. The ratio of the single-sideband up-converted AM noise power to carrier power is given by

$$\frac{P_{\mathrm{AM},u}}{P_c} = \frac{1}{2}\frac{\langle\delta i_t{}^2\rangle}{\langle i_t{}^2\rangle} = \frac{\langle\delta i_t{}^2\rangle}{i_t{}^2},$$

or, after substitution of eqs (5.31) and (5.35),

$$\frac{P_{\mathrm{AM},u}}{P_c} = \frac{1}{4}\frac{1}{[1-D(\gamma v_a)]^2}\frac{\langle\delta I_{c0}{}^2\rangle}{I_{c0}{}^2}. \tag{5.36}$$

In sec. 7.2 we shall see that this equation can also be derived directly [46]) from our IMPATT-diode model, using the results obtained in secs 3.2.2 and 3.2.3.

The down-conversion of oscillator noise is governed by the factor Λ defined by (see eq. (5.15))

$$\Lambda = \frac{\delta V_{i_t}}{\varrho\, R_{Bt}} = \left(\frac{\mathrm{d}i_t}{\mathrm{d}I_{c0}}\right)\left(\frac{\partial}{\partial i_t}\delta V_{0r}\right)\frac{1}{R_{Bt}}, \tag{5.37}$$

where δV_{0r} is given by eq. (3.45), for which we shall write

$$\delta V_{0r} = -\zeta\, v_a{}^2. \tag{5.38}$$

In spite of the poor agreement between theory and experiment found for the effect of d.c. restorage as discussed in sec. 3.2.5, we believe it to be appropriate to investigate the factor Λ somewhat further. From eqs (3.35), (5.24), (5.33), (5.35), (5.37) and (5.38) it can be found after straightforward calculations that

$$\Lambda = -\frac{2\zeta}{\gamma^2}\frac{1}{I_{st}}\frac{1}{R_{Bt}}f(\gamma v_a), \tag{5.39}$$

where

$$f(\gamma v_a) = \frac{I_1(\gamma v_a)}{I_0(\gamma v_a)}\frac{\gamma v_a}{B(\gamma v_a)}\frac{1+B(\gamma v_a)}{1-D(\gamma v_a)}.$$

In fig. 5.7 the function $f(\gamma v_a)$ is plotted for the minimum and the maximum value of $\omega_{a,\mathrm{st}}^2/\omega_0^2$ as given in table 5-I. It is easily shown that

$$\lim_{\gamma v_a \to 0} f(\gamma v_a) = 2$$

and

$$\lim_{\gamma v_a \to \infty} f(\gamma v_a) = \gamma v_a \left(1 - \frac{\omega_{a,\mathrm{st}}^2}{\omega_0^2}\right).$$

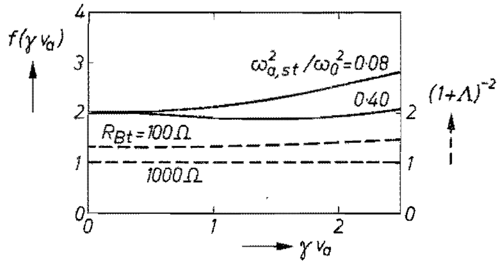

Fig. 5.7. The function $f(\gamma v_a)$ describing the signal-level dependence of the down-conversion factor Λ for $\omega_{a,\mathrm{st}}^2/\omega_0^2$ equal to 0·08 and 0·40, being the upper and lower limits of $\omega_{a,\mathrm{st}}^2/\omega_0^2$ in table 5-I. The function $(1 + \Lambda)^{-2}$ for diode no. 7 in table 5-I has been plotted for a total bias resistance R_{Bt} = 100 and 1000 Ω, respectively.

We note that the limit for $\gamma v_a \to 0$ is a constant $\neq 0$, so that Λ is non-zero at the start of the oscillations. This is due to the fact that we are dealing with the derivative of δV_{0r} with respect to i_t and not with δV_{0r} itself, which is zero at the start of the oscillations. Also given in fig. 5.7 is the factor $(1 + \Lambda)^{-2}$ for diode no. 7 of table 5-I, assuming $\zeta = 6 . 10^{-3}\ \mathrm{V}^{-1}$, for $R_{Bt} = 1000\ \Omega$ and $R_{Bt} = 100\ \Omega$. The latter value was chosen to approximate the situation $R_B = 0$ for this diode. The value of ζ was estimated from fig. 3.19*b* by taking the slope of the tangent in the origin, using eq. (3.32) and the data given in table 5-I. We conclude that the factor $(1 + \Lambda)^{-2}$ is very close to unity even for $R_{Bt} = 100\ \Omega$. So we might expect the effect of down-conversion to be very slight for this diode even at low values of the bias resistance R_B. This conclusion is, of course, only valid within the RVM of the diode.

Finally we conclude from fig. 5.7 and the data given in table 5-I that within the RVM of the diode eq. (5.37) can be approximated by

$$\Lambda = -4 \frac{\zeta}{\gamma^2} \frac{1}{I_{\mathrm{st}}} \frac{1}{R_{Bt}}.$$

6. LINEAR THEORY OF IMPATT-DIODE-OSCILLATOR NOISE

6.1. Introduction

In chapter 5 we outlined some of the results of the general theory of oscillator noise and applied these results to the special case of an IMPATT-diode oscillator. In this chapter, and also in chapter 7, the oscillator noise will be discussed starting from the noise properties of the IMPATT diode itself, according to the diagram in fig. 6.1.

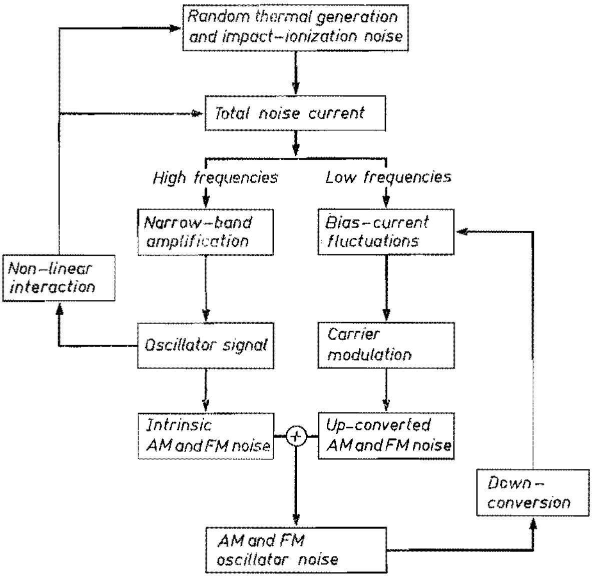

Fig. 6.1. Block diagram of the origin of IMPATT-diode-oscillator noise.

IMPATT-diode-*oscillator* noise of course also originates from the random character of the thermal-generation and impact-ionisation processes. The noise connected with these processes has been discussed in chapter 4 for the case of a non-oscillating diode. There can be a comparable discussion for the oscillating diode taking its large-signal properties into account. Again we shall arrive at a total noise current flowing through the diode [11]). As in chapter 5, we shall discuss the r.f. and l.f. components of this current separately, taking the r.f. components first.

If noise is disregarded, an oscillator loop has to be undamped completely to make stable oscillations possible. In that case the total loop resistance is zero and, consequently, the quality factor of the loop is infinitely high and the spectrum width is zero. If noise is taken into account its r.f. components can be considered as an input signal into the loop. Hence the loop does not have to be undamped completely to obtain a certain amount of output power. The output signal now consists of narrow-band, amplified noise 70,80,81), and the total loop resistance, R_t, is slightly larger than zero. This last makes the quality factor Q of the loop finite. Consequently the spectrum of the output signal has a finite width $2\,\Delta\omega_0$,

$$2\,\Delta\omega_0 = \omega_0/Q = \omega_0{}^2\,R_t\,C \neq 0, \tag{6.1}$$

where C is the total capacitance of the oscillating diode.

The "input noise" caused by the noise-generation mechanism in the IMPATT diode is amplified and filtered by the circuit. In this chapter we assume the signal level so low that the output signal can be taken to consist mainly of *linearly* amplified noise, while the non-linearity only enters as the mechanism ensuring that the amount of amplification in the "noise amplifier" remains finite according to the non-linear theory described in sec. 3.2. This is the reason for calling this chapter "Linear theory of IMPATT-diode-oscillator noise".

The linear amplification precludes the possibility of mixing products of the components of the noise current itself, and of the noise current and the signal current. Hence the linear theory accounts only for the intrinsic oscillator noise, i.e. the noise caused by the r.f. components of the total noise current. At higher signal levels the signal dependence of the noise generation and the influence of the signal level on the total noise current have to be considered more carefully. In the diagram in fig. 6.1 this is indicated schematically by "non-linear interaction". Non-linear oscillator noise will be discussed in chapter 7. In that chapter the effects of up-conversion and down-conversion will be discussed, too, since these effects only arise via a non-linearity. For the discussions in the present chapter it is sufficient to know that in the experimental situation the conditions in the bias circuit can be chosen so as to make the effects of up-conversion and down-conversion negligible. This can be concluded from eqs (5.16) and (5.37).

Sections 6.3 and 6.4 deal with the FM and AM components of the intrinsic oscillator noise, respectively. In sec. 6.5 the possibilities of reducing oscillator noise will be discussed. We continue now with a discussion of the width and form of the output spectrum.

6.2. Width and form of the output spectrum

By analogy with the discussion of the noise in the non-oscillating diode we start the present discussion from the Read–Langevin equation for the total conduction current in the avalanche region

$$\tau_i \frac{\mathrm{d}}{\mathrm{d}t} I_c(t) = I_c(t)\,(\overline{\alpha}\,l_a - 1) + g_n. \tag{6.2}$$

As stated in the introduction to this chapter we assume that the signal level is so low that the noise is amplified linearly. On this assumption we obtain from eq. (6.2):

$$j\,\omega\,\tau_i\,i_{nc} = I_{c0}\,\overline{\alpha}'\,v_{na} + (2\,q\,I_{c0}\,\mathrm{d}f)^{1/2}, \tag{6.3}$$

by taking the first-order perturbation of that equation. Equation (6.3) describes the relation between the conduction noise current i_{nc} and the noise voltage v_{na} in a frequency band df around frequency ω. The difference between eq. (6.3) and the equivalent equation for the non-oscillating diode, eq. (4.10), is that eq. (6.3) describes the response to small deviations from a stationary low-level oscillation while eq. (4.10) describes the response to small deviations from the d.c. situation. It should be emphasised that the similarity between eqs (4.10) and (6.3) only arises because we restrict ourselves to low signal levels.

Along the lines as indicated at the end of sec. 4.2 we arrive at the equation for the total noise current flowing through the diode (see also eq. (4.8)),

$$\langle i_{nt}{}^2\rangle = \frac{2\,q\,I_{c0}\,\mathrm{d}f}{\omega^2\,\tau_i{}^2}\,\frac{|\Phi|^2}{\omega^2\,C_d{}^2\,(1-\omega_a{}^2/\omega_0{}^2)^2}\,\frac{1}{|Z_t|^2}, \tag{6.4}$$

where Z_t is the total impedance in the oscillating loop. Equation (6.4) contains the large-signal avalanche frequency ω_a as defined by eq. (3.25). As in sec. 5.4.2, we assume that for the singly tuned, low-Q_L circuit used the oscillator loop may be considered as a simple LCR series resonance circuit. Then Z_t reads as

$$Z_t = R_t + jX_t = R_s + R_c + R_L + R_{\mathrm{depl}} + j\omega L + 1/j\omega C, \tag{6.5}$$

where R_t has been decomposed according to fig. 3.10. We next assume, for the narrow frequency range $\omega = \omega_0 \pm \Omega$ of interest, the total loop resistance R_t, the inductance L and the capacitance C to be frequency-independent and to have a value equal to their value at the oscillation frequency ω_0. From eqs (6.1) and (6.5) we then obtain

$$|Z_t|^2 = R_t{}^2\left[1+\left(\frac{\omega-\omega_0}{\Delta\omega_0}\right)^2\right]. \tag{6.6}$$

As will be clear from the introduction to this chapter, the output power delivered to the load resistance R_L is given by

$$P_L = \frac{1}{2\pi}\int_0^\infty \frac{\langle i_{nt}{}^2\rangle(\omega)}{\mathrm{d}f}\,R_L\,\mathrm{d}\omega, \tag{6.7}$$

where $\langle i_{nt}{}^2\rangle/\mathrm{d}f$ is the power-density spectrum of the total noise current given by eq. (6.4). Via eqs (6.4) and (6.6) the factor $1 + (\omega-\omega_0)^2/(\Delta\omega_0)^2$ enters into the integral of eq. (6.7). This factor is the only highly frequency-dependent factor in the integration, since the quality factor Q of the almost undamped loop is very high (10^4 to 10^6), so that $\Delta\omega_0$ is small. Taking this consideration into account we obtain the relation

$$P_L = \frac{q}{2\pi} \frac{|\Phi|^2}{\tau_i^2} \frac{I_{c0} R_L C}{\omega_0^2 R_t C_d^2} \frac{1}{(1-\omega_a^2/\omega_0^2)^2} \int_{-2Q}^{\infty} \frac{\mathrm{d}x}{1+x^2},$$

where $x = (\omega - \omega_0)/\Delta\omega_0$. For the high values of Q the value of the integral is well approximated by π. After substitution we find

$$R_t = \frac{q}{2} \frac{|\Phi|^2}{\tau_i^2} \left\{ \omega_0^2 C_d \left[\frac{W}{l_d} - \left(1 - \frac{\sin\theta}{\theta}\right) \frac{\omega_{a,st}^2}{\omega_0^2} \right] \left(1 - \frac{\omega_{a,st}^2}{\omega_0^2}\right) \right\}^{-1} \frac{I_{c0} R_L}{P_L}, \quad (6.8)$$

where use has been made of eq. (5.21). It should be noted that P_L in this equation is still unknown, and consequently R_t is still unknown. However, the value of P_L can be obtained from the noise-free oscillator theory since we may expect that

(a) R_t is very much smaller than $R_L + R_s + R_c$, so that its effect on the value of the impedance of the oscillating diode is negligible;

(b) most of the output power is contained in a narrow frequency band around the oscillation frequency, i.e. the centre frequency of the spectrum.

For an experimental determination of R_t, P_L can simply be read from a power meter. In fig. 6.2 theoretical values of R_t for 5 diodes presented in table 5-I

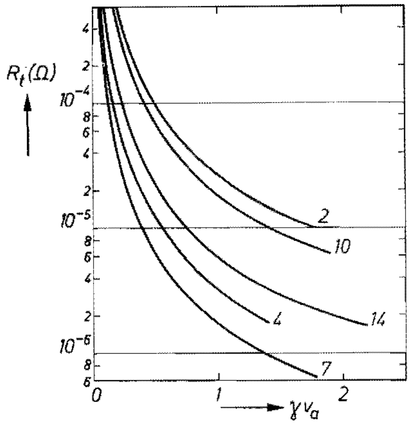

Fig. 6.2. The total loop resistance R_t at $\omega = \omega_0$ as a function of γv_a for 5 diodes given in table 5-I. The circuit is assumed to be fixed.

are given as a function of γv_a ($0 < \gamma v_a \leqslant (\gamma v_a)_{\max}$) *). The values were calculated using eqs (3.30), (3.32), (6.8) and the constants given in table 5-I. From fig. 6.2 we conclude that, except for extremely low values of γv_a, actually $R_t \ll R_L$. Furthermore, we conclude that R_t decreases with increasing signal level, i.e. with increasing values of γv_a. The latter is caused by the fact that P_L increases more than linearly with I_{c0} (note that I_{c0} and P_L in eq. (6.8) are not independent variables).

Once R_t is known, we also know the halfwidth of the spectrum:

$$2\,\Delta\omega_0 = \frac{q\,|\Phi|^2}{2\,\tau_i^2}\left[\frac{W}{l_d} - \left(1 - \frac{\sin\theta}{\theta}\right)\frac{\omega_{a,\mathrm{st}}^2}{\omega_0^2}\right]^{-2}\frac{I_{c0}\,R_L}{P_L}. \qquad (6.9)$$

In many practical cases this equation can be approximated by

$$2\,\Delta\omega_0 = \frac{q\,|\Phi|^2}{2\,\tau_i^2}\left(\frac{l_d}{W}\right)^2\frac{I_{c0}\,R_L}{P_L},$$

as was already discussed in connection with eq. (5.28).

Making use of the relation $P_L = \frac{1}{2}\,|i_t|^2\,R_L$, where i_t is the amplitude of the r.f. current at $\omega = \omega_0$, we can simply write $2\,\Delta\omega_0 = \text{constant}\times I_{c0}/|\,i_t|^2$. From this relation we conclude that for a fixed value of I_{c0} the spectrum width decreases with increasing signal level. This can be understood from the discussion given in the introduction of this chapter. If I_{c0} is fixed the noise-excitation current is fixed. For increasing signal levels the loop has to be undamped more and more which means that R_t becomes ever smaller. Consequently the spectrum width decreases. Equation (6.9) will be discussed in more detail in sec. 6.5.

Figure 6.3*a*–*f* shows a series of photographs **) taken from the display screen of a spectrum analyser (HP852A). The diode under test was diode no. 10 of table 5-I ($R_L = 5{\cdot}1\ \Omega$). The signal level increases going from fig. 5.3*a* to fig. 5.3*f*. We conclude that the spectrum width first decreases with increasing signal level, but then increases at higher signal levels. In fig. 6.4 we plotted the theoretical spectrum width calculated from eq. (6.9) and the constants given in table 5-I. We also plotted the spectrum width obtained from figs 5.3*b*–*f*. Since it is impossible to determine this width directly from the photographs with any accuracy, we assumed that the spectrum can be described by a Lorentz curve, i.e. by a curve of the form $1/(1 + x^2)$. By so doing, the width can be calculated, for example, from the ratio of the noise power (in the 100-kHz band

---

*) The value of $(\gamma v_a)_{\max}$ concerns the range of validity of the diode model, RVM, with regard to the output power and large-signal impedance, hence not with regard to the linear noise theory.

**) The author is indebted to H. Tjassens for making these results available.

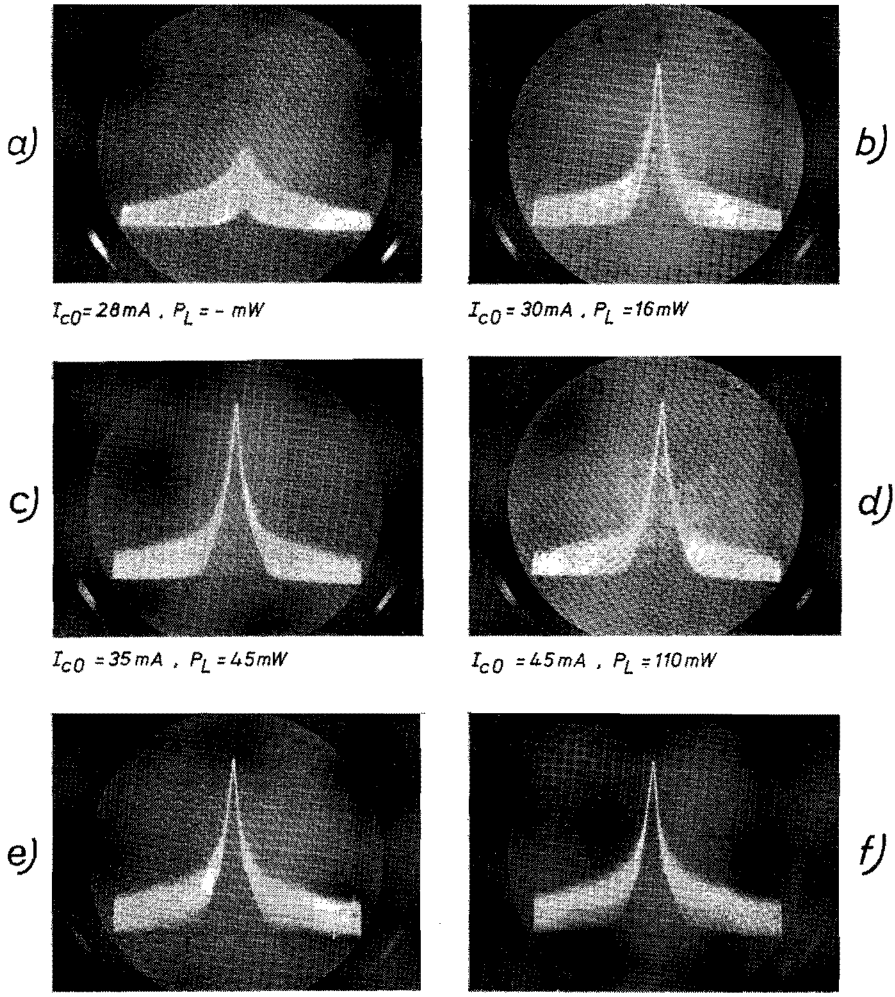

$I_{c0} = 28 mA$, $P_L = -$ mW

$I_{c0} = 30 mA$, $P_L = 16 mW$

$I_{c0} = 35 mA$, $P_L = 45 mW$

$I_{c0} = 45 mA$, $P_L = 110 mW$

$I_{c0} = 55 mA$, $P_L = 181 mW$

$I_{c0} = 70 mA$, $P_L = 270 mW$

Fig. 6.3. The output spectrum, photographed from the display screen of a spectrum analyser, of diode no. 10 in table 5-I ($R_L = 5{\cdot}1\ \Omega$) for various values of the output power. Horizontal scale 1 MHz/division, vertical scale 10 dB/division. Bandwidth 100 kHz.

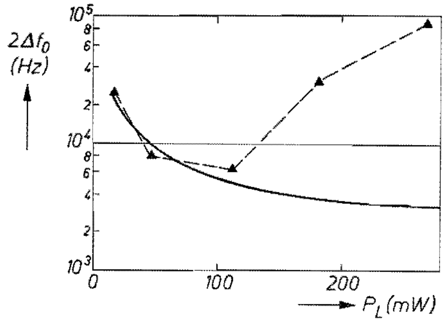

Fig. 6.4. Calculated half-width of the output spectrum (drawn curve) and experimental half-width (triangles) determined from the photographs given in fig. 6.3.

used) at a distance of 1 MHz from the carrier to the carrier power. From fig. 6.4 we conclude that at low signal levels there is good agreement between theory and experiment. At higher signal levels the linear oscillator-noise theory is clearly no longer applicable. Figures 6.3 and 6.4 were presented mainly as an illustration. In secs 6.3 and 6.4 the linear oscillator noise will be traced more accurately, using the noise-measuring equipment described in sec. 5.2.

The use of a Lorentz curve in the description of the output spectrum can be accounted for as follows. In the derivation of the expression of the ratio of the intrinsic AM to FM noise power as described in sec. 5.4.2, we assumed that for the oscillators used the oscillator loop may be considered as a simple LCR resonance circuit. At the end of that section we found good agreement between theory and experiment, and concluded that the LCR-circuit representation can indeed be used. In the present chapter we also used this representation and moreover assumed the circuit quantities to have constant values in the frequency band $\omega_0 \pm \Omega$ of interest. These assumptions imply that in this theory the output spectrum is symmetrical around the frequency ω_0 and can be described by a Lorentz curve. If we account for the frequency dependence of R_{depl} and C, it is found from a numerical investigation that over the frequency range investigated, i.e. $\omega_0 \pm 100 \times 2\,\Delta\omega_0$ the spectrum still follows a Lorentz curve in a very good approximation. This is also found from experiments, an example of which is given in fig. 6.5. In this figure the spectrum already presented in fig. 5.1 is shown together with a Lorentz curve fitted at 200 kHz from the carrier (the deviations very close to the carrier are predominantly caused by the long-term instability of the oscillator and the spectrum analyser during the writing of the spectrum).

In chapter 5 we decomposed the spectrum in a carrier containing all the output power and in upper and lower sidebands. Since the spectrum is now known, the relevance of this decomposition can be estimated. An example is given in fig. 6.6 where we plotted the output power contained in a frequency

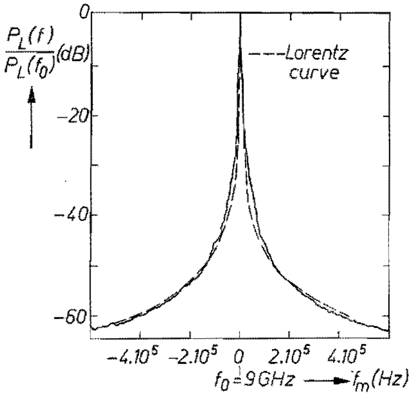

Fig. 6.5. The output spectrum of fig. 5.1, together with a Lorentz curve fitted at $\Omega/2\pi = 200$ kHz.

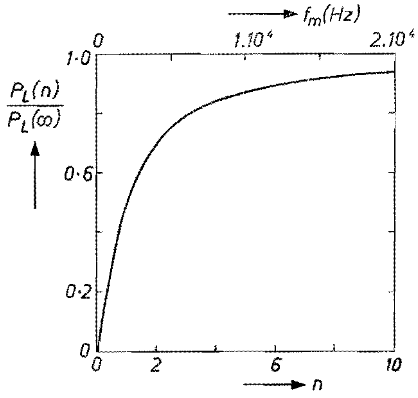

Fig. 6.6. The normalised output power obtained by integration of the noise power dissipated in the load resistance over intervals $f_0 \pm n\,(2\,\Delta f_0)$ as a function of n, and as a function of $f_m = \Omega/2\pi$ in case $2\,\Delta f_0 = 4000$ Hz.

band ($f_0 \pm n\,\Delta f_0$), normalised to the value of the output power for $n = \infty$. The distance to the carrier, f_m, is also indicated in the case $2\,\Delta f_0 = 4$ kHz. This value corresponds to $\Delta f_{\text{rms}} = 250$ Hz in a 100-Hz band assuming eq. (5.6) to be applicable. From fig. 6.6 we conclude that the frequency band $f_0 \pm 20$ kHz already contains more than 90% of the total output power. In the present example 99·4% of the total output power is contained in the frequency band $f_0 \pm 200$ kHz.

We finally emphasise that our theory for the form and width of the output spectrum makes no pronunciation on the type of intrinsic noise involved: FM, AM or a mixture of both.

6.3. Intrinsic FM oscillator noise

It is found experimentally that the intrinsic oscillator noise of a singly tuned, low-loaded-Q IMPATT-diode oscillator is predominantly FM noise. It is very probable that this is found because of the amplitude-limiting non-linearity of the diode. In figs 5.5 and 5.6 we have seen that the AM noise power is at least 40 dB below the FM noise power at not too extreme low values of the signal level. Hence it is reasonable to assume that the spectrum of the output signal is determined by the FM noise only, and to check whether this noise can actually be described by eq. (6.9). For the latter purpose we express the spectrum width in terms of quantities which are more commonly used in FM-noise measurements, such as Δf_{rms} and P_{FM}/P_c. Form eqs (5.6) and (6.9) it follows for $f_m \gg 2\,\Delta f_0$ that

$$(\Delta f_{\mathrm{rms}})^2 = \frac{q\,|\Phi|^2}{4\,\tau_i^2}\,R_L\,\mathrm{d}f\left[\frac{W}{l_d}-\left(1-\frac{\sin\theta}{\theta}\right)\frac{\omega_{a,\mathrm{st}}{}^2}{\omega_0{}^2}\right]^{-2}\frac{I_{c0}}{P_L}, \qquad (6.10)$$

while eq. (5.5) states that

$$\frac{P_{\mathrm{FM}}}{P_c} = \frac{(\Delta f_{\mathrm{rms}})^2}{2 f_m{}^2}\,.$$

In these equations the noise contribution of a single sideband is considered. The conversion from Δf_{rms} to P_{FM}/P_c can easily be made using fig. 6.7.

The r.m.s. frequency deviation given by eq. (6.10) does not depend on $\Omega = 2\,\pi f_m$. This is due to the Lorentz-curve shape of the spectrum. The constant Δf_{rms} has been found experimentally for silicon [5,82,83]) and germanium [84]) diodes. For gallium-arsenide diodes an increase of Δf_{rms} has been observed [85,86]) for values of $f_m \lesssim 100$ kHz. This effect has been attributed to the up-conversion of a $1/f$ type of noise present in these diodes [86]). At first sight this up-conversion into FM oscillator noise is in contradiction to the conclusion arrived at in sec. 5.4 that there is no up-converted FM noise. In sec. 7.2 it will be discussed that this conclusion, inferred from an idealised model, has to be regarded with some reserve and that up-converted FM noise can be present. In our experiments where $f_m = 200$ kHz, that is larger than the 100 kHz mentioned above, it is assumed tht the $1/f$ type of noise which might be present in the GaAs diode may be neglected.

It is difficult to estimate theoretically the range of validity on the linear oscillator-noise theory. As a first check of the theory we investigated [63,87]) experimentally several types of diodes at a signal level such that $\gamma v_a = 1$, i.e. $I_{c0} = 1{\cdot}12\ I_{\mathrm{st}}$ as follows from eq. (3.25). From table 5-I it is known that $(\gamma v_a)_{\max} > 1$ for all diodes investigated. This, of course, is a prerequisite condition which has to be fulfilled when one is checking the linear oscillator-noise

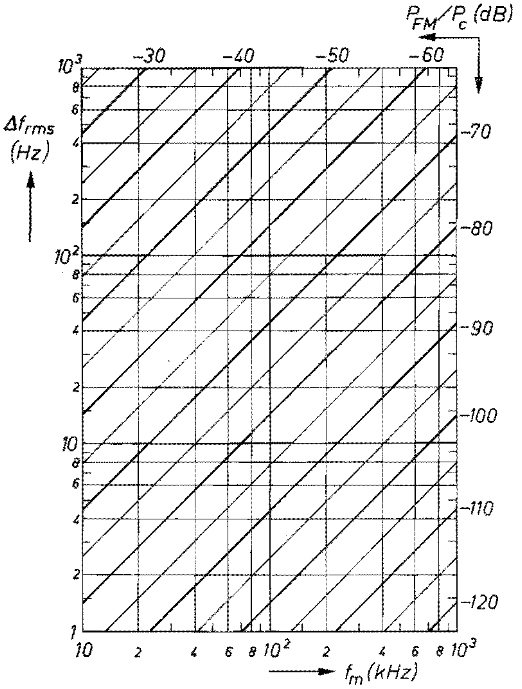

Fig. 6.7. Conversion of P_{FM}/P_c to Δf_{rms}. For example, at $f_m = 200$ kHz, $P_{\mathrm{FM}}/P_c = -70$ dB corresponds to $\Delta f_{\mathrm{rms}} = 90$ Hz, where P_{FM} and Δf_{rms} are related to the same bandwidth.

theory. Results of Δf_{rms}, experimental as well as theoretical, are presented in table 6-I. The lines along which we arrived at the data given in columns 5 and 6 of table 6-I are given schematically in fig. 6.8. The bias current at the start of the oscillations, I_{st}, was read from a current meter, after which the d.c. current was adjusted to 1·12 I_{st} and the power P_L was read from a power meter. All data were substituted into eq. (6.10), and the results for Δf_{rms} obtained in this way (the theoretical results), are given in the 5th column of table 6-I. The bandwidth df was taken 100 Hz. In addition, we measured the ratio $P_{\mathrm{FM},i}/P_c$ at a distance of 200 kHz from the carrier in a 100-Hz band following the procedure outlined in sec. 5.2. The experimental values of Δf_{rms} derived from $P_{\mathrm{FM},i}/P_c$ are given in the 6th column of table 6-I. In particular when taking into account the large number of independent measurements needed, comparison of the data in columns 5 and 6 leads to the conclusion that there is good agreement between theory and experiment. So, at least at low signal levels, the assumption that the intrinsic oscillator noise is predominantly FM noise which can be described by expressing the spectrum width in terms of the r.m.s. frequency deviation only, resulted in a good agreement between theory and experiment.

For the Si p^+–n diode no. 2, the Si n^+–p diode no. 8, and the GaAs Schottky-

TABLE 6-I

Calculated and experimentally determined r.m.s. frequency deviation of the diodes given in table 5-I. The signal level is always chosen such that $\gamma v_a = 1$, i.e. $I_{c0} = 1{\cdot}12\ I_{st}$. Bandwidth $df = 100$ Hz; the distance to the carrier $f_m =$ 200 kHz

no.	type	R_L (Ω)	P_L (mW)	Δf_{rms} calculated (Hz)	Δf_{rms} measured (Hz)	θ (rad)
2	Si p^+–n ($V_{BR} =$ 66 V)	3·1	9	414	432	1·2
4	Si p^+–n ($V_{BR} =$ 100 V)	1·6	12	130	131	1·9
7	Si n^+–p ($V_{BR} =$ 111 V)	0·5	7	77	58	2·3
10	Ge n^+–p ($V_{BR} =$ 32 V)	6·8	15	265	300	1·6
14	n-GaAs S.B. ($V_{BR} =$ 50 V)	2·2	17	130	185	1·1

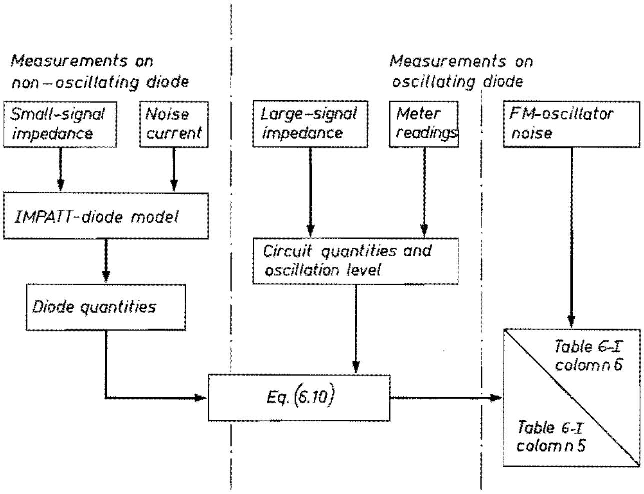

Fig. 6.8. Block diagram of the experimental check of eq. (6.10). A similar diagram is applicable to eq. (6.12).

barrier diode no. 14 mentioned in table 5-I we investigated the FM noise as a function of the signal level. The results of this investigation, carried out along the same lines as in fig. 6.8, are presented in figs 6.9 and 6.10. In this case we

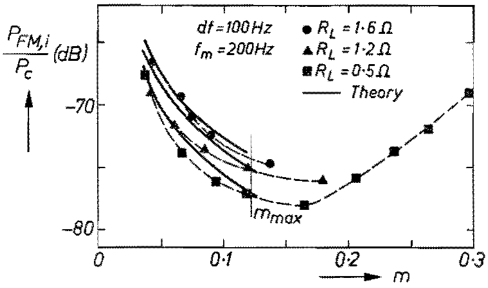

Fig. 6.9. The ratio of the single-sideband intrinsic FM noise power to the carrier power as a function of the modulation depth for the silicon n^+–p diode no. 8 in table 5-I for three values of the load resistance. See also fig. 3.16.

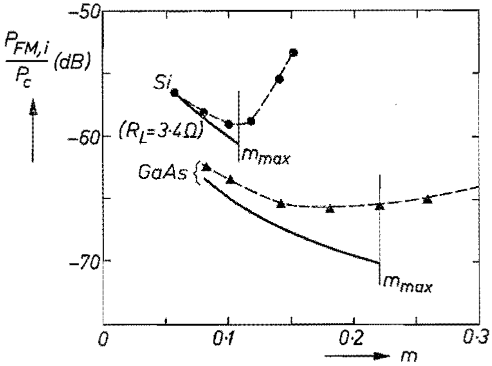

Fig. 6.10. The ratio of the single-sideband intrinsic FM noise power to the carrier power as a function of the modulation depth for the silicon p^+–n diode no. 2 and the gallium-arsenide diode no. 14 in table 5-I.

expressed the FM noise in terms of $P_{\mathrm{FM},i}/P_c$ in a 100-Hz band. The noise data are given as a function of the modulation depth m defined as the ratio of the total a.c. voltage across the diode to the breakdown voltage. The experimentally determined maximum modulation depth $m_{\max}$ within the RVM of the diode is indicated. The value of $m_{\max}$ was derived from $(\gamma v_a)_{\max}$. The theoretical curves were calculated from

$$\frac{P_{\mathrm{FM},i}}{P_c} = K_{\mathrm{FM}} \frac{I_{c0}}{P_L}, \tag{6.11}$$

where, for the fixed circuit used in each measurement, K_{FM} is given by

$$K_{\mathrm{FM}} = \frac{q\,|\Phi|^2}{4\,\Omega^2\,\tau_i^{\,2}} \left[\frac{W}{l_a} - \left(1 - \frac{\sin\theta}{\theta}\right)\frac{\omega_{a,\mathrm{st}}^{\;2}}{\omega_0^{\;2}}\right]^{-2} R_L\,\mathrm{d}f.$$

The theoretical curves can be calculated for $m \leqslant m_{\max}$ only. From figs 6.9 and 6.10 we learn that all experimental curves for $P_{\mathrm{FM},i}/P_c$ as a function of m show the same general behaviour. See also fig. 6.4, where $2\,\Delta f_0$ is given as a function of P_L for the Ge n^+-p diode no. 10. First, at low values of m, the noise decreases with increasing m, as it should according to our linear noise theory. Second, at high values of m, the noise increases with increasing signal level which is in contradiction to this theory. In chapter 7 we shall see that the increase in noise at high values of m is predominantly caused by the signal dependence of the total noise current which, we repeat, is assumed to be independent of the signal level in the linear noise theory.

To the author's knowledge the decreasing part of the experimental curves has not been discussed explicitly in the literature, whereas it is this part in particular that can be described by our linear theory. Cowley et al.[88]) have reported the increasing part of the curves but not the decreasing part. This is most probably due to their measuring method, as they measured the noise as a function of the load resistance at a fixed (high) bias current and a fixed frequency. Since they did not measure up to very high values of this resistance they did not observe the decrease in noise with increasing signal level at low values of m. When an estimate is made for the diode parameters needed in eq. (6.10) for the diodes studied by Cowley et al. it is found that eq. (6.10) accounts reasonably well for the nosie data at the highest values of the load resistance reported by these authors.

From figs 6.9 and 6.10 we conclude that, for the diodes investigated, the linear oscillator-noise theory can be used up to a modulation depth of about 0·1, which is roughly about 30% of the maximum attainable modulation depth [47]). For the gallium-arsenide diode the agreement at the lowest values of m is not as good as for the silicon diodes. We believe that deviation found for the gallium-arsenide diode, even at a low value of m, might be caused by the effect of diffusion of the free carriers, which was not accounted for in the analysis. As has been shown by Hulin and Goedbloed [60]) the effect of carrier diffusion in gallium-arsenide diodes is much more pronounced than in silicon diodes. However, we also learn from fig. 6.10 that for the GaAs diode investigated, the deviation at low values of m is still less than 3 dB. It has also been found [60]) that in germanium diodes the effect of carrier diffusion is pronounced. However, the determination of the experimental noise data for the germanium diode, fig. 6.4, was too crude to draw conclusions.

6.4. Intrinsic AM oscillator noise

In the foregoing section we concluded that the assumption that the spectrum width is predominantly caused by FM noise and can be described by our expression for this spectrum width led to good agreement between theory and experiment. Consequently the linear noise theory does not provide directly for an expression for the intrinsic AM oscillator noise. The latter expression, however, can be obtained by using results for the ratio of the intrinsic AM to FM noise power as obtained in sec. 5.4.2. The expression for this ratio was confirmed experimentally as valid over the whole range $m \leqslant m_{\text{max}}$. It is then obvious to combine eqs (5.28) and (6.10) to an expression for the ratio of the single-sideband intrinsic AM noise power to carrier power

$$\frac{P_{\text{AM},i}}{P_c} = \frac{2q}{\omega_0^2\,\tau_i^2}\,B^2(\gamma v_a)\,\frac{I_{c0}\,R_L}{P_L}\,\mathrm{d}f, \tag{6.12}$$

where $B(\gamma v_a)$ is given by eq. (5.27). We note that eq. (6.12) does not explicitly contain the transit-time function Φ and the ratio W/l_a as is the case for the FM noise. Therefore the AM noise depends much less on the transit time than the FM noise. Furthermore, the ratio $P_{\text{AM},i}/P_c$ is independent of Ω, the distance from the carrier, which is in agreement with experimental results reported by Josenhans [5]).

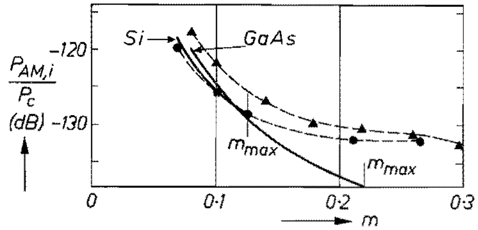

Fig. 6.11. The ratio of the single-sideband intrinsic AM noise power to the carrier power as a function of the modulation depth for the silicon n^+–p diode no. 7 and the gallium-arsenide diode no. 14 in table 5-I. See also fig. 5.6.

In fig. 6.11 a comparison is made between theory and experiment for the same gallium-arsenide diode as in fig. 6.10, and for the silicon n^+–p diode reported in fig. 5.6, sec. 5.4.2. The results were obtained along the same lines as sketched in fig. 6.8 for the FM noise. For the silicon diode we observe that once again agreement between theory and experiment is good and that this agreement for the gallium-arsenide diode is less good, just like the FM noise of this diode. Therefore, we believe that here, too, the diffusion of the free carriers might play a role. But, again at low values of m the deviation is less than 3 dB, as it should be since the ratio $P_{\text{AM},i}/P_{\text{FM},i}$ for this diode agreed well with theory, as was shown in fig. 5.6.

The intrinsic AM noise in a Read diode oscillator has been discussed by Johnson and Robinson [89]). Their expression for $P_{\text{AM},i}/P_c$, eq. (10) of ref. 89, differs from our eq. (6.12), when the same conditions are considered. We believe that this is due mainly to the fact that they did not take into account the effects of frequency and bias-current fluctuations on the admittance of the avalanche region (eq. (1) of ref. 89). Neglecting frequency fluctuations is not justified since the intrinsic noise is predominantly FM noise. The bias-current fluctuations cannot be neglected since the variations of the a.c. voltage across the avalanche region are related to (r.f.) bias-current fluctuations through the avalanche frequency which is a constant for an oscillating diode in their diode model as well as in ours. Furthermore, if frequency fluctuations are taken into account, their assumption that the sum of the load impedance and the unperturbed diode impedance vanishes, has also to be reconsidered.

6.5. Reduction of intrinsic oscillator noise

As shown by several authors, the oscillator noise can be reduced either by circuit techniques 75,76,82,90–92), or by injection-phase-locking techniques 11,75,93,94) or by effects of harmonics 95–97). In but few papers, however, the reduction of oscillator noise is discussed starting from device parameters 15,32,98). We shall do this in the present section for the reason that if the noise can be reduced by device modelling, it can be reduced further by the other techniques mentioned above. We shall first give a brief discussion of the reduction of FM noise on the basis of eq. (6.10), and of the AM noise on the basis of eq. (6.12).

Equation (6.10) reads

$$(\Delta f_{\mathrm{rms}})^2 = \frac{q\,|\Phi|^2}{4\,\tau_i^2}\left[\frac{W}{l_d} - \left(1 - \frac{\sin\theta}{\theta}\right)\frac{\omega_{a,st}^{\;2}}{\omega_0^{\;2}}\right]^{-2}\frac{I_{c0}\,R_L}{P_L}\,\mathrm{d}f,$$

while from eqs (3.23), (3.24) and (3.31) it is easily derived that

$$\frac{I_{c0}\,R_L}{P_L} = \frac{\omega_0^{\;2}\,C_0^{\;2}}{(\mathrm{Im}\,\Phi)^2}\left(\frac{W}{l_d}\right)^2\frac{(R_L + R_s + R_c)^2}{2\,I_{c0}}\left(\frac{I_0(\gamma v_a)}{I_1(\gamma v_a)}\right)^2. \tag{6.13}$$

From these equations we can draw the following conclusions:

(1a) The r.m.s. frequency deviation is inversely proportional to the intrinsic response time τ_i. From fig. 4.5, where τ_i is given as a function of the length of the avalanche region, we conclude that if diodes with the same length of avalanche region are compared, the germanium and gallium-arsenide diodes have an advantage over silicon diodes, as far as τ_i is concerned. Using this argument, the improvement of the noise-to-carrier ratio over silicon diodes as observed experimentally by Rulison et al. 84) for germanium diodes and by Baranowsky et al. 85) for gallium-arsenide diodes can be understood. However, as we shall see later in this section, the conclusion that germanium diodes have a better noise performance than silicon diodes 84) in general is not correct. Hence a more careful formulation of the conclusion is necessary.

(1b) The r.m.s. frequency deviation is proportional to the transit-time function Φ. For values of the transit angle of the drift region θ, where $\theta < 2\pi$, it is found that $|\Phi|$ decreases with increasing value of θ. However, when the transit-time function is considered, we must bear in mind that the factor $I_{c0}\, R_L/P_L$ depends on Im Φ. From eqs (6.10) and (6.13) it then follows that the explicit transit-angle dependence of Δf_{rms} is given by

$$|\Phi|^2/(\mathrm{Im}\,\Phi)^2 = 1 + \tan^2 \varphi,$$

where use has been made of eq. (3.9), and we neglected

$$[1 - (\sin \theta)/\theta]\, \omega_{a,\mathrm{st}}{}^2/\omega_0{}^2$$

compared to W/l_a. We recall that $\tan \varphi$ is the slope of the $X(R)$ curve of the diode under breakdown conditions. The dependence of $\tan \varphi$ on θ for various values of the ratio l_a/l_d has already been presented in fig. 3.4. From that figure we conclude that for the values of l_a/l_d found experimentally for our diodes, see table 5-I, $\tan \varphi \to \infty$ for $\theta \to 0$ and for $\theta \to 2\pi$, while the minimum value of $\tan \varphi$ is attained for $\pi < \theta < 2\pi$.

(1c) At first sight the r.m.s. frequency deviation increases with increasing area since it is proportional to C_0. However, a more careful consideration indicates that this conclusion is not true in general. This is due to the fact that the bias current I_{c0} is not an independent variable: I_{c0} has to be larger than the start oscillation current while the latter current, among other things, also depends on the diode area.

Next we briefly discuss the expression for the intrinsic AM noise, eq. (6.12), again together with eq. (6.13) for the factor $I_{c0}\, R_L/P_L$. The AM noise is given by

$$\frac{P_{\mathrm{AM},i}}{P_c} = \frac{2q}{\omega_0{}^2\, \tau_i{}^2}\, B^2(\gamma v_a)\, \frac{I_{c0}\, R_L}{P_L}\, \mathrm{d}f,$$

where $B(\gamma v_a)$ is given by eq. (5.27). From eqs (6.12) and (6.13) we can draw the following conclusions:

(2a) The AM noise decreases with increasing value of τ_i, see also conclusion (1a).

(2b) The direct dependence of $P_{\mathrm{AM},i}/P_c$ on θ is now determined by

$$(\mathrm{Im}\,\Phi)^{-2} = [(1 - \cos \theta)/\theta]^{-2},$$

the minimum value of which is obtained for $\theta \approx 3\pi/4$.

(2c) At first sight the AM noise increases with increasing total resistance and increasing diode area. This conclusion turns out not to be valid in general. This again is caused by I_{c0}, which also depends on the diode area, as does $\omega_0{}^2/\omega_{a,\mathrm{st}}{}^2$ which forms part of the function $B(\gamma v_a)$.

We next present some of the results of computer investigations of eqs (6.10) and (6.12), taking all dependent and independent variables into proper account. We shall successively answer questions how the oscillator noise can be reduced by a proper choice of the value of (1) the transit angle, (2) the junction area, and (3) the thickness of the epitaxial layer used in the fabrication of the diodes.

Question 1

What is the value of the transit angle θ corresponding to minimum FM and AM noise for the types of diode used in our singly tuned, low-Q oscillator circuit?

The question is answered assuming that the following conditions are fulfilled.

(a) The output power P_L is 20 mW, which is an acceptable value for the output power of a local oscillator.

(b) The oscillation frequency is 10 GHz.

(c) The signal level is such that $\gamma v_a = 1$. This value was chosen because the results obtained in secs 6.3 and 6.4 indicate that the linear noise theory can be used up to $\gamma v_a = 1$.

(d) The depletion layer is never restricted by the substrate so that the ratio l_d/W can be assumed to be a constant for a given type of diode. The saturated drift velocity is known from table 3-I, so that W can be calculated from θ, ω_0 and l_d/W.

(e) The diode area $A = 2 \, . \, 10^{-8}$ m^2.

(f) The total loss resistance $R_s + R_c$ is a constant equal to 1·3 Ω. This was assumed to limit the number of variables as, strictly speaking, R_c is not a constant [38]), because the diode capacitance, which in this case is a function of θ, is part of the transformer between the diode chip and the coaxial line.

(g) The values of $\overline{\alpha}'$ and τ_i needed in the calculations were assumed to be given by

$$\overline{\alpha}' = p \, l_a^{\,q}$$

and

$$\tau_i = \tau_D + p \, l_a^{\,q},$$

where the values of the constants p, q and τ_D were obtained from the experimental and theoretical results discussed in chapter 4. The values of these constants are listed in table 6-II.

The computer calculations were carried out along the following lines. From eqs (3.31) and (3.32) it follows that

$$P_L = \frac{\omega_0^{\,4} \, C_a^{\,2}}{2} \left(\frac{\tau_i}{\overline{\alpha}'} \right)^2 \left(1 - \frac{\omega_0 \, (R_L + R_s + R_c)}{(1 - \cos \theta)/\theta + \omega_0 \, C_d \, (R_L + R_s + R_c)} \right)^2 R_L (\gamma v_a)^2 . \tag{6.14}$$

TABLE 6-II

Experimental relations for the intrinsic response time as a function of the length of the avalanche region: $\tau_i = \tau_D + p\, l_a^q$, and for the field derivative of the average ionisation coefficient: $\bar{\alpha}' = p\, l_a^q$, see chapter 4

material/ type	τ_i (s)			$\bar{\alpha}'$ (V^{-1})	
	τ_D (s)	p ($s\,m^{-1}$)	q	p ($V^{-1}\,m^{-1}$)	q
Si p^+–n	$0{\cdot}6 \,.\, 10^{-12}$	$1{\cdot}03 \,.\, 10^{-7}$	0·76	$4{\cdot}94 \,.\, 10^{-6}$	–0·75
Si n^+–p	$0{\cdot}6 \,.\, 10^{-12}$	$1{\cdot}03 \,.\, 10^{-7}$	0·76	$4{\cdot}94 \,.\, 10^{-6}$	–0·75
Ge n^+–p	$3{\cdot}4 \,.\, 10^{-12}$	$3{\cdot}04 \,.\, 10^{-6}$	0·97	$3{\cdot}92 \,.\, 10^{-6}$	–0·81
n-GaAs S.B.	$3{\cdot}2 \,.\, 10^{-12}$	$5{\cdot}00 \,.\, 10^{-6}$	1·00	$1{\cdot}71 \,.\, 10^{-5}$	–0·70

In this equation for a given value of θ, R_L is now the only unknown quantity, since all other quantities directly follow from the conditions (a) to (g), given above. Thus R_L can be solved from eq. (5.14) using an iterative calculation procedure. The value of $\omega_{a,\mathrm{st}}^2$ now follows from eq. (3.31), which, rewritten, reads

$$\omega_{a,\mathrm{st}}^2 = \frac{\omega_0^3\,(R_L + R_c + R_s)\,C_d}{(1 - \cos\theta)/\theta + \omega_0\,C_d\,(R_L + R_s + R_c)}\,. \qquad (6.15)$$

The next step is to calculate I_{c0} from

$$I_{c0} = \frac{\omega_{a,\mathrm{st}}^2\,C_a}{2\gamma v_a}\left(\frac{\tau_i}{\bar{\alpha}'}\right)\frac{I_1(\gamma v_a)}{I_0(\gamma v_a)}\,. \qquad (6.16)$$

This equation easily follows from eqs (3.4) and (3.30). Since all relevant diode and circuit quantities are now known, Δf_{rms} and $P_{\mathrm{AM},i}/P_c$ can be calculated. The calculations were performed for a silicon n^+–p, a silicon p^+–n, a germanium n^+–p, and an n-type gallium-arsenide Schottky-barrier diode, respectively, since for these diodes we know the value of the various diode parameters. The results of these calculations are presented in fig. 6.12. From fig. 6.12*a* we draw the following conclusions for the FM noise:

(1) The r.m.s. frequency deviation shows a minimum for $\theta \approx 4{\cdot}5$ radians. Moreover, the position of the minimum is almost the same for all types of diodes investigated. Further investigation showed that variations of P_L, A, γv_a and $R_s + R_c$ affected the minimum value of Δf_{rms} but hardly affected the value of θ where this minimum was reached. From this we conclude that θ is a relevant parameter along the abscissa when comparing noise properties of

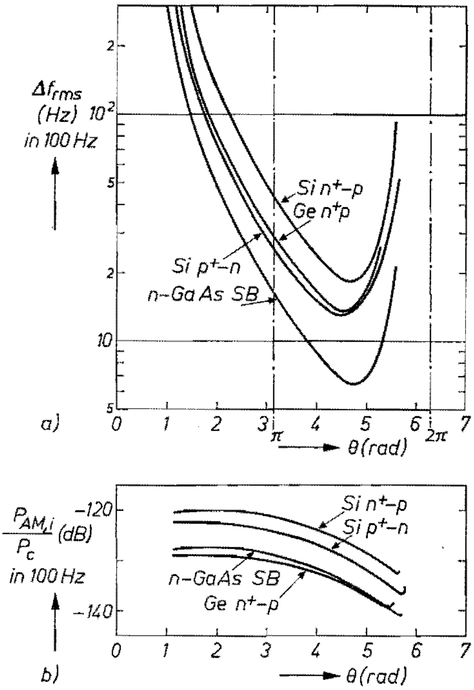

Fig. 6.12. (*a*) The calculated r.m.s. frequency deviation, single-sideband ($df = 100$ Hz), as a function of the transit angle θ of the drift region for 4 types of diodes. The main boundary conditions are $P_L = 20$ mW, $f_0 = 10$ GHz, $\gamma v_a = 1$, $A = 2.10^{-8}$ m², $R_s + R_c = 1 \cdot 3\ \Omega$. (*b*) The calculated ratio of the single-sideband AM noise power to the carrier power ($df = 100$ Hz), for the same diodes and for the same boundary conditions as given in fig. 6.12*a*.

our oscillators equipped with diodes of various types and geometrical dimensions.

(2) The value of Δf_{rms} can be reduced considerably by choosing a relatively large transit angle for the diode. In many cases the transit angle θ is chosen $\approx 3\pi/4$ rad, so as to optimise the output power of the oscillator. However, if not much output power is needed, and a low-noise oscillator is wanted, it is advantageous to choose a higher value of θ. This conclusion is in conformity with the experimental results presented in table 6-I. We believe that a considerable part of the noise reduction found by Goldwasser et al.[91]) has to be ascribed to the fact that the transit angle of the diode used was larger than π rad, and not only to the circuit techniques used.

(3) For a given value of θ the gallium-arsenide diode has the best noise performance, followed by the silicon p^+–n and germanium n^+–p diode, while the silicon n^+–p diode has the worst noise performance. However, for a given length W of the depletion layer, say 5 μm, the situation is completely different. This is shown in fig. 6.13 where the same values of Δf_{rms} as in fig. 6.12*a* are plotted as a function of W. Comparing the results given in figs 6.12*a* and 6.13

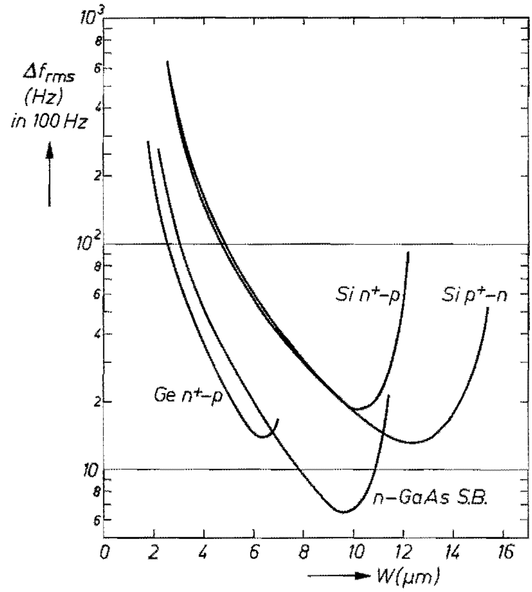

Fig. 6.13. The calculated r.m.s. frequency, as given in fig. 6.12*a*, but now as a function of the length *W* of the depletion layer.

it is clear that a statement like "germanium and gallium-arsenide diodes always have an improved noise performance over silicon diodes" is in general incorrect. We must be careful as to what types are involved when we compare diodes.

(4) It is certainly possible to make low-noise oscillators equipped with silicon diodes. This is interesting from a technological point of view. In general the silicon technology is preferred to the gallium-arsenide technology, while epitaxially grown germanium is rarely manufactured. It should be noted, however, that germanium is an interesting material for IMPATT-diode oscillators since it combines good noise behaviour, a low breakdown voltage, a good conversion efficiency [38]) and a well-known technology.

(5) For a given value of θ the Δf_{rms} of the silicon n^+–p diode is larger than that of the silicon p^+–n diode. This is caused predominantly by the fact that for the n^+–p diodes l_a, and hence also τ_i, is smaller than l_a for the p^+–n diodes.

From fig. 6.12*b* we observe that the AM noise does not depend as pronouncedly on θ as the FM noise does. The minimum AM noise is obtained at a value of $\theta \approx 5{\cdot}5$ radians.

For values of θ near 2π radians, both the FM and AM noise strongly increase with increasing θ. This is caused by the fact that Im $\Phi = 0$ for $\theta = 2\pi$. This makes the output power $P_L = 0$, as can be concluded from eq. (6.13). Consequently, the FM and AM noise become infinitely high when θ approaches 2π, as the bias current needed to obtain the output power required becomes infinitely high. The increase in bias current, and also in breakdown voltage, with increasing values of θ makes the practical realisation of the oscillator with minimum noise at $\theta \approx 4{\cdot}5$ rad difficult because the power dissipated in the diode becomes very large.

Question 2

What is the optimum junction area for low oscillator noise for the types of diode used in our singly tuned, low-Q oscillator circuit?

The question is answered assuming that the conditions of question 1 are fulfilled with the value of θ fixed at $\theta = \pi$ rad, and with the exception of condition (e). The junction area A was varied from $0{\cdot}3 \,.\, 10^{-8}$ m^2 up to $6{\cdot}0 \,.\, 10^{-8}$ m^2. From fig. 6.14*a* we learn that at low values of A, Δf_{rms} strongly depends on A, and that the optimum junction area for the FM noise is about $3 \,.\, 10^{-8}$ m^2. Figure 6.14*b* shows that the AM noise decreases with increasing junction area for the range of A investigated. It serves no useful purpose to investigate the oscillator noise for still higher values of A since the practical

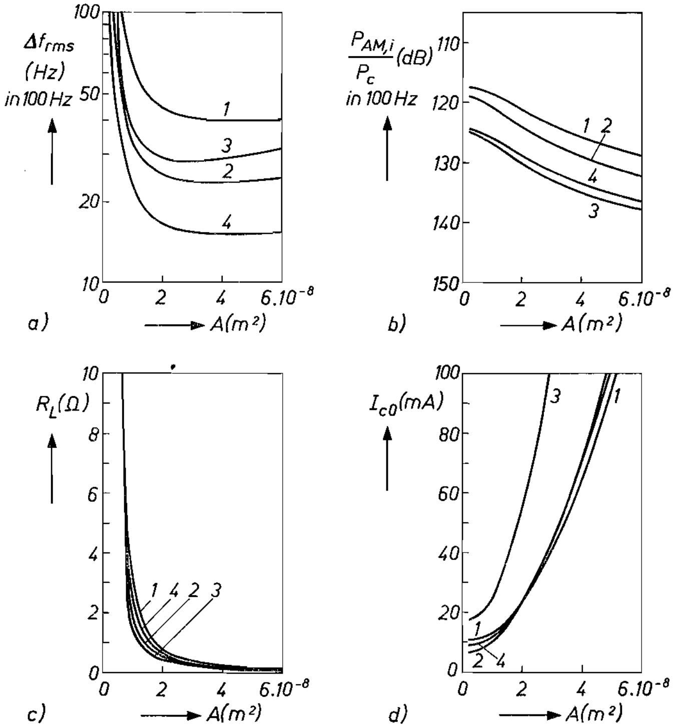

Fig. 6.14. Results of calculations as a function of the junction area for 4 types of diodes. The main boundary conditions are $P_L = 20$ mW, $f_0 = 10$ GHz, $\gamma v_a = 1$, $\theta = \pi$ rad, $R_s + R_c = 1{\cdot}3\,\Omega$. 1 : Si n^+–p; 2 : Si p^+–n; 3 : Ge n^+–p; 4 : n-GaAs S.B.
(*a*) The r.m.s. frequency deviation ($\mathrm{d}f = 100$ Hz). (*b*) The ratio of the single-sideband AM noise power to the carrier power ($\mathrm{d}f = 100$ Hz). (*c*) The load resistance R_L needed in the actual circuit. (*d*) The bias current I_{c0} needed to obtain 20 mW (note that here $I_{c0} = 1{\cdot}12\, I_{\mathrm{st}}$, since $\gamma v_a = 1$).

realisation of the oscillator must be possible. Figure 6.14*c* shows that the load resistance corresponding to $A = 3 \, . \, 10^{-8}$ m^2 is about 0·2–0·4 Ω, which is difficult to realise in a practical situation. Hence this puts a restriction on the magnitude of the junction area in practice. The power which can be dissipated in the diode also restricts this magnitude. From fig. 6.14*d* we conclude that I_{c0} strongly increases with increasing junction area, and hence the power dissipated likewise.

Question 3

What is the influence on the oscillator noise of the series resistance of the "unswept" region of the epitaxial layer, and what is the influence on the noise caused by a restriction of the depletion layer by the substrate?

The question is answered for a silicon n^+–p diode with the conditions (a), (b), (c), (e) and (g) of question 1, and the conditions

(h) the transit angle of the non-restricted diode is $\theta = \pi$ (as in question 2);

(i) the minimum loss resistance which arises from circuit losses and contact losses is 1 Ω;

(j) the signal level is so low that it does not affect the value of the series resistance of the unswept material [48], so that we consider the passive resistance only [99];

(k) in the range of interest it is assumed that a restriction of the depletion layer by the substrate does not affect the position and shape of the avalanche region.

The results of the calculations are given in fig. 6.15. The horizontal axis gives the thickness of the epitaxial layer counted, in this figure, from the left-hand-side boundary of the depletion layer. The length l_a of the avalanche region and of the non-restricted depletion layer, W_0, are indicated. From fig. 6.15 we conclude that for the conditions quoted the optimum FM-noise performance is found for just punch-through of the depletion layer. Both the restriction of the depletion layer and the series resistance of the unswept layer give rise to an increase in FM noise. The reverse effect is found for the AM noise.

In the foregoing we tried to gain some insight into the reduction of oscillator noise by means of a proper choice of the device parameters. As mentioned at the beginning of this section a further reduction of the noise is possible by using circuit techniques and/or locking techniques. For example, diode no. 7 of table 5-I was placed in an oscillator circuit based on ideas put forward by Kurokawa [100] *). We then obtained an output power of about 60 mW with $\Delta f_{\mathrm{rms}} = 0{\cdot}8$ Hz (in 100 Hz at 200 kHz from the carrier), which is even slightly better than an X-13 klystron [93]. IMPATT-diode oscillators, in particular those equipped with silicon diodes, have the reputation of being noisy oscil-

---

*) The circuit was built in our laboratory by H. Tjassens [101].

lators. From the foregoing it might be clear that if one needs a low-noise oscillator, one should use an IMPATT-diode oscillator.

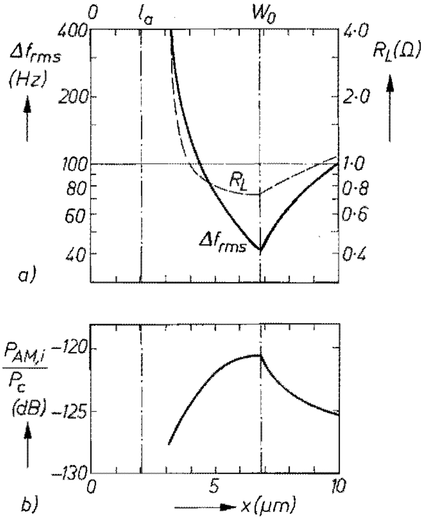

Fig. 6.15. Results of calculations as a function of the amount of restriction of the depletion layer by the substrate ($x \leqslant W_0$), and as a function of the length of unswept region ($x > W_0$), for a silicon n^+–p diode: $P_L = 20$ mW, $f_0 = 10$ GHz, $\gamma v_a = 1$, $\theta = \pi$ rad. The resistivity of the epitaxial layer was assumed to be 3·2 Ω cm.
(*a*) The r.m.s. frequency deviation (df = 100 Hz) and the load resistance. (*b*) The ratio of the single-sideband AM noise power to the carrier power.

7. NON-LINEAR IMPATT-DIODE-OSCILLATOR NOISE

7.1. Introduction

In this chapter we allow for non-linear effects with regard to the oscillator noise as distinct from the linear treatment of this noise given in the previous chapter. Therefore the present chapter deals with the dependence of the noise generation on the signal level and with modulation noise (with the term modulation noise we denote the effect of the r.f. noise on the l.f. noise and the reverse, i.e. down-conversion as well as up-conversion). This type of noise was already treated partly in sec. 5.4.3, where we derived expressions for it on the basis of the general theory of oscillator noise. The interaction of low- and high-frequency components of the noise described as modulation noise should be distinguished from the interaction arising from mixing of the noise at several frequencies and the harmonics of the signal.

In sec. 7.3 the discussion is again limited to the intrinsic oscillator noise. In that section the difference between the measured oscillator noise and that predicted by the linear noise theory will be discussed. A brief account will be given on large-signal noise theories presented in the literature.

7.2. Modulation noise

In this section we discuss the right-hand-side branch of the diagram fig. 6.1 presented in sec. 6.1, i.e. we discuss the inter-relationship between the oscillator noise and the l.f. components of the total noise current flowing through the diode. The frequency of these components is assumed to be sufficiently low, compared with the oscillation frequency, to be thought of as bias-current fluctuations. In the present discussion the signal level can have any value within the RVM of the diodes.

The connection between l.f. noise and r.f. oscillator noise, viz. up-conversion and down-conversion, has already been discussed briefly in sec. 5.4.3. In that section the general theory of oscillator noise was applied to the IMPATT-diode oscillator. We there concluded that there is no up-conversion of l.f. noise into FM oscillator noise. This conclusion can also be obtained from eq. (3.29b) in sec. 3.2, since this equation states that the oscillation frequency is influenced neither by the bias current nor by the signal level. In sec. 5.4.3, furthermore, an expression was derived to describe the up-conversion of l.f. noise into AM oscillator noise and, finally, we made some remarks on the down-conversion of oscillator noise. We shall continue with the effect of down-conversion first.

Assuming there is no correlation between the l.f. and r.f. components of the bias-current fluctuations, it is easily found by substitution of the intrinsic part of δi_t (eq. (5.16)) in eq. (5.30) that

$$\langle \delta I_{c0}{}^2 \rangle = \varrho^2\, \varLambda^2\, \frac{P_{\mathrm{AM},i}}{P_c} + \frac{\langle e_l{}^2 \rangle}{R_{Bt}{}^2\,(1+\varLambda)^2}.$$

Substituting $\varrho = \mathrm{d}I_{c0}/\mathrm{d}i_t$ from eq. (5.35) gives, with $P_c = \frac{1}{2}\, i_t{}^2\, R_L$:

$$\langle \delta I_{c0}{}^2 \rangle = 2\, I_{c0}{}^2\, [1 - D(\gamma v_a)]^2\, \frac{P_{\mathrm{AM},i}}{P_c}\, \varLambda^2 + \frac{\langle v_{n0}{}^2 \rangle}{R_{Bt}{}^2\,(1+\varLambda)^2}, \qquad (7.1$$

where $R_{Bt} = R_0 + R_B$ is the total bias-loop resistance, $\langle v_{n0}{}^2 \rangle = \langle e_l{}^2 \rangle$ is the mean-square value of the l.f.-noise-voltage source in series with the diode, which is assumed to cause the l.f. noise present, and $\varLambda$ is the factor governing the down-conversion. $\varLambda$ is given by eq. (5.39), and in the present discussion it is sufficient to know that $\varLambda$ is, among other things, inversely proportional to R_{Bt}. In sec. 5.4.3 a theoretical estimate was made of the value of $(1 + \varLambda)^2$ and it was found that this value was close to unity, even for low values of the total bias resistance. We shall show now that experimental evidence that $(1 + \varLambda)^2 \approx 1$, at least within the RVM of the diode, can be obtained from a further investigation of eq. (7.1). Estimating the magnitude of the two terms on the right-hand side of this equation it is found for the diodes investigated that eq. (7.1) is well approximated by

$$\langle \delta I_{c0}{}^2 \rangle = \frac{\langle v_{n0}{}^2 \rangle}{R_{Bt}{}^2\,(1+\varLambda)^2}, \qquad (7.2)$$

for normal values of R_{Bt}. The value of $\langle \delta I_{c0}{}^2 \rangle$ can be determined from the value of the noise voltage across the known bias resistor R_B. Assuming $\varLambda \ll 1$, $\langle v_{n0}{}^2 \rangle$ can be calculated from eq. (7.2) using the experimental values of $\langle \delta I_{c0}{}^2 \rangle$ and R_0 *). The values of $\langle v_{n0}{}^2 \rangle$ found in this way for an Si n^+-p diode are presented in fig. 7.1*c*. From this figure we conclude that the mean-square value of the l.f.-noise-voltage source is independent of R_B, and hence of R_{Bt} **). Since $\varLambda$ is inversely proportional to R_{Bt}, we can conclude that $(1 + \varLambda)^2 \approx 1$. Hence the effect of down-conversion is negligible in this case. Further investigations within the RVM, also using other types of diodes, have never been

---

*) The theory of the noise-free IMPATT diode of chapter 3 does not provide an accurate expression for the l.f. diode resistance R_0. Moreover the actual value of R_0 is very much influenced by temperature effects as was discussed in sec. 3.2.5. Hence, we have to use the experimental value R_0 (at the frequency f_m). The a.c. measuring current has to be taken very small in order to avoid non-linear effects via up-conversion.

**) The value of R_0 is assumed to be independent of R_B in order to avoid a very complicated diode model. This assumption is supported by the experimental observations that the bias voltage, the output power and the oscillation frequency are all independent of R_B. We tried to confirm the assumption experimentally, and found it to be correct within the experimental error which, however, is rather large at low values of R_B. This is the reason why we made the a priori assumption of a constant R_0 when R_B is varied (note that R_0 can vary with the signal level).

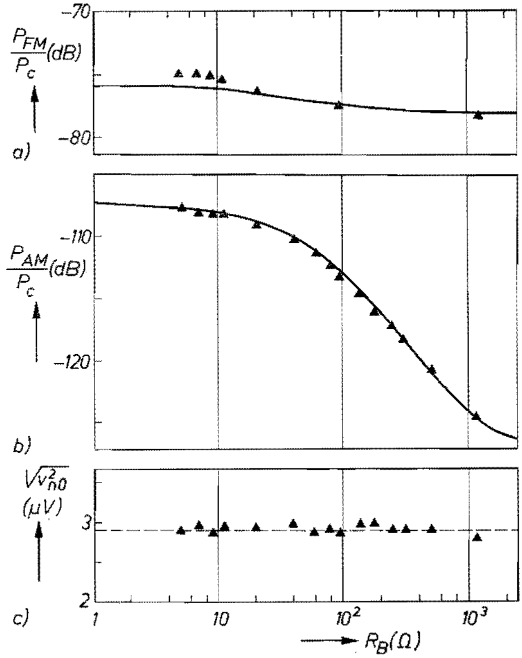

Fig. 7.1. Modulation noise of diode no. 7 in table 5-I (Si n^+–p, $V_{\mathrm{BR}} = 111$ V) as a function of the bias resistance at 200 kHz. The bias current is fixed; the modulation depth is 0·09.
(*a*) Total FM noise at 200 kHz from the carrier in a 100-Hz band. (*b*) Total AM noise at 200 kHz from the carrier in a 100-Hz band. (*c*) Open-circuit noise voltage of the bias circuit at 200 kHz in a 100-Hz band.

fruitful in demonstrating experimentally the occurrence of down-conversion. A final discussion will be given at the end of this section. We now continue with a discussion of the up-converted oscillator noise, in which we shall neglect a possible effect of down-conversion.

Equation (5.36), which describes the up-conversion of the bias-current noise into AM oscillator noise, has been obtained from an application of the general theory of oscillator noise. However, this equation can also be derived directly from our IMPATT-diode model [46]). For that purpose we combine eqs (3.33) and (3.34) to the following equation for the relative variations of the output power as a function of those of the bias current

$$\frac{\delta P_L}{P_L} = \frac{2}{1 - D(\gamma v_a)} \frac{\delta I_{c0}}{I_{c0}} + \frac{1}{[1 - D(\gamma v_a)]^2} \frac{\delta I_{c0}{}^2}{I_{c0}{}^2},$$

where $D(\gamma v_a)$ is given by eq. (3.35). When determining noise powers the mean value of δI_{c0} is zero. Hence, the above equation reduces to

$$\frac{\langle \delta P_L \rangle}{P_L} = \frac{1}{[1 - D(\gamma v_a)]^2} \frac{\langle \delta I_{c0}{}^2 \rangle}{I_{c0}{}^2}, \tag{7.3}$$

Equation (7.3) gives the change in the average output power due to the l.f. noise current imposed on the bias current. From that equation we obtain for the ratio of the single-sideband up-converted AM noise power to carrier power

$$\frac{P_{\mathrm{AM},u}}{P_c} = \frac{1}{4}\,\frac{1}{[1 - D(\gamma v_a)]^2}\,\frac{\langle \delta I_{c0}{}^2 \rangle}{I_{c0}{}^2}, \tag{7.4}$$

where $P_{\mathrm{AM},u}$ and $\langle \delta I_{c0}{}^2 \rangle$ have to be measured in the same bandwidth, at a distance of f_m from the carrier and at a frequency f_m, respectively. Equations (7.4) and (5.36) are identical. Assuming no correlation between the l.f. and r.f. components of the total noise current, the noise powers of the up-converted and intrinsic noise are additive, that is

$$\frac{P_{\mathrm{AM}}}{P_c} = \frac{P_{\mathrm{AM},u}}{P_c} + \frac{P_{\mathrm{AM},i}}{P_c}. \tag{7.5}$$

Furthermore, eq. (7.2) now reads

$$\langle \delta I_{c0}{}^2 \rangle = \frac{\langle v_{n0}{}^2 \rangle}{R_{Bt}{}^2} = \frac{\langle v_{n0}{}^2 \rangle}{(R_B + R_0)^2}. \tag{7.6}$$

From eqs (7.4) and (7.6) we conclude that for a given and fixed adjustment of the oscillator the amount of up-converted noise can be varied by varying the bias resistance R_B only. Results of experiments on a silicon n^+–p diode are given in fig. 7.1*b*, those for an *n*-GaAs Schottky-barrier diode in fig. 7.2. In both figures the theoretical curves (drawn curves) were calculated from eqs (7.4)

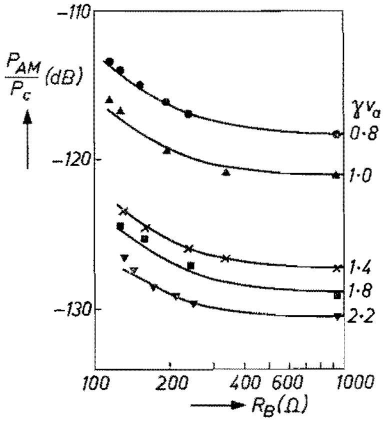

Fig. 7.2. Total AM noise of diode no. 14 in table 5-I (*n*-GaAs S.B., $V_{\mathrm{BR}} = 50$ V) as a function of the bias resistance for several values of γv_a. The noise was measured at 200 kHz from the carrier in a 100-Hz band.

to (7.6), using the experimental values of R_0, R_B and $\langle \delta I_{c0}^2 \rangle$. Theory and experiment were fitted at $R_B = 1200\ \Omega$ to obtain the value of $P_{\mathrm{AM},i}/P_c$, in all cases studied. The value of $P_{\mathrm{AM},i}/P_c$ was taken independent of R_B, since down-conversion is neglected. From figs 7.1*b* and 7.2 we conclude that the agreement between theory and experiment is good.

Figure 7.1*a* shows that the FM noise really is somewhat influenced by R_B. Hence, the idealised diode model, which predicts that the FM noise does not depend at all on the l.f. noise because it is not up-converted, has to be refined. The presence of up-converted FM noise is not quite unexpected because in sec. 3.2.3 we already found a slight shift in oscillation frequency when the bias current was varied. If this shift is present, it automatically ensures that bias-current fluctuations are up-converted into oscillation-frequency fluctuations. The shift of the oscillation frequency could be explained by mentioning that a change of bias current causes a change in bias voltage which, in turn, varies the cold capacitance of the diode, and consequently the oscillation frequency. It was concluded in sec. 3.2.3 and shown in fig. 3.14 that, within the RVM, the fourth power of the oscillation frequency is proportional to the d.c. voltage across the diode. Using this conclusion, a phenomenological expression for the up-converted FM noise can be derived as follows.

As is discussed in sec. 5.1, the signal frequency can be written in the form

$$f = f_0 + \Delta f \cos (2\pi f_m t), \tag{7.7}$$

where f_0 is the frequency of the carrier (the oscillation frequency) and Δf the amplitude of the frequency deviation due to the FM noise present in the noise sideband, of width $\mathrm{d}f$, at f_m from the carrier. On the other hand, we know that the oscillation frequency is a function of the bias voltage. Hence, we can also write

$$f = f_0 + \frac{\partial f_0}{\partial V_0} \langle v_n^2 \rangle^{1/2} \cos 2\pi f_m t, \tag{7.8}$$

where $\langle v_n^2 \rangle$ is the mean-square value of the l.f.noise voltage across the diode. Assuming $f_0^4 = K V_0$, we obtain from eqs (7.7), (7.8) and (5.5) the relation

$$\frac{P_{\mathrm{FM},u}}{P_c} = \frac{1}{32} \frac{K^2}{f_m^2 f_0^6} \frac{R_0^2}{R_{Bt}^2} \langle v_{n0}^2 \rangle, \tag{7.9}$$

where, as in the case of the up-converted AM noise, we assumed that the l.f. noise is caused by a voltage source $\langle v_{n0}^2 \rangle$ in series with the diode. If no correlation is present between the intrinsic and up-converted noise, the FM noise is given by

$$\frac{P_{\mathrm{FM}}}{P_c} = \frac{P_{\mathrm{FM},u}}{P_c} + \frac{P_{\mathrm{FM},i}}{P_c}. \tag{7.10}$$

The theoretical curve in fig. 7.1*a* was calculated from eqs (7.9) and (7.10), and the experimental values of K, R_0, R_B and $\langle \delta I_{c0}{}^2 \rangle$. The intrinsic FM noise was determined in the same way as was done for the intrinsic AM noise needed in eq. (7.5). We conclude that the agreement between theory and experiment is rather good *).

In conclusion we remark that the up-converted noise is indeed predominantly AM noise, which is in agreement with experimental observations made by Scherer [102]) and Thaler [103]). It should be noted that the results given in fig. 7.1, say at $R_B = 10\ \Omega$, that $P_{\mathrm{FM},u}/P_c \approx 10^{-8}$ while $P_{\mathrm{AM},u}/P_c \approx 10^{-11}$. We thus see that the up-converted FM noise is larger by a factor of 10^3 compared to the up-converted AM noise. However, since the intrinsic FM and AM noise differ by a factor of 10^4 to 10^5, the up-conversion into FM noise can still be neglected, whereas the up-conversion into AM noise is not negligible.

In the investigation of the up-converted noise it was found experimentally that the value of $\langle v_{n0}{}^2 \rangle$ increased with the signal level over its small-signal value, measured at the same value of the bias current. On the other hand it was found that at a fixed value of the bias current, $\langle v_{n0}{}^2 \rangle$ of the oscillating diode did not change when the bias resistance was varied. Hence, the signal dependence of $\langle v_{n0}{}^2 \rangle$ cannot be explained by the effect of down-conversion. The increase of intrinsic AM and FM noise with respect to their values predicted by the linear oscillator-noise theory of chapter 6, as is found experimentally, cannot be explained by a mechanism including the effect of down-conversion either. These conclusions are in contradiction with those of Weidmann [77,78]), and of Mouthaan and Rijpert [79]), who concluded that the up-conversion–down-conversion loop influences the oscillator noise a great deal, even at intermediate signal levels. In our opinion this discrepancy is partly caused by the fact they did not take into account the signal dependence of the driving noise source, which is found to occur without the effect of modulation noise. Hence, in this respect, their theories are small-signal theories. Moreover, they did not give a full account of the combined dependence of the diode impedance on ω_0, Ω, i_t and I_{c0}, as can be verified by comparing their theories with the oscillator-noise theory put forward by Vlaardingerbroek [12]). Follow-

---

*) Another origin for the up-conversion into FM noise could be the complex avalanche frequency which was found in the extended small-signal model of the diode. In sec. 3.1.4 we defined this complex avalanche frequency by the relation $\overline{\omega}_{a1}{}^2 = \omega_{a1}{}^2\,(1 - j\sigma)$, where the real quantity σ resulted from the extension of the diode model with respect to that summarised in sec. 2.4. If we assume the avalanche frequency to be a complex quantity in the large-signal model, too, we find from an equation equivalent to eq. (3.29) that

$$\sigma = -\mathrm{Im}\, g(\omega_0)/\mathrm{Re}\, g(\omega_0).$$

Thus we now find that the oscillation frequency is also determined by the imaginary part of the avalanche frequency. Consequently, up-converted FM noise results if (but only if) σ depends on the bias current. Unfortunately, it is not possible to obtain a theoretical estimate of the large-signal dependence of σ.

ing our conclusions, for example, the lack of agreement between theory and experiment at low and intermediate signal levels found in fig. 11 of ref. 79, can be understood. It should be emphasised that, with these authors, we think that the up-conversion–down-conversion loop can be of importance at signal levels near the saturation of the oscillator.

7.3. Excess noise

In secs 6.3 and 6.4 we concluded that with increasing signal level the measured intrinsic FM and AM noise becomes larger than the intrinsic noise predicted by the linear oscillator-noise theory. On the other hand, this deviation between experiment and theory was not observed when the ratio of the intrinsic AM to FM noise was considered, as can be concluded from fig. 5.6. Furthermore, as already mentioned in the previous section, the l.f. noise increases with the signal level with respect to its small-signal value, where this increase could not be ascribed to the effects of modulation noise. From all those observations we draw the conclusion that the common origin of the FM, AM and l.f. noise, viz. the total noise current, grows with the signal level. In fig. 7.3 a survey is presented of the available data for the excess noise Δ (in dB) as a function of the modulation depth, where Δ is defined by

$$\Delta = (P_{\mathrm{FM},i}/P_c)_{\mathrm{meas.}}/(P_{\mathrm{FM},i}/P_c)_{\mathrm{lin.theory}} \qquad (7.11)$$

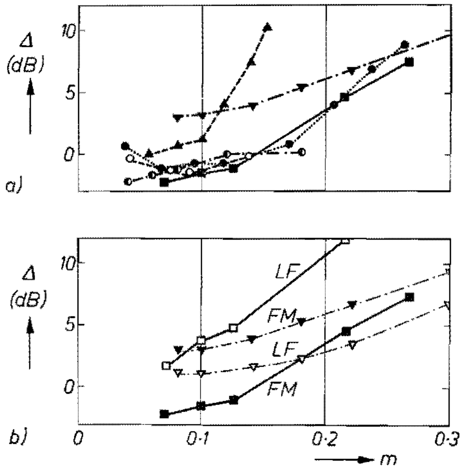

Fig. 7.3. Excess noise established experimentally compared to the noise predicted by the linear noise theory.
(*a*) Data derived from FM-noise measurements and calculations: black triangles: Si p^+–n, $V_{\mathrm{BR}} = 66$ V, $R_L = 3{\cdot}4\ \Omega$ (diode no. 2 in table 5-I); black squares: Si n^+–p, $V_{\mathrm{BR}} = 111$ V (diode no. 7 in table 5-I); dots: Si n^+–p, $V_{\mathrm{BR}} = 111$ V, $R_L = 0{\cdot}5\ \Omega$; half-filled circles; idem, $R_L = 1{\cdot}2\ \Omega$; circles: idem, $R_L = 1{\cdot}6\ \Omega$ (diode no. 8 in table 5-I); black triangles upside down: n-GaAs S.B., $V_{\mathrm{BR}} = 50$ V (diode no. 14 in table 4-I). (*b*) Data derived from l.f.-noise measurements (circles) together with the corresponding data derived from FM-noise data (dots), where black squares and triangles as under (*a*).

when the FM-noise data are used, or by

$$\Delta = \langle v_{n0}{}^2 \rangle_{\text{meas.}} / \langle v_{n0}{}^2 \rangle_{\text{small-signal}} \tag{7.12}$$

when the l.f.-noise data are used. The data for the AM noise were not used since we found the ratio $P_{\text{AM},i}/P_{\text{FM},i}$ to be well described by the linear theory, so that these data would coincide with their corresponding FM-noise data. The theoretical value of the intrinsic FM noise was calculated from eq. (6.11) which reads

$$\frac{P_{\text{FM},i}}{P_c} = K_{\text{FM}} \frac{I_{c0}}{P_L},$$

where the value of the constant K_{FM} was obtained from the data given in table 5-I, and the values of I_{c0} and P_L were obtained from meter readings. For the data presented in fig. 7.3 we assumed the above equation to be valid for *all* values of m, so that we obtain some insight into the noise behaviour outside the RVM, too. The value of the small-signal l.f.-noise voltage was obtained from measurements on the non-oscillating diode, since in sec. 4.5 we concluded that the theoretical expression for this noise, eq. (4.18), could only be used in a small bias-current range. The excess-noise data obtained for the l.f. noise are given in fig. 7.3*b*, together with their corresponding FM-noise data. We conclude from this figure that for the GaAs diode the FM and l.f. excess noise differ a constant factor at all values of m, while the l.f. excess noise of the Si diode at low values of m increases more rapidly than the corresponding FM noise.

In spite of the "Milky Way" character of fig. 7.3, this figure clearly demonstrates *) the increase of excess noise with the signal level. Furthermore, we see that this increase is more rapid as m increases. At low values of m, diodes with positive as well as negative values of Δ (in dB) are present. We believe that this effect is caused predominantly by an error in the constant K_{FM}, which value was derived from a number of independent measurements.

7.3.1. *Discussion*

In the literature, several papers have been put forward in which the large-signal noise of the IMPATT diode (used either in an oscillator or in an amplifier) is discussed from a theoretical standpoint. We shall now briefly discuss some aspects of these theories and compare some of the results with our experimental data.

---

*) The data of the Si n^+-p diode at the lowest values of m can be left out of consideration since these data were obtained near the minimum power needed for a correct functioning of the noise-measuring equipment. From repeated measurements we know that an error of ± 2 dB is then possible.

The first large-signal noise theory was presented by Inkson [9]). In his theory he assumes the signal level so (extremely) high that the conduction current leaving the avalanche region can be considered as consisting of a sequence of very sharp pulses. When a pulse has left the avalanche region a very small conduction current is maintained by the diode over a large part of each cycle. A new pulse builds up from this minimum current. Inkson calculated the jitter in pulse amplitude and of the interval between successive pulses due to the random process of ionisation. From these results he calculated the AM and FM noise of the output signal. Unfortunately the sharp-pulse approximation used does not apply to the situation within the RVM of our diode model (which is believed to be practically the same as Inkson's diode model). Within the RVM the signal level is still too low to use this approximation, and therefore no comparison of theory and experiment is possible. However we think the basic idea of Inkson's theory to be correct and useful. The behaviour of the minimum current from which the pulse builds up is then of paramount importance. Van Iperen [104]) recently pointed out that at signal levels outside the RVM ($m > m_{\max}$) a non-negligible amount of impact ionisation occurs in the drift region. This implies that at high signal levels the avalanche and the drift regions can no longer be treated separately. Van Iperen also pointed out that the ionisation in the drift region very much influences the value of the minimum current in the avalanche region. We think it possible to obtain a better understanding of the oscillator-noise behaviour outside the RVM by combining the ideas set forth by Inkson and Van Iperen.

Although Inkson's theory is not applicable in its present form, it nevertheless predicts the following behaviour of the oscillator noise, which is qualitatively in agreement with the experimental observations:

(a) as the bias current is increased the output signal rapidly becomes very noisy;
(b) the noise can be reduced by widening the avalanche region of the device compared to the drift region;
(c) the noise can be reduced by increasing the diode area.

In the remainder of this discussion the signal level is again restricted to signal levels within the RVM. Furthermore, we consider the excess noise as a function of γv_a instead of m (the ratio $m/\gamma v_a$ for the diode investigated is given in table 7-I). Moreover, we carry out a "smoothing" procedure on the assumption that the excess noise is zero for γv_a equal to zero, and that this noise increases monotonically with the signal level. The excess noise found after applying this procedure to the data in fig. 7.3 is given in fig. 7.4a, and indicated by $\bar{\Delta}(\gamma v_a)$. The value of $\bar{\Delta}(\gamma v_a)$ was calculated from

$$\bar{\Delta}(\gamma v_a) = \Delta(\gamma v_a) - \Delta(0) \text{ (dB)}. \qquad (7.13)$$

The value of the correction factor $\Delta(0)$ was found from the intersection of the hypothetical "smooth" curve through each series of data and the axis $\gamma v_a = 0$.

TABLE 7-I

Correction factor $\Delta(0)$, and the ratio of the modulation depth, m, to the normalised voltage across the avalanche region, γv_a, as determined from experimental data

no.	type	V_{BR} (V)	FM/l.f.	$\Delta(0)$ (dB)	$m(\gamma v_a)^{-1}$
2	Si p^+–n	66	FM	0·8	0·059
7	Si n^+–p	111	FM	2·8	0·070
	—	—	l.f.	0·4	—
8	Si n^+–p	111	FM	2·8	0·065
14	n-GaAs S.B.	50	FM	$-2{\cdot}5$	0·100

The values of $\Delta(0)$ used are listed in table 7-I, where it should be noted that $\Delta(0)$ is a constant for each series of excess-noise data. From fig. 7.4*a* we conclude that the excess noise which follows from the FM-noise data increases for all diodes more or less in like manner with the signal level, while those obtained from the l.f.-noise data on the Si n^+–p diode increase more rapidly. For comparison, to be explained below, the graphs of $I_0{}^2(\gamma v_a)$ and $I_0(\gamma v_a)$ are also presented in fig. 7.4.

The first large-signal noise theory for arbitrary signal level was presented by Convert [13,105]). From his theory it can be concluded that the primary noise current, in our study discussed in sec. 4.2 under small-signal conditions, is now also proportional to $I_0{}^2(\gamma v_a)$. The same conclusion can be drawn from the large-signal theory of Hines [17]). The theories of Kuvås [14]), Fikart [15]) and Sjölund [16]) show that the primary noise current increases with the signal level almost proportionally with $I_0{}^2(\gamma v_a)$, where the exact proportionality depends on the ratio $\omega_{a1}{}^2/\omega_0{}^2$. The results of the theories mentioned *) are given in fig. 7.4*b*, for the range of values of $\omega_{a1}{}^2/\omega_0{}^2$ listed in table 5-I, by the shaded areas.

Comparing these results with the experimental data in fig. 7.4*a* we find that only the l.f. data of the Si n^+–p diode vary proportionally to $I_0{}^2(\gamma v_a)$. This can be understood from the results of the large-signal noise theory of Hines [17]). His approach of the noise problem differs completely from those given in refs 13, 14 and 15. Hines considers the influence of noise perturbations, at frequencies $\omega_0 \pm \Omega$ and Ω, on the diode periodically driven at frequency ω_0. He then carefully traces all mixing terms which arise from the non-linear behaviour of the diode, and takes full account of the impedances of the diode

---

*) The theory of Sjölund is limited to values of $\gamma v_a \leqslant 1$ [106]).

and the circuit at frequencies $\omega_0 \pm \Omega$ and Ω. From Hines's theory it then can be concluded that the l.f. noise varies proportionally with the primary noise current, and hence the l.f. excess noise with $I_0{}^2(\gamma v_a)$, as found for the silicon diode. The l.f. noise of the *n*-GaAs Schottky-barrier diode found experimentally does not agree with this conclusion. This is attributed to the fact that the l.f. noise is very sensitive to the actual d.c.-current distribution in the junction. It was found from l.f.-noise-current measurements that in the Si n^+-p diode investigated the d.c.-current distribution was far more uniform than in the GaAs diode investigated. Furthermore, Hines reaches the conclusion that the r.f. noise at frequency $\omega_0 + \Omega$ is determined by the noise generation at $\omega_0 + \Omega$ and $\omega_0 - \Omega$, and vice versa, and thus also by the impedances at these frequencies. This is found to give reduction of the signal dependence of the r.f. excess noise compared to the l.f. noise. In fig. 7.4*a* it is shown that the r.f. excess noise varies proportionally with (somewhat arbitrarily chosen) $I_0(\gamma v_a)$. Although Hines primarily considered an IMPATT-diode amplifier, the conclusions mentioned are found to be correct for the IMPATT-diode oscillator too, as will be published by Goedbloed and Vlaardingerbroek [107]), who worked out a large-signal oscillator-noise theory based on the ideas set forth by Convert [105]) and Hines [17]).

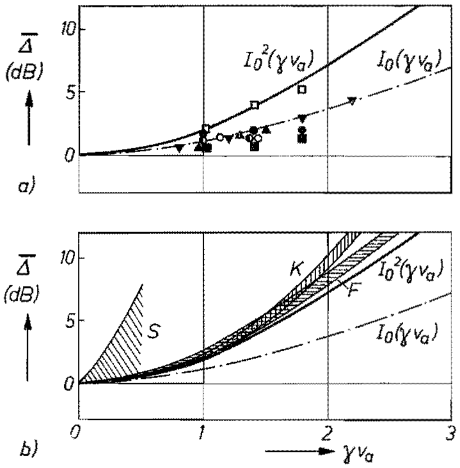

Fig. 7.4. Excess-noise data as a function of γv_a.
(*a*) Data derived from those in fig. 7.3, using eq. (7.13) and the data given in table 7-I.
(*b*) Signal dependence of the noise generation predicted by the theories of Kuvås (K), Fikart (F) and Sjölund (S), see text.

We think the theory presented recently by Fikart [16]) to be an important contribution in the description of oscillator noise. In his paper, which is based on the general theory of oscillator noise given by Vlaardingerbroek [12]) and the large-signal noise theory of Kuvås [14]), Fikart made a comparison between theory and experiment. He found good agreement at high signal levels. However, in our opinion, he compares theory and experiment at signal levels beyond the RVM of his diode model, in particular where he compares his theory with the experimental data presented by Goedbloed [98]). We therefore think that the agreement between theory and experiment found could be fortuitous. On the other hand, we think that Fikart's theory can lead to a good description of the oscillator noise within the RVM.

REFERENCES

1) W. T. Read, Bell Syst. tech. J. **37**, 401, 1958.
2) R. L. Johnston, B. C. DeLoach and B. G. Cohen, Bell Syst. tech. J. **44**, 369, 1965.
3) V. M. Val'd-Perlov, A. V. Krasilov and A. S. Tager, Radio Eng. Electron. Phys. **11**, 1764, 1966.
4) B. C. DeLoach and R. L. Johnston, Trans. IEEE **ED-13**, 181, 1966.
5) J. Josenhans, Proc. IEEE (Lett.) **54**, 1478, 1966.
6) M. S. Gupta, Proc. IEEE **59**, 1674, 1971.
7) M. E. Hines, Int. Solid-State Circuits Conf. Dig. (Philadelphia, Pa.) 82, 1966.
8) M. E. Hines, Trans. IEEE **ED-13**, 158, 1966.
9) J. C. Inkson, Int. J. Electron. **25**, 1, 1968.
10) M. T. Vlaardingerbroek, Electron. Lett. **5**, 521, 1969.
11) M. T. Vlaardingerbroek and J. J. Goedbloed, Philips Res. Repts **25**, 452, 1970.
12) M. T. Vlaardingerbroek, Electron. Lett. **7**, 648, 1971.
13) G. Convert, Proc. IEEE (Lett.) **59**, 1266, 1971.
14) R. L. Kuvås, Trans. IEEE **ED-19**, 220, 1972.
15) A. Sjölund, Solid-State Electron. **15**, 971, 1972.
16) J. L. Fikart, Thesis University of Alberta, Edmonton, Canada, 1973.
17) M. E. Hines, Proc. IEEE **60**, 1534, 1972.
18) J. J. Goedbloed, De Ingenieur **83**, ET63, 1971 (in Dutch).
19) A. S. Groove, Physics and technology of semiconductor devices, John Wiley and Sons Inc., 1967, Ch. 6.
20) C. B. Norris and J. F. Gibbons, Trans. IEEE **ED-14**, 38, 1962.
21) K. G. McKay, Phys. Rev. **94**, 877, 1954.
22) S. M. Sze, Physics of semiconductor devices, John Wiley and Sons Inc., 1969, Ch. 2.
23) A. G. Chynoweth, Phys. Rev. **109**, 1537, 1958.
24) W. Shockley, Solid-State Electron. **2**, 35, 1961.
25) S. L. Miller, Phys. Rev. **105**, 1246, 1957.
26) J. E. Caroll, Hot electron microwave generators, Edward Arnold Ltd., London, Ch. 2.
27) A. van der Ziel, Noise, Prentice-Hall Inc., New York, 1954, Ch. 12.
28) R. B. Emmons and G. Lukovsky, Trans. IEEE **ED-13**, 297, 1966.
29) C. A. Lee, R. L. Batdorf, W. Wiegmann and G. Kaminsky, J. appl. Phys. **38**, 2787, 1967.
30) S. T. Fisher, Trans. IEEE **ED-14**, 313, 1967.
31) B. B. van Iperen, private communication.
32) M. Claassen, Proc. MOGA 70 (Amsterdam, The Netherlands), Kluwer, Deventer, The Netherlands, 1970, p. 12·26.
33) R. L. Kuvås and C. A. Lee, J. appl. Phys. **41**, 1743, 1970.
34) G. Convert, Proc. IEEE (Lett.) **59**, 1265, 1971.
35) J. J. Goedbloed, Solid-State Electron. **15**, 635, 1972.
36) R. Hulin, M. Claassen and W. Harth, Electron. Lett. **6**, 849, 1970.
37) G. A. Acket and M. T. Vlaardingerbroek, Festkörperprobleme, IX, Verlag F. Vieweg u. Sohn, Braunschweig, 1969, p. 280.
38) B. B. van Iperen and H. Tjassens, Philips Res. Repts **27**, 38, 1972.
39) D. de Nobel and H. G. Kock, Proc. IEEE (Lett.) **57**, 2088, 1969.
40) R. Hulin, private communication.
41) A. S. Tager, Sov. Phys. Uspekhi **9**, 892, 1967.
42) B. Boittiaux, E. Constant, B. Kramer, M. Lefebvre, G. Vaesken and A. Semichon, Acta electronica **12**, 157, 1969.
43) H. K. Gummel and D. L. Scharfetter, Bell Syst. tech. J. **45**, 1797, 1966.
44) D. Delagebeaudeuf, L'Onde électr. **48**, 722, 1968.
45) M. Abramowitz and I. A. Stegun, Handbook of mathematical functions, Dover Publ. Inc., New York, p. 376.
46) J. J. Goedbloed, Proc. MOGA 70 (Amsterdam, The Netherlands) Kluwer, Deventer, The Netherlands, 1970, p. 12·36.
47) B. B. van Iperen and H. Tjassens, Proc. MOGA 70 (Amsterdam, The Netherlands), Kluwer, Deventer, The Netherlands, 1970, p. 7·27.
48) B. B. van Iperen and H. Tjassens, Proc. IEEE (Lett.) **59**, 1032, 1971.
49) R. H. Haitz, H. L. Stover and N. J. Tolar, Trans. IEEE **ED-16**, 438, 1969.
50) E. Allamando, Thesis University of Lille, France, 1968.
51) A. S. Tager, Sov. Phys. solid State **6**, 1919, 1965.
52) R. J. McIntyre, Trans. IEEE **ED-13**, 164, 1966.

53) M. Gilden and M. E. Hines, Trans. IEEE **ED-13**, 169, 1966.
54) H. Melchior and W. T. Lynch, Trans. IEEE **ED-13**, 829, 1966.
55) H. K. Gummel and J. L. Blue, Trans. IEEE **ED-14**, 569, 1967.
56) W. Shockley, J. A. Copeland and R. P. James, "The impedance field method of noise calculation in active semiconductor devices", in Quantum theory of atoms, molecules and the solid state, Academic Press, 1966.
57) H. Statz, R. A. Pucel and H. A. Haus, Proc. IEEE (Lett.) **60**, 645, 1972.
58) T. Misawa, Solid-State Electron. **13**, 1369, 1970.
59) G. Persky and D. J. Bartelink, J. appl. Phys. **42**, 4414, 1971.
60) R. Hulin and J. J. Goedbloed, Appl. Phys. Lett. **21**, 69, 1972.
61) E. Constant, B. Kramer and L. Raczy, C. R. Acad. Sci. Paris ser. B. **265**, 385, 1967.
62) R. H. Haitz and F. W. Voltmer, J. appl. Phys. **39**, 3379, 1968.
63) J. J. Goedbloed, ESDERC Conference (Munich, March 1971).
64) I. M. Naqvi, J. Jap. Soc. appl. Phys. Suppl. **40**, 241, 1971.
65) R. L. Kuvås and C. A. Lee, J. appl. Phys. **41**, 3108, 1970.
66) R. H. Haitz, J. appl. Phys. **38**, 2935, 1967.
67) G. Gibbons and T. Misawa, Solid-State Electron. **11**, 1007, 1968.
68) C. R. Crowell and S. M. Sze, Appl. Phys. Lett. **9**, 242, 1966.
69) J. G. Ondria, Trans. IEEE **MTT-16**, 767, 1968.
70) A. G. van Nie, Philips Res. Repts **25**, 437, 1970.
71) B. Schiek and J. Köhler, private communication.
72) O. Schreiber and N. Hecker, Nachr. techn. Z. **22**, 158, 1969.
73) H. P. M. Rijpert, private communication.
74) K. Kurokawa, Trans. IEEE **MTT-16**, 234, 1968.
75) K. Kurokawa, Bell Syst. techn. J. **48**, 1937, 1969.
76) H. J. Thaler, G. Ulrich and G. Weidmann, Trans. IEEE **MTT-19**, 692, 1971.
77) G. Weidmann, ESDERC Conference (Munich, March 1971).
78) G. Weidmann, Nachr. Techn. Z. **23**, 368, 1970.
79) K. Mouthaan and H. P. M. Rijpert, Philips Res. Repts **26**, 394, 1971.
80) W. A. Edson, Proc. IRE **48**, 1454, 1960.
81) G. Klein and J. J. Zaalberg van Zelst, Precision electronics, Philips Technical Library, Centrex, Eindhoven, 1967, p. 317.
82) J. G. Ondria and J.-C. R. Collinet, IEEE J. solid-State Circuits **SC-4**, 65, 1969.
83) J. R. Ashley and F. M. Palka, Proc. IEEE (Lett.) **58**, 155, 1970.
84) R. L. Rulison, G. Gibbons and J. G. Josenhans, Proc. IEEE (Lett.) **55**, 223, 1967.
85) J. J. Baranowski, V. J. Higgens, C. K. Kim and L. D. Armstrong, Microwave J. **12**, 71, 1969.
86) R. Perichon, Thesis University of Lille, France, 1971.
87) J. J. Goedbloed, Electron. Lett. **7**, 445, 1971.
88) A. M. Cowley, Z. A. Fazarine, R. D. Hall, S. A. Hamilton, C. S. Yen and R. A. Zettler, IEEE J. solid-State Circuits **SC-5**, 338, 1970.
89) H. Johnson and B. B. Robinson, Proc. IEEE (Lett.) **59**, 1272, 1971.
90) W. Harth and G. Ulrich, Electron. Lett. **5**, 7, 1969.
91) R. E. Goldwasser, J. Berenz, C. A. Lee and G. C. Dalman, Proc. MOGA 70 (Amsterdam, The Netherlands), Kluwer, Deventer, The Netherlands, 1970, p. 12·19.
92) K. Schünemann and B. Schiek, Electron. Lett. **7**, 659, 1971.
93) M. E. Hines, J.-C.R. Collinet and J.G. Ondria, Trans. IEEE **MT-16**, 738, 1968.
94) B. Schiek and K. Schünemann, Arch. el. Übertr. **26**, 310, 1972.
95) A. S. Tager and A. M. Tsebiyer, Radio Eng. Electron. Phys. **14**, 1110, 1969.
96) R. Perichon, Trans. IEEE **MTT-18**, 988, 1970.
97) K. Mouthaan, Philips Res. Repts **25**, 33, 1970.
98) J. J. Goedbloed, Proc. 1971 European Microwave Conference (Stockholm, Sweden), Suppl., p. 6.
99) B. B. van Iperen, H. Tjassens and J. J. Goedbloed, Proc. IEEE (Lett.) **57**, 1341, 1969.
100) K. Kurokawa, Trans. IEEE **MT-19**, 793, 1971.
101) H. Tjassens, Proc. 1973 European Microwave Conf. (Brussels, Sept. 1973).
102) E. F. Scherer, IEEE Trans. **MTT-16**, 781, 1968.
103) H. J. Thaler, ESDERC Conference (Munich, March 1969).
104) B. B. van Iperen, Proc. IEEE (Lett.), to be published.
105) G. Convert, Revue Thomson-CSF **3**, 419, 1971.
106) A. Sjölund, private communication.
107) J. J. Goedbloed and M. T. Vlaardingerbroek, to be published.

Summary

This thesis deals with the noise in singly tuned low-loaded-Q IMPATT-diode oscillators. Since the ultimate aim of our studies is to describe the amplitude and frequency fluctuations of the oscillator signal, starting from the processes which take place inside the diode, the diode model adopted is of great importance. That model is introduced in chapter 2. In that chapter we first give a brief review of the phenomenon of impact ionisation in semiconductor diodes that leads to avalanche breakdown of these diodes, and derive the principal assumption on which the diode model is based, namely that in an avalanching junction, carrier generation by impact ionisation and carrier drift occur in separate regions of the depletion layer. These regions are called avalanche region and drift region, respectively. The chapter continues with a discussion of the avalanche region in which the highly non-linear avalanche process takes place. An equation is derived for the conduction current in that region. It is shown that several rather crude assumptions have to be made to arrive at the relatively simple, generalised Read equation, which is found to give an adequate description of the conduction current mentioned. The introduction of the diode model is completed with a discussion of the drift region, and with a vector diagram of voltages and currents in which the origin of the negative resistance of the diode can be traced. The chapter ends with a summary of the basic assumptions in the diode model.

Chapter 3 presents a discussion of the noise-free behaviour of the IMPATT diode. It is shown that the value of all diode parameters in the diode model can be derived from small-signal-impedance measurements carried out at a fixed microwave frequency as a function of the bias current through the diode. To have some insight into the validity of the diode model used, this model is extended. Using the results of numerical calculations, it is then found that the simple model of chapter 2 is sufficient in all cases of interest. Chapter 3 continues with a discussion of the large-signal behaviour of the diode. Much attention is paid to the range of validity of the noise-free, large-signal theory (denoted by RVM), because if the model fails to describe the quasi-stationary quantities, such as large-signal impedance and the output power of the oscillator, we can have no illusions about the description of the oscillator noise derived from the same model. A method, based on the conclusion that if the external circuit is fixed, the oscillation frequency and the avalanche frequency are constants, is used to determine the RVM from simple measurements of output power versus bias current. Furthermore, microwave measurements are discussed, from which the large-signal impedance of the diode, the loss resistance of the circuit and the load resistance can be determined. Finally, the theory is extended to include the second-order field derivative of the ionisation coefficient of the carriers which should make it possible to explain the variation

of the bias voltage of the oscillating diode with the signal level of the oscillations. The experiments are found not to confirm this.

Chapter 4 deals with the noise of the non-oscillating diode. The fluctuations of the avalanche process enter the mathematical description via a Langevin term added to the continuity of electrons and holes, assuming the fluctuations to be shot noise. The total current through the diode is calculated, and it is found that this current can be assumed to arise from a hypothetical noise current in the avalanche region. The only diode parameter which determines this current is the intrinsic response time of the avalanche process. This response time is determined from microwave measurements for several diode structures, such as Si n^+–p, Si p^+–n, n-Si Schottky-barrier, Ge n^+–p, and n-GaAs Schottky-barrier diodes. As in chapter 3 the diode model was extended, which resulted in restrictions on the measuring frequency and the bias current in the experimental determination of the response time. Furthermore it was concluded that, in the frequency range of interest, the noise contribution of the avalanche process predominates. Finally, the field derivative of the ionisation coefficient could be determined from the experimental data for the diodes mentioned.

Chapter 5 starts with a discussion of some ways in which the fluctuations of the output signal of an oscillator can be described. This is followed by a description of the noise-measuring equipment and the oscillator-noise-measuring procedures. The chapter continues with a review of the general, phenomenological theory of oscillator noise, after which this theory is applied to the special case of an IMPATT-diode oscillator. This resulted in an expression for the ratio of the intrinsic AM and FM noise power in singly tuned, low-Q_L circuits. This expression predicts that the AM noise is at least 40 dB below the FM noise in these circuits. Within the RVM, the expression was verified by experiments on an Si n^+–p and an n-GaAs Schottky-barrier diode. Outside the RVM, the general theory was found to describe adequately the ratio mentioned. The chapter ends with a first discussion of the up-conversion of bias-current noise into oscillator noise, and the reverse effect, the down-conversion of oscillator noise into bias-current noise. It is concluded that in the model used no up-conversion into FM noise is present. An expression is derived (from the general theory) for the up-converted AM noise, as is an expression for the factor governing the down-conversion.

In chapter 6 we deal with the linear theory of oscillator noise, which is based on the fact that the output signal of an oscillating loop consists of narrow-band amplified noise. This theory is restricted to low signal levels, so that the output power can be assumed mainly as linearly amplified noise, while the non-linearity only enters as the mechanism ensuring that the amount of noise amplification remains finite. The linear amplification precludes the possibility of mixing products, hence the linear theory does not account for modulation noise. The theory provides an expression for the form and width of the output spectrum.

It is found that the spectrum can be described by a Lorentz curve. As the intrinsic noise is found to be predominantly FM noise, it is assumed that the output spectrum is determined by FM noise alone, and an expression is derived for this type of noise. If the oscillator circuit is fixed, the theory predicts that the FM noise decreases with increasing signal level. The theory is confirmed, up to a modulation depth of about 0·1, by experiments on Si p^+–n, Si n^+–p, and n-GaAs Schottky-barrier diodes. (The modulation depth is defined as the ratio of the a.c. voltage across the diode to the breakdown voltage). In contradiction with the theory the FM noise is found to increase at higher modulation depths. An expression for the intrinsic AM noise is obtained by combining the expression for the FM noise with that for the ratio of the intrinsic AM and FM noise derived in chapter 5. Again up to a modulation depth of about 0·1, the theory is verified by experiments. At higher signal levels the AM noise is almost a constant. Finally, there is discussed as to how oscillator noise can be reduced by means of a proper choice of device parameters. Among other things, it is found that the FM noise can be minimised by choosing the transit angle about 4·5 rad.

Chapter 7 deals with non-linear noise in IMPATT-diode oscillators. The up-converted and down-converted noise is treated first. It is found that, within the RVM, the down-conversion of oscillator noise can be neglected, and, furthermore, that the up-converted noise is indeed predominantly AM noise. The theoretical results are confirmed by experiments on a Si n^+–p diode and an n-GaAs Schottky-barrier diode. The chapter ends with a discussion of the difference between the measured noise and the noise predicted by the linear noise theory of chapter 6. It is concluded that the common origin of the AM, FM and l.f. noise, viz. the total noise current flowing through the diode, grows with the signal level over its small-signal value.

Samenvatting

Dit proefschrift behandelt de ruis van lawine-looptijdoscillatoren (IMPATT-diode-oscillatoren) met enkelvoudige afstemming en lage belaste kwaliteitsfactor. Het doel van deze studie is de amplitude- en frequentie-fluctuaties van het oscillatorsignaal af te leiden uit de processen die in de diode plaats vinden. Derhalve is de keuze van een goed model van de diode van groot belang. In hoofdstuk 2 wordt een model ingevoerd. In dat hoofdstuk geven we eerst een kort overzicht van het verschijnsel botsingsionisatie in halfgeleiderdiodes, dat aanleiding geeft tot lawinedoorslag. We komen dan tot de hoofdveronderstelling waarop het model van de diode gebaseerd is, namelijk dat de generatie van ladingdragers door botsingionisatie en de drift van deze ladingdragers plaats vinden in afzonderlijke delen van het depletiegebied, en wel in respectievelijk het lawinegebied en het driftgebied. Dan volgt een bespreking van het lawinegebied waarin het, uitgesproken niet-lineaire, lawine-proces plaats vindt. Daarbij wordt een vergelijking afgeleid voor de geleidingsstroom in dat gebied. Er moeten verschillende tamelijk grove veronderstellingen gemaakt worden om tot een gegeneraliseerde vergelijking van Read te komen die nog betrekkelijk eenvoudig is en toch het gedrag van deze stroom goed weergeeft. De invoering van het diodemodel wordt besloten met een bespreking van het driftgebied, en met een vectordiagram van spanningen en stromen waarin het ontstaan van de negatieve weerstand van de diode nagegaan kan worden. Het hoofdstuk eindigt met een overzicht van de basisveronderstellingen waarop het diodemodel berust.

Hoofdstuk 3 geeft een bespreking van het ruisvrije gedrag van de IMPATT-diode. Er wordt aangegeven hoe de waarden van de parameters van het model alle afgeleid kunnen worden uit metingen van de impedantie voor kleine signalen als functie van de gelijkstroom door de diode, uitgevoerd bij een vaste microgolffrequentie. Ten einde een indruk te krijgen van de deugdelijkheid van het gebruikte model, wordt dit verfijnd. Gebruik makend van resultaten van numerieke berekeningen wordt geconcludeerd dat het eenvoudige in hoofdstuk 2 ingevoerde diodemodel, in alle gevallen waarin wij geïnteresseerd zijn, acceptabel is. Hoofdstuk 3 gaat voort met een bespreking van het gedrag van de diode bij grote signalen. Veel aandacht wordt besteed aan het geldigheidsgebied van de theorie voor ruisvrije grote signalen, omdat we niet de illusie kunnen hebben dat de oscillatorruis beschreven kan worden met het diodemodel, wanneer dit reeds faalt in de beschrijving van de quasi-stationaire grootheden zoals de impedantie voor grote signalen en het uitgangsvermogen van de oscillator. Een methode, gebaseerd op de conclusie dat bij een gegeven extern circuit de oscillatiefrequentie en de lawinefrequentie constantes zijn, wordt beschreven om het voornoemde geldigheidsgebied te bepalen uit eenvoudige metingen van het uitgangsvermogen als functie van de gelijkstroom. Dit geldigheidsgebied wordt in dit proefschrift aangeduid met RVM (Range of Validity of

the noise-free large-signal Model). Voorts worden metingen van de impedantie bij microgolffrequenties besproken, waaruit de diode-impedantie voor grote signalen, de verliesweerstand van het circuit en de belastingweerstand bepaald kunnen worden. Tot slot wordt de theorie uitgebreid door de tweede afgeleide naar het electrisch veld van de ionisatiecoëfficient van de ladingdragers in de beschouwingen op te nemen. Dit zou het mogelijk moeten maken de verandering van de gelijkspanning over de oscillerende diode, als gevolg van een verandering van de grootte van het oscillatorsignaal, te verklaren. De experimenten bevestigen dit echter niet.

Hoofdstuk 4 is gewijd aan de ruis van de niet-oscillerende diode. De fluctuaties in het lawineproces komen mathematisch tot uiting in een aan de continuiteitsvergelijking voor de electronen en de gaten toegevoegde Langevinterm; daarbij wordt aangenomen dat de fluctuaties het karakter van hagelruis hebben. De totale ruisstroom door de diode wordt berekend en het blijkt dat deze stroom gedacht kan worden te zijn veroorzaakt door een stroombron in het lawinegebied. De enige diodeparameter die de grootte van deze bron bepaalt blijkt de intrinsieke responsietijd van het lawineproces te zijn. Deze tijdconstante is voor verschillende diodestructuren, zoals Si-p^+-n, Si-n^+-p, Si-n-metaal, Ge-n^+-p en GaAs-n-metaal diodes, bepaald uit microgolfmetingen. Evenals in hoofdstuk 3 wordt het diodemodel uitgebreid, hetgeen leidt tot het stellen van voorwaarden met betrekking tot de meetfrequentie en de grootte van de gelijkstroom bij de experimentele bepaling van de responsietijd. Voorts blijkt in het frequentiegebied waarin wij zijn geinteresseerd de ruisbijdrage van het lawineproces te overheersen. Tot slot kan de eerste afgeleide van de ionisatiecoëfficient naar het electrisch veld bepaald worden uit de experimentele gegevens voor voornoemde diodes.

Hoofdstuk 5 begint met een bespreking van enkele manieren waarop de fluctuaties van het uitgangssignaal van een oscillator beschreven kunnen worden. Dit wordt gevolgd door een beschrijving van de ruis-meetopstelling en de procedures voor het meten van de oscillatorruis. Het hoofdstuk wordt vervolgd met een overzicht van de algemene, phenomenologische theorie van oscillatorruis, waarna deze wordt toegepast op het speciale geval van een IMPATT-diode-oscillator. Dit resulteert in een uitdrukking voor het intrinsieke AM- en het intrinsieke FM-ruisvermogen in een enkelvoudig afgestemd circuit met lage kwaliteitsfactor. Deze voorspelt dat de intrinsieke AM-ruis tenminste 40 dB lager is dan de intrinsieke FM-ruis. Binnen het RVM werd deze uitdrukking juist bevonden voor het beschrijven van de meetresultaten verkregen voor een Si-n^+-p en een GaAs-n-metaal diode. Buiten het RVM bleek de algemene theorie de verhouding goed te beschrijven. Het hoofdstuk eindigt met een eerste bespreking van het omzetten van ruis van het voedingscircuit in ruis van de oscillator, en het omgekeerde, het omzetten van ruis van de oscillator tot ruis in het voedingscircuit. De conclusie is dat er geen omzetting in FM-ruis plaats vindt. Uit de algemene ruistheorie wordt een uitdrukking afgeleid voor de omzetting van ruis in het voedingscircuit in AM-ruis van de oscillator, en tevens wordt de factor, die de omzetting naar ruis in het voedingscircuit bepaalt, aan een nadere beschouwing onderworpen.

In hoofdstuk 6 behandelen we de lineaire theorie van oscillatorruis die gebaseerd is op het feit dat het uitgangssignaal van een oscillerende kring bestaat uit smal-bandig versterkte ruis. Deze theorie is beperkt tot dusdanig kleine signalen dat aangenomen kan worden dat het uitgangssignaal voornamelijk bestaat uit lineair versterkte ruis, waarbij de niet-lineariteit slechts naar voren komt in het mechanisme dat er voor zorgt dat de versterking van de ruis eindig blijft. De lineaire versterking sluit de mogelijkheid van mengproducten uit, derhalve doet deze theorie geen uitspraak over modulatieruis. De theorie geeft een uitdrukking voor de vorm en de breedte van het uitgangsspectrum, waarbij blijkt dat de vorm beschreven kan worden door een Lorentz-kromme. Daar de intrinsieke ruis voornamelijk uit FM-ruis blijkt te bestaan, veronderstellen we dat de vorm van het spectrum uitsluitend bepaald wordt door FM-ruis, en een uitdrukking voor dit type ruis wordt afgeleid. De theorie voorspelt dat bij gegeven oscillatorcircuit de FM-ruis afneemt met toenemend signaal. Tot een modulatiediepte van ca. 0,1 wordt de theorie bevestigd door resultaten van metingen aan Si-p^+-n, Si-n^+-p en GaAs-n–metaal diodes. (De modulatiediepte is hier gedefinieerd als de verhouding van de wisselspanning over de diode en zijn doorslagspanning.) In tegenstelling tot de theorie neemt de gemeten FM-ruis bij grotere signalen weer toe. Een uitdrukking voor de intrinsieke AM-ruis wordt verkregen door die voor de FM-ruis te combineren met de in hoofdstuk 5 afgeleide verhouding van intrinsieke AM- en FM-ruis. De theorie wordt tot een modulatiediepte van ca. 0,1 weer bevestigd door metingen. Bij grotere signalen is de AM-ruis min of meer een constante. Tot slot wordt besproken hoe de ruis van de oscillator verminderd kan worden door een juiste keuze van de diodeparameters. Onder andere blijkt de FM-ruis geminimaliseerd te kunnen worden door de loophoek ongeveer 4,5 radiaal te maken.

Hoofdstuk 7 betreft niet-lineaire ruis in IMPATT-diode-oscillatoren. Het verband tussen de ruis in het voedingscircuit en de oscillatorruis wordt eerst behandeld. Het blijkt dat binnen het RVM het omzetten van oscillatorruis in ruis in het voedingscircuit verwaarloosd kan worden, en voorts dat de ruis van het voedingscircuit inderdaad voornamelijk in AM-ruis wordt omgezet. De theorie wordt bevestigd door metingen aan een Si-n^+-p en een GaAs-n–metaal diode. Het hoofdstuk wordt besloten met een bespreking van het verschil tussen de gemeten ruis en de ruis die voorspeld wordt door de lineaire ruistheorie uit hoofdstuk 6. Geconcludeerd wordt dat de gemeenschappelijke bron van de AM-, FM- en laagfrequent-ruis, d.w.z. de totale ruisstroom door de diode, met toenemende grootte van de signalen een toenemend verschil vertoont vergeleken met zijn waarde bij kleine signalen.

Curriculum vitae

De schrijver van dit proefschrift is in 1937 te Biervliet geboren. In 1954 behaalde hij het einddiploma H.B.S.-B aan de Gemeentelijke H.B.S. A en B, te Utrecht. In september van datzelfde jaar trad hij in dienst bij de N.V. Philips' Gloeilampenfabrieken te Eindhoven. Hier was hij, met een onderbreking van 21 maanden in verband met zijn militaire verplichtingen, tot september 1961 als assistent verbonden aan het Natuurkundig Laboratorium. In die periode was hij onder leiding van Ir. W. Bähler werkzaam in de Electro-Mechanische Groep, hoofdzakelijk op het gebied van wervelstroom-koppelingen en -motoren. In oktober 1961 begon hij zijn studie aan de Gemeentelijke Universiteit van Amsterdam, alwaar hij in juni 1964 het candidaatsexamen in de Wis- en Natuurkunde (a_n) aflegde, en in december 1967 het doctoraalexamen Experimentele Natuurkunde. Van november 1964 tot augustus 1967 was hij als wetenschappelijk assistent in dienst van de Stichting F.O.M. werkzaam op het Natuurkundig Laboratorium van de Gemeentelijke Universiteit van Amsterdam. Aldaar verrichtte hij, onder leiding van Dr. C. A. J. Ammerlaan, onderzoek op het gebied van gammabestraling van met lithium gecompenseerd silicium. In december 1967 trad hij wederom in dienst bij de N.V. Philips' Gloeilampenfabrieken te Eindhoven, alwaar hij thans werkzaam is in de groep "Microwave Device Physics" van het Natuurkundig Laboratorium. Het in dit proefschrift beschreven onderzoek is uitgevoerd in de periode mei 1969 tot mei 1972.

STELLINGEN

bij het proefschrift van

J. J. Goedbloed

6 november 1973
T.H. Eindhoven

I

Ten onrechte concludeert Haitz dat zijn metingen van ruis bij lage frequenties verricht aan lawinediodes, informatie bevatten omtrent de intrinsieke responsietijd van het lawineproces.

R. H. Haitz, J. appl. Phys. **38**, 2935, 1967.

II

De conclusie van Fikart en Goud dat de AM-ruis in lawine-looptijd-oscillatoren minder sterk varieert met de grootte van het oscillatorsignaal dan de FM-ruis, is weliswaar juist, doch verdient enige aanvulling.

J. L. Fikart en P. Goud, J. appl. Phys. **44**, 2284, 1973.

III

Het gebruik van het begrip ruismaat bij oscillatoren is weinig zinvol.

Microwaves **11**, 40, 1972.

IV

De berekeningen die Zwicker et al. geven van de faseverschuiving tussen de recombinatiestraling in halfgeleidermaterialen en het gemoduleerde licht dat deze straling veroorzaakt, is onnodig ingewikkeld.

H. R. Zwicker, D. L. Keune, N. Holonyak Jr. en R. D. Burnham, Solid-State Electron. **14**, 1023, 1971.

V

In een “bulk-CCD” kunnen grotere ladingpakketten getransporteerd worden dan in een “oppervlakte-CCD” wanneer de pakketten in beide gevallen met dezelfde snelheid worden getransporteerd, dit in tegenstelling tot wat Walden et al. beweren.

R. H. Walden, R. H. Krambeck, R. J. Strain, J. McKenna, N. L. Schryer en G. E. Smith, Bell Syst. techn. J. **51**, 1635, 1972.

VI

De getalwaarden van de parameters van de wisselwerkingspotentiaal van helium–waterstof-systemen, bepaald uit moleculaire-bundel-experimenten volgens de methoden gangbaar bij atomaire systemen, zullen afhangen van de temperatuur van de bronkamer.

H. P. Butz, R. Feltgen, H. Pauly, H. Vehmeyer en R. M. Yealland, Z. Phys. **247**, 60, 1971.
W. F. Heukels en J. van der Ree, J. chem. Phys. **57**, 1393, 1972.
H. V. Lilenfeld, J. L. Kinsey, N. C. Lang en E. K. Parks, J. chem. Phys. **57**, 4593, 1972.

VII

Hoewel de theorie van Zachos en Ripper voor de verdeling van het electromagnetische veld in een halfgeleider-laserdiode een goede beschrijving geeft van de experimentele resultaten, is deze theorie toch niet consistent met de vergelijkingen van Maxwell.

T. H. Zachos en J. E. Ripper, IEEE J. Quant. Electron. **QE-5**, 29, 1969.

VIII

Bij de bepaling van de diëlectrische constante van licht-gereduceerd rutiel houdt Chu onvoldoende rekening met de mogelijke beïnvloeding van zijn resultaten door oppervlakte-toestanden.

C. W. Chu, Phys. Rev. B **1**, 4700, 1970.

IX

De door Rossel et al. bij MOS-transistoren gevonden veldafhankelijkheid van de evenredigheidsconstante tussen de verandering van de spanning op de stuurelectrode bij constant gehouden stroom door de afvoerelectrode, en de logaritme van de tijd, komt niet overeen met het tunnelmodel dat zij introduceren om deze veldafhankelijkheid te verklaren.

P. Rossel, H. Martinot en D. Esteve, Solid-State Electron. **13**, 425, 1970.

X

Bij de huidige stand van de technologie is het zinvol lawine-fotodiodes te gebruiken voor het onderzoek naar de homogeniteit van een halfgeleidermateriaal.

XI

Mede om te komen tot een betere vakantiespreiding, zonder de zomervakantie te verlengen, dient de jaarovergang op scholen verschoven te worden naar het eind van de maand maart.

XII

Het aantal nederlandse beoefenaars van de bergsport neemt nog steeds toe; dit ondanks de wijze waarop de nederlandse televisie aandacht besteedt aan deze tak van sport.